New Finite Element Mesh for Efficient Modeling of Spatial

Flexible Link Articulated Systems

BY

ASHRAF M HAMED

B.Sc. in Mechanical Engineering, Cairo University, Egypt, 2005
M.Sc. in Mechanical Engineering, University of Illinois at Chicago, USA, 2010

THESIS

Submitted as partial fulfillment of the requirements
for the degree of Doctor of Philosophy in Mechanical Engineering
in the Graduate College of the
University of Illinois at Chicago, 2014

Chicago, Illinois

Defense Committee:

Ahmed Shabana, Chair and Advisor, Mechanical Engineering
Craig Foster, Civil and Materials Engineering
Paramsothy Jayakumar, U.S. Army
Eduard Karpov, Civil and Materials Engineering
Antonio Recuero, Mechanical Engineering
Thomas Royston, Mechanical Engineering

ACKNOWLEDGEMENTS

I would like to thank my graduate advisor Dr. Ahmed Shabana for his extensive guidance, valuable suggestions, and persistent encouragement during my studies at the University of Illinois at Chicago. His advice on both research as well as on my career have been invaluable. I would like also to thank my committee members: Dr. Craig Foster, Dr. Paramsothy Jayakumar, Dr. Eduard Karpov, Dr. Antonio Recuero and Dr. Thomas Royston for their constructive advice. I am particularly grateful for Dr. Paramsothy Jayakumar and Dr. Antonio Recuero for their tremendous help that allowed me to complete my thesis.

I owe thanks to all my colleagues at the Dynamic Simulation Laboratory I worked over the years. I learned a lot from each one of them and for that I am very grateful.

Lastly, I would like to thank my family for all their love and encouragement. For my parents, who raised me with a love of science and supported me in all my pursuits. For my sisters, who helped me a lot. And most of all for supportive, encouraging, and patient wife Yasmeen for her help and support during the program.

TABLE OF CONTENTS

iv

v

LIST OF TABLES

LIST OF FIGURES

SUMMARY

Existing multibody system (MBS) algorithms treat articulated system components that are not rigidly connected as separate bodies connected by joints that are governed by nonlinear algebraic equations. As a consequence, these MBS algorithms lead to a highly nonlinear system of coupled differential and algebraic equations. Existing finite element (FE) algorithms, on the other hand, do not lead to a constant mesh inertia matrix in the case of arbitrarily large relative rigid body rotations. In this thesis, new FE/MBS meshes that employ linear connectivity conditions and allow for arbitrarily large rigid body displacements between the finite elements are introduced. The large displacement FE *absolute nodal coordinate formulation* (ANCF) is used to obtain linear element connectivity conditions in the case of large relative rotations between the finite elements of a mesh. It is shown that a linear formulation of the planner pin (revolute) joints that allow for finite relative rotations between connected elements can be systematically obtained using ANCF finite elements. The algebraic joint constraint equations, which can be introduced at a preprocessing stage to efficiently eliminate redundant position coordinates, allow for deformation modes at the pin joint definition point, and therefore, this new joint formulation can be considered as a generalization of the planner pin joint formulation used in rigid MBS analysis. The new pin joint deformation modes, that are the results of C^0 continuity conditions, allow for the calculations of the pin joint strains which can be discontinuous as the result of the finite relative rotation between the elements. This type of discontinuity is referred to in this thesis as *non-structural discontinuity* in order to distinguish it from the case of *structural discontinuity* in which the elements are rigidly connected. Because ANCF finite elements lead to a constant mass matrix, an identity generalized mass matrix can be obtained for the FE mesh despite the fact that

the finite elements of the mesh are not rigidly connected. The relationship between the non-rational ANCF finite elements and the B-spline representation is used to shed light on the potential of using ANCF as the basis for the integration of computer aided design and analysis (ICADA). When cubic interpolation is used in the FE/ANCF representation, C^0 continuity is equivalent to a knot multiplicity of three when computational geometry methods such as B-splines are used. Nonetheless, B-spline and NURBS representations cannot be used to effectively model T-junctions that can be systematically modeled using ANCF finite elements that employ gradient coordinates that can be conveniently used to define element orientations in the reference configuration.

This thesis also examines the limitations of using B-spline representation as an analysis tool by comparing its geometry with the nonlinear finite element absolute nodal coordinate formulation (ANCF) geometry. It is shown that while both B-spline and ANCF geometries can be used to model non-structural discontinuities using linear connectivity conditions, there are fundamental differences between B-spline and ANCF geometries. First, while B-spline geometry can always be converted to ANCF geometry, the converse is not true; that is, ANCF geometry cannot always be converted to B-spline geometry. Second, because of the rigid structure of the B-spline recurrence formula, there are restrictions on the order of the parameters and basis functions used in the polynomial interpolation; this in turn can lead to models that have significantly larger number of degrees of freedom as compared to those obtained using ANCF geometry. Third, in addition to the known fact that B-spline does not allow for straight forward modeling of T-junctions, B-spline representation cannot be used in a straight forward manner to

model structural discontinuities. It is shown that the planner ANCF linear joints can be extended to the spatial analysis and new spatial chain models, governed by linear connectivity conditions, can be developed. The modes of the deformations at the definition points of the joints that allow for rigid body rotations between ANCF finite elements are discussed. Similar to the planner case, the use of the linear connectivity conditions with ANCF spatial finite elements leads to a constant inertia matrix and zero Coriolis and centrifugal forces. The fully parameterized structural ANCF finite elements used in this thesis allow for the deformation of the cross section and capture the coupling between this deformation and the stretch and bending. A new chain model that employs different degrees of continuity for different coordinates at the joint definition points is developed. In the case of cubic polynomial approximation, C^1 continuity conditions are used for the coordinate line along the joint axis; while C^0 continuity conditions are used for the other coordinate lines. This allows for having arbitrary large rigid body rotation about the axis of the joint that connects two flexible links.

The ideal compliant joints developed can be formulated, for the most part, using linear algebraic equations, allowing for the elimination of the dependent variables at a preprocessing stage, thereby significantly reducing the problem dimension and array storage needed. Furthermore, the constraint equations are automatically satisfied at the position, velocity, and acceleration levels. When using the proposed approach to model large scale chain systems, differences in computational efficiency between the augmented formulation and the recursive methods are eliminated, and the CPU times resulting from the use of the two formulations become similar regardless of the complexity of the system. The elimination of the joint constraint equations and the associated dependent variables also contribute to the solution of a

SUMMARY (continued)

fundamental problem encountered in the analysis of closed loop chains and mechanisms by eliminating the need to repeatedly change the chain or mechanism independent coordinates. It is shown that the concept of the knot multiplicity used in computational geometry methods, such as B-spline and NURBS (Non-Uniform Rational B-Spline), to control the degree of continuity at the breakpoints is not suited for the formulation of many ideal compliant joints. As explained in the thesis, this issue is closely related to the inability of B-spline and NURBS to model structural discontinuities. Another contribution of this thesis is demonstrating that large deformation ANCF finite elements can be effective, in some MBS applications, in solving small deformation problems. This is demonstrated using a heavily constrained tracked vehicle with flexible link chains. Without using the proposed approach, modeling such a complex system with flexible links can be very challenging. The analysis presented in the thesis also demonstrates that adding significant model details does not necessarily imply increasing the complexity of the MBS algorithm.

A new simplified spatial elastic Euler-Bernoulli beam force model was developed in an attempt to improve the computational efficiency of the flexible link chain tracked vehicle. The developed force model accounts for the coupling between bending and axial deformations. The model can be considered as a generalization of the two-dimensional force model developed by Berzeri et al (2001). Despite the simplicity of the proposed force model, it accounts for the elastic nonlinearity in the strain-displacement relationship. This force model can be used in the case of small deformations and only accounts for bending and axial deformations. It employs constant stiffness matrices that can be calculated at a preprocessing stage. This helps in reducing the computational effort needed to evaluate the elastic forces. The simplified Euler-Bernoulli

SUMMARY (continued)

elastic force model is compared to the elastic line and continuum mechanics approaches. This comparison serves as a verification of the proposed model. The comparison is held using a heavily constrained tracked vehicle with flexible link chains. The track chain links are connected using linear absolute nodal coordinate joints. It is shown that the Euler-Bernoulli force model results are in a good agreement with the elastic line and continuum mechanics approaches results. It is also shown that the proposed force model is computationally more efficient compared to both these elastic force models.

CHAPTER 1

INTRODUCTION

Most existing finite element (FE) algorithms allow for developing meshes in which the finite elements are rigidly connected. In the case of finite rigid body rotations, some of the existing finite element algorithms employ an incremental solution procedure based on a co-rotational formulation that leads to a highly nonlinear mesh inertia matrix. These FE meshes are routinely used to describe mechanical system components which, in general, have complex shapes that cannot be described using smooth geometry. When the FE method is used in the multibody system (MBS) analysis (Roberson and Schwertassek, 1988; Schiehlen, 1997), it is useful to distinguish between two types of geometric discontinuities; *structural discontinuities*, and *non-structural discontinuities*. Conventional finite element meshes have only structural discontinuities that represent T-, V-, and L-junctions. This type of discontinuities, as previously mentioned, is described in conventional FE/MBS analysis using finite elements that are rigidly connected; that is, the relative motion between the elements is pure deformation. Structural geometric discontinuities have represented a fundamental issue in flexible MBS analysis for decades. Figure 1 (Shabana, and Wehage, 1984) shows an example of a vehicle that was analyzed approximately three decades ago by using MBS computational methods. Figure 2 (Shabana, and Wehage, 1984) shows the twist of two different models of the vehicle that have two different frame designs.

Figure 1 Torsion of the truck frame
(Shabana and Wehage, 1984)

Figure 2 Comparing of frame twist of two vehicle designs
(Shabana and Wehage, 1984)

The interest three decades ago was to develop a new flexible MBS formulation to study

the torsional characteristics of the new frame of this vehicle, shown in Fig. 3 (Shabana, and

Wehage, 1984), when the vehicle components including the frame experience arbitrary rigid

body displacement (Shabana and Wehage, 1984). This frame, as shown in the figure, has structural geometric discontinuities that define T- and V-junctions.
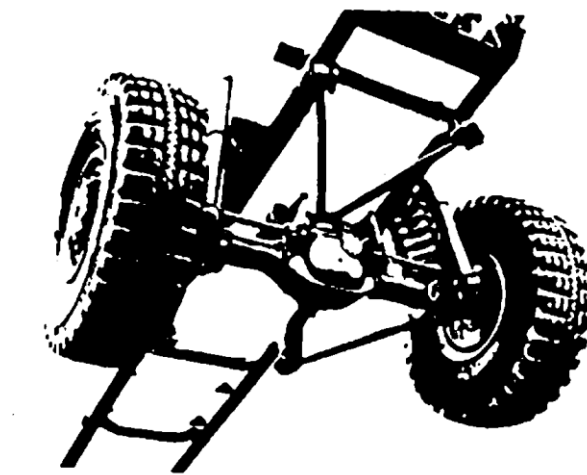
Figure 3 T-Junctions of the truck frame
(Shabana and Wehage, 1984)

The challenge at this time was to develop an accurate kinematic representation of the complex geometry of this frame that is invariant under rigid body rotations. This was a challenging problem since structural finite elements (beam, plates, and shells) that existed at this time employed infinitesimal rotations as nodal coordinates, and as a result, these elements produced shapes that are not invariant under general rigid body displacement. Therefore, the goal was to be able to connect elements (segments) defined by local polynomials that are not invariant under rigid body displacement and develop a formulation in which the structure deformed shape is invariant under such a displacement. This fundamental geometry and analysis problem was solved using the FE *floating frame of reference* (FFR) *formulation* that allows modeling T- and V-junctions even when the local polynomials cannot correctly describe rigid body displacements. The FE/FFR formulation also defines a local linear problem that can be used to filter out

3

insignificant high frequency modes of vibration while preserving the invariance properties in the case of rigid body displacements. Crucial to preserving the rigid body invariant property in the case of structural discontinuities is the use of the concept of the *intermediate element coordinate system.* This coordinate system has an origin that is rigidly attached to the origin of the structure coordinate system and has axes that are initially parallel to the axes of the finite element coordinate system. Using this coordinate system, the finite elements that can have different orientations can be connected rigidly using linear algebraic constraint equations at a preprocessing stage. Therefore, the FE/FFR formulation provided a general solution for accurately modeling structural geometric discontinuities even in cases when the local polynomials define shapes that are not invariant under rigid body rotations.

The second type of discontinuities represents *non-structural discontinuities* that characterize the motion of MBS applications; example of which is chain of links connected by pin joints as the one shown in Fig. 4. Each link is permitted to undergo an independent rigid body rotation. If the links are considered to be flexible bodies, the relative motion between the links is a combination of rigid body and deformation displacements. Nonetheless, the dynamics of a simple planar rigid-link chain is governed by highly nonlinear equations as the result of the geometric nonlinearities due to the finite relative rotations.
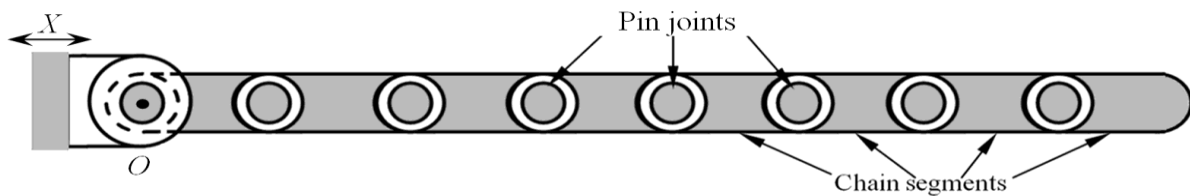
Figure 4 Eight-link chain system

4

Existing FE algorithms and computer programs, however, do not allow for generating a FE mesh for such chains using linear connectivity conditions. One of the goals of this thesis is to demonstrate that a FE mesh of such chains that consist of flexible links can be developed. This will allow developing one FE mesh that includes one or more chains with flexible links, each of which can have independent relative finite rotations. For a tracked vehicle as the one shown in Fig. 5, the two chains can be described using one FE mesh in which connectivity conditions between the links are described using linear algebraic constraint equations. Such a finite element mesh can be systematically developed using the large displacement FE *absolute nodal coordinate formulation* (ANCF) that has a representation that is equivalent to the representation used in the computational geometry and computer aided design (CAD) methods such as B-splines (Piegl and Tiller, 1997, Sanborn and Shabana, 2009; Lan and Shabana, 2010; Mikkola et al, 2013); both representations are related by a linear transformation.

Figure 5 Tracked vehicle

5

ANCF finite elements have several desirable features and correctly describe rigid body motion; that is, the shape of the element is invariant under a rigid body displacement, and such a displacement does not change the strain state of the element (Dmitrochenko.and Pogorelov, 2003; Dufva et al., 2005; Garcia-Vallejo et al., 2008; Kerkkänen et al., 2006; Schwab and Meijaard, 2010; Tian et al., 2009, 2010; Yoo et al., 2004; Yakoub and Shabana, 2001; Shabana and Mikkola, 2003; Shabana, 1998; Abbas et al., 2010). The connectivity conditions between ANCF finite elements in the case of some mechanical joints such as pin and spherical joints can be described using linear algebraic constraint equations that can be imposed at a preprocessing stage to eliminate the dependent variables. Furthermore, the FE element mesh developed using ANCF finite elements has a constant mass matrix and zero Coriolis and centrifugal forces. Since the mass matrix is constant, the ANCF large displacement Cholesky coordinates can be used to obtain an identity generalized inertia matrix for the FE mesh in which the elements can experience arbitrary relative rotations with respect to each other (Shabana, 1998). For articulated systems, the proposed procedure allows for treating a subsystem or the entire system using one FE mesh (one flexible body). Existing MBS algorithms are not designed to handle such a FE mesh since MBS components which are not rigidly connected are treated as separate bodies connected by joints governed by nonlinear algebraic equations. It is explained in this thesis how such a linear FE mesh can be developed.

Having nonlinear joint constraints is not the only problem with existing finite element formulations. Another problem, that might be more serious, is the geometry description used which cannot be exactly converted to the geometry developed by computational geometry methods such as B-spline and NURBS (**N**on-**U**niform **R**ational **B**-**S**plines) representations. This fact has motivated researchers in the computational mechanics community to adopt the methods

of computational geometry as analysis tools instead of using conventional FE formulations. While the methods of computational geometry, such as B-spline, have several desirable analysis features; these methods have serious limitations when used as analysis tools. The B-spline recurrence formula and the rigid definition of the knot vector make B-spline less attractive as compared to the *absolute nodal coordinate formulation* (ANCF) geometry description. While B-spline geometry can always be converted exactly to ANCF geometry (Piegl and Tiller, 1997, Sanborn and Shabana, 2009; Lan and Shabana, 2010; Mikkola et al, 2013), the converse is not always true. ANCF geometry does not restrict the order of the parameters or the number of basis functions used in the interpolating polynomials. This advantage, as will be demonstrated in the thesis, allows for developing finite elements with fewer degrees of freedom as compared to those developed using the B-spline geometry.
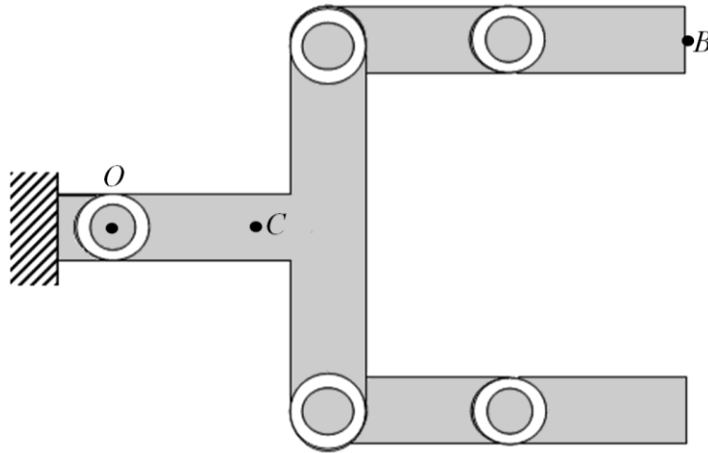
Figure 6 Structural and non-structural discontinuities

Another fundamental difference between B-spline and ANCF geometric descriptions lies in modeling discontinuities. Figure 6 shows a chain which has a structural discontinuity at point C and non-structural discontinuity at point O. At the junction at C, only deformation degrees of freedom are allowed, while at point O, relative rigid body rotation is permitted. Nonetheless,

7

the degree of continuity at both points is C^0. B-spline can be used as an analysis tool to describe the non-structural C^0 discontinuity at point O, but because of its rigid recurrence structure and the definition of its knot vector and knot multiplicity, B-spline cannot be used in the motion analysis of structural C^0 continuity at point C since B-spline C^0 description leads to a rigid body mode; that is, the elimination of one control point by reducing the knot multiplicity by one is not sufficient for eliminating the modes of rigid body rotations between two B-spline segments. ANCF geometry, on the other hand, can be used in the analysis of both structural and non-structural discontinuities (Hamed et al., 2011; Shabana et al, 2012).

Important multibody system (MBS) applications that can be used to shed light on the fundamental differences between B-spline and ANCF geometries are chain applications. Chains are highly nonlinear systems that are subjected to repeated impulse forces during their functional use. Geometric nonlinearities are the result of the large relative displacements between the chain links. The repeated impulsive forces as the result of the chain link contact with the rollers and other system components introduce high frequencies to the nonlinear chain dynamic model. For these reasons, the nonlinear dynamic analysis of chain systems represents one of the most challenging computational problems. In fact the simplest rigid-link chains are highly nonlinear because of the large relative rotations between the chain links (Roberson and Schwertassek, 1988; Schiehlen, 1997). In the case of rigid-link chains, the geometric nonlinearities that result from these rotations lead to highly nonlinear chain inertia forces that include the quadratic velocity Coriolis and centrifugal forces. Furthermore, the contact between the rigid-chain links and the sprockets and rollers that may exist in the system is often described using compliant force models; leading to high frequencies that require the use of very small time integration step

in order to accurately capture the changes in the velocities, accelerations, and forces. For these reasons, efficient and accurate modeling of chain systems remains a challenging MBS computational problem even in the simpler case in which the chain links are assumed to be rigid. Because of the geometric nonlinearities and the high frequencies, it is important to use an efficient solution algorithm if the flexibility of the chain links is considered. Flexible-link chains require the use of significantly larger number of degrees of freedom in order to capture the link deformation modes. Some of these deformation modes may also introduce high frequencies in addition to the high frequencies resulting from the contact between the chain links and rollers as well as other components in the system. It is also important in some applications to capture certain coupled deformation modes that cannot be captured using conventional structural finite elements such as beams and plates that are based on simplified kinematic assumptions. For example, in tracked vehicle applications, the chain links are subjected to significant tensile and compressive forces. The coupling between the deformation of the link cross section and other modes of deformation can be significant and must be taken into account in order to develop a more realistic model. It is, therefore, important to employ FE formulation that captures the effect of these coupled deformation modes and allows for an efficient MBS implementation. As mentioned earlier, ANCF finite elements are used in the thesis to develop new FE meshes for chain applications. In these FE meshes, the flexible-link pin joints are defined using linear connectivity conditions despite the large relative rotation allowed between the chain links. This leads to an efficient elimination of the dependent variables at a preprocessing stage. Furthermore, the use of the linear connectivity conditions with ANCF finite elements leads to a constant chain inertia matrix and zero Coriolis and centrifugal forces. It is demonstrated for the first time that a three-dimensional flexible-link chain model that is based on linear connectivity conditions and

9

has a constant mass matrix and zero Coriolis and centrifugal forces can be developed using spatial fully parameterized ANCF finite elements.

The use of The ANCF formulation comes at the expense of having more complex elastic force expressions. It is for this reason that many investigations have been devoted to proposing new and analyzing existing elastic force models aimed at the precise and efficient description of beams, plates, shells, and solid elements. Earlier works on ANCF beams dealt with continuum mechanics (CM) (Omar and Shabana, 2001; Yakoub and Shabana, 2001) and elastic line (EL) formulations (Hussein et al, 2007; Dmitrochenko et al, 2009; Schwab and Meijaard, 2010). The study of beams using continuum mechanics is computationally expensive due to the fact that it demands a three-dimensional numerical integration and includes some higher-frequency modes of deformation that are not always significant in the application under consideration. A simplification of three-dimensional continuum mechanics formulations became popular with application to ANCF (Schwab and Meijaard, 2005; Hussein et al, 2007; Dmitrochenko et al, 2009; Schwab and Meijaard, 2010). The use of the absolute coordinates to define Green-Lagrange strains and curvatures is the basis for what is called the elastic line approach. In this method, strain components are defined on of the beam centerline, while the curvature expression is used to define the bending strains. The elastic line was proved to offer good results and lower the computation time significantly. In addition, several successful attempts using variational principles to match the EL beam dynamics with existing finite-element formulations were documented in the literature (Schwab and Meijaard, 2005; 2010). Other force models based on Euler-Bernoulli beam theory were also introduced in the literature (Berzeri et al, 2001; Gerstmayr and Shabana, 2006; Gerstmayr and Irschik, 2008; Hamed et al, 2014). A simple force model, which can be used in the analysis of small deformation based on a three-dimensional

ANCF Euler-Bernoulli beam is introduced. The developed force model accounts for the coupling between bending and axial deformations. The model can be considered as a generalization of the two-dimensional force model developed by Berzeri et al (2001). Despite the simplicity of the proposed force model, it accounts for the elastic nonlinearity in the strain-displacement relationship. The new simplified force model is verified by comparing its results with the results obtained using more general elastic force formulations. It is shown that the new force model is very efficient compared to the continuum mechanics and elastic line approaches. However, it is important to mention that the proposed force model can be only used in the small deformation analysis and it does not consider shear and cross section deformations.

1.1. Scope and Organization of the Thesis

This thesis is organized in six chapters including this introductory chapter. In this section, the organization and scope of the thesis as well as a summary of the contents and contributions of its chapters are presented.

Chapter 2 explains how the linear FE meshes can be developed for planar applications. It starts by discussing the nonlinearities of the large rotation constraints in existing FE algorithms and computer codes. After which, the concept of knot multiplicity used in computational dynamics is discussed. The chapter then introduces how the ANCF formulation can be used to model both structural and nonstructural discontinuities using linear constraints. It is also shown that higher degrees of continuity can be applied between the ANCF elements using linear constraint equations. The main contributions of this chapter can be summarized as follows:

1. It is demonstrated that the concept of the *knot multiplicity* used in computational geometry methods can be used with ANCF finite elements to model plannar pin joints.

11

The conclusions made are not applicable only to pin joints, but apply to both structural and non-structural discontinuities. This general approach will allow for developing different types of joints with different degrees of continuity, including C^0 continuity that allows for relative rigid body rotation. This general approach will allow developing joints in which coordinates of the same types (such as gradient vectors) are subjected to different continuity conditions.

2. The deformation modes resulting from imposing lower degree of continuity using ANCF finite elements will be discussed. Numerical results will be presented to demonstrate how these deformation modes can be captured using ANCF finite elements. These deformation modes were not discussed in the work of Garcia-Vallejo et al. (2003) which was focused on planar pin joint only.

3. This chapter also demonstrates that T-junctions, which represent a special case of structural discontinuity, can be modeled using ANCF finite elements. It is shown, with an example, that one model can include T-junction representing special case of structural discontinuity and pin joints representing non-structural discontinuities.

Chapter 3 introduces a generalization of the proposed plannar joint formulation to the spatial analysis. It is shown that the constraints equations of the spherical and revolute (pin) joints will remain linear in the spatial analysis. This chapter also examines the limitations of using B-spline representation as an analysis tool by comparing its geometry with the nonlinear finite element *absolute nodal coordinate formulation* (ANCF) geometry. The chapter starts by explaining how surfaces can be defined in B-spline representation. This introduction is followed by a discussion of the limitations of using B-spline representation as analysis tool in comparison

12

with ANCF analysis. The proposed linear meshes which can be used in modeling structural and nonstructural discontinuities are also introduced in this chapter which ends with a numerical results section, in which, belt and chain drives are used to demonstrate the use of the formulations developed. The main contributions of this chapter can be summarized as follows.

1. The chapter addresses the important issue of using computational geometry methods such as B-spline and NURBS as analysis tools. As demonstrated in this thesis, the B-spline recurrence formula has several drawbacks when used as an analysis tool. This fact is used to demonstrate the generality of the ANCF geometry.

2. This chapter also presents a new three-dimensional continuum based pin joint model that leads to linear connectivity conditions and constant mass matrix when used with ANCF finite elements. The proposed new class of ideal joints account for the distributed inertia and elasticity at the joint definition point. Additional degrees of freedom are introduced in order to capture modes of deformation that cannot be captured using existing formulations that employ rigid triads or unit vectors to formulate the joint equations.

Chapter 4 continues discussing the limitations of using B-spline surfaces as analysis tool (Iso-geometric analysis) in comparison to the absolute nodal coordinate formulation (ANCF). The limitations are discussed by extensively examining the new class of ideal compliant joints which accounts for the distributed inertia and elasticity. This is demonstrated using a heavily constrained tracked vehicle with flexible link chains. Without using the proposed approach, modeling such a complex system with flexible links can be very challenging. The analysis presented in this chapter also demonstrates that adding significant model details does not necessarily imply increasing the complexity of the MBS algorithm. The chapter starts with a

brief introduction about different multibody finite element formulations and a brief literature review of the tracked vehicle multibody models. This is followed by a discussion about modeling different types of discontinuities in multibody system analysis. This section explains the differences of the computational algorithms used in simulation of ANCF chains when linear and nonlinear constraints are used. The chapter then expands on the discussion of the linear compliant joints by introducing linear pin joint model that can be used with the Euler-Bernoulli beam element. It also proposes a new sliding joint model that employs a set of linear and simple nonlinear constraints. The proposed sliding joint model is used, accompanied with other factors, to show the generality of using ANCF as analysis tool in comparison to Iso-geometric analysis. Later on, the reasons why ANCF is the educated choice, when modeling small deformation flexible link tracked vehicle, are discussed. A simplified Euler-Bernoulli visco-elastic force model that accounts for the coupling between axial and bending deformation is proposed. The chapter ends with a numerical results section, in which heavily constrained tracked vehicle models are used to demonstrate the use of the formulations developed. The main contributions of this chapter can be summarized as follows.

1. It is shown that when the ideal compliant joints developed are used, linear connectivity conditions are used to eliminate the dependent variables at a preprocessing stage. Hence, the constraint equations are automatically satisfied at the position, velocity, and acceleration levels. Therefore, when using the proposed approach to model large scale chain systems, differences in computational efficiency between the augmented formulation and the recursive methods are eliminated, and the CPU times resulting from the use of the two formulations become similar regardless of the complexity of the system.

2. Furthermore, the elimination of the joint constraint equations and the associated dependent variables contribute to the solution of a fundamental singularity problem encountered in the analysis of closed loop chains and mechanisms. It is known that in the case of closed loop chains and mechanisms, the set of independent coordinates must be repeatedly changed in order to avoid singularity of the constraint Jacobian matrix (Nakanishi and Shabana, 1994). This problem can be avoided by using the new ANCF finite element meshes that allow for the elimination of the constraint equations and the dependent variables at a preprocessing stage.

3. While small deformation MBS problems can be effectively solved using the FFR approach that allows for filtering out high frequency contents, there are small deformation problems that can be solved more efficiently using large deformation formulation such as the absolute nodal coordinate formulation (ANCF). In these small deformation problems, the inclusion of high frequency modes may be necessary. An example of these problems is a flexible-link chain of a tracked vehicle where each link is modeled using one finite element only. The use of ANCF finite elements can be advantageous as compared to the use of the FFR formulation.

4. The necessity of using the new concepts developed in modeling complex systems is demonstrated using a heavily constrained tracked vehicle with flexible-link chains. Without using the proposed approach modeling such a complex system with flexible links can be very challenging.

5. In order to efficiently simulate the complex tracked vehicle model, a simplified force model, which can be used in the analysis of small deformation based on a three-dimensional ANCF Euler-Bernoulli beam, is introduced. The developed force model

15

accounts for the coupling between bending and axial deformations. The model can be considered as a generalization of the two-dimensional force model developed by Berzeri et al (2001).

A verification of the proposed Euler-Bernoulli elastic force model is introduced in **Chapter 5**. The force model is verified by comparing its results to both the continuum mechanics and elastic line approaches. It is shown that the new elastic force model is very efficient compared to the other force models. The chapter starts by briefly explaining the continuum mechanics and elastic line force formulation approaches. The main differences between the proposed Euler-Bernoulli force model and the other force models are also explained. The chapter ends with a numerical results section, in which, heavily constrained tracked vehicle models are used in the verification of the elastic force model.

The thesis ends with **Chapter 6,** which gives summary of and conclusions drawn from this thesis.

CHAPTER 2

CONCEPTS OF LINEAR ANCF JOINTS

Materials presented in this chapter are taken from "Hamed, A.M., Shabana, A.A, Jayakumar, P., Letherwood, D.M.: Non-structural Geometric Discontinuities in Finite Element/Multi-body System Analysis. Journal of Nonlinear Dynamics, 2011." Please refer to Appendix A for copyright transfer.

Existing multibody system (MBS) algorithms treat articulated system components that are not rigidly connected as separate bodies connected by joints that are governed by nonlinear algebraic equations. As a consequence, these MBS algorithms lead to a highly nonlinear system of coupled differential and algebraic equations. Existing finite element (FE) algorithms, on the other hand, do not lead to a constant mesh inertia matrix in the case of arbitrarily large relative rigid body rotations. In this chapter, planner FE/MBS meshes that employ linear connectivity conditions and allow for arbitrarily large rigid body displacements between the finite elements are introduced. The large displacement FE *absolute nodal coordinate formulation* (ANCF) is used to obtain linear element connectivity conditions in the case of large relative rotations between the finite elements of a mesh. It is shown in this chapter that a linear formulation of plannar pin (revolute) joints that allow for finite relative rotations between the connected elements can be systematically obtained using ANCF finite elements. The algebraic joint constraint equations, which can be introduced at a preprocessing stage to efficiently eliminate redundant position coordinates, allow for deformation modes at the pin joint definition point, and therefore, this new joint formulation can be considered as a generalization of the pin joint formulation used in rigid MBS analysis. The new pin joint deformation modes, that are the results of C^0 continuity conditions, allow for the calculations of the pin joint strains which can be discontinuous as the result of the finite relative rotation between the elements. This type of

discontinuity is referred to in this thesis as *non-structural discontinuity* in order to distinguish it from the case of *structural discontinuity* in which the elements are rigidly connected. Because ANCF finite elements lead to a constant mass matrix, an identity generalized mass matrix can be obtained for the FE mesh despite the fact that the finite elements of the mesh are not rigidly connected. The relationship between the non-rational ANCF finite elements and the B-spline representation is used in this chapter to shed light on the potential of using ANCF as the basis for the integration of computer aided design and analysis (ICADA). When cubic interpolation is used in the FE/ANCF representation, C^0 continuity is equivalent to a knot multiplicity of three when computational geometry methods such as B-splines are used. Nonetheless, B-spline and NURBS representations cannot be used to effectively model T-junctions that can be systematically modeled using ANCF finite elements that employ gradient coordinates that can be conveniently used to define element orientations in the reference configuration. Numerical results are presented in order to demonstrate the use of the new formulation in developing new chain models.

2.1. <u>Large Rotation Nonlinearities</u>

Existing FE algorithms and computer codes allow for developing meshes in which the finite elements are rigidly connected. In the case of arbitrarily large relative rigid body rotations between the finite elements of one mesh, incremental solution procedure based on a co-rotational formulation is used. This FE solution procedure leads to a highly nonlinear inertia matrix and due to the nature of the incremental approach used and the set of coordinates employed, existing FE algorithms and computer programs are not suited for the analysis of complex multibody systems that are characterized by geometric nonlinearities that result from the independent rigid

body rotations of the finite elements. In most formulations, including rigid body dynamics formulations, such non-structural geometric discontinuities are governed by nonlinear algebraic constraint equations which lead to highly nonlinear inertia matrix. For such articulated systems, components which are not rigidly connected are treated as separate bodies when MBS algorithms are used. Consider, for example, the simple planar double-pendulum example shown in Fig. 7.
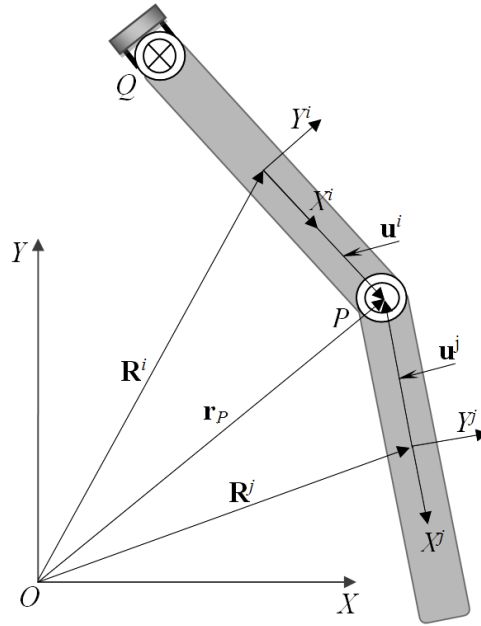
Figure 7 Double pendulum example

The pendulum consists of two rigid bodies, i and j, connected by a pin (revolute) joint at point P whose local position vector is defined in the two body coordinate systems by the vectors $\bar{\mathbf{u}}_P^i$ and $\bar{\mathbf{u}}_P^j$, respectively. The global position vector of this point in terms of the coordinates of bodies i and j are denoted as $\mathbf{r}_P^i$ and $\mathbf{r}_P^j$, respectively. In this simple planar rigid

body example, the kinematic constraint conditions of the pin joint can be written as $\mathbf{r}_P^i = \mathbf{r}_P^j$. This

equation can be written more explicitly in terms of the coordinates of bodies i and j as

$$\mathbf{R}^i + \mathbf{A}^i \bar{\mathbf{u}}_P^i = \mathbf{R}^j + \mathbf{A}^j \bar{\mathbf{u}}_P^j \tag{2.1}$$

where $\mathbf{R}^i$ and $\mathbf{R}^j$ define the global position vector of the origins of the coordinates systems of

the two bodies, and $\mathbf{A}^i$ and $\mathbf{A}^j$ are the transformation matrices that define the orientations of the

two bodies. In the planar analysis, the vectors and matrices that appear in Eq. 2.1 can be written

as

$$
\left.
\begin{aligned}
&\bar{\mathbf{u}}_P^k = [\bar{x}^k \quad \bar{y}^k], \qquad \mathbf{R}^k = [R_x^k \quad R_y^k] \\
&\mathbf{A}^k = \begin{bmatrix} \cos(\theta^k) & -\sin(\theta^k) \\ \sin(\theta^k) & \cos(\theta^k) \end{bmatrix}, \quad k = i, j
\end{aligned}
\right\} \tag{2.2}
$$

The geometric nonlinearities of the connectivity conditions of Eq. 2.1 characterize all

MBS formulations including the augmented and embedding techniques. In the augmented

formulation, the technique of Lagrange multipliers is used to adjoin the nonlinear constraint

equations to the dynamic equations of motion. The resulting coupled system of

differential/algebraic equations is highly nonlinear. In the embedding technique, on the other

hand, redundant coordinates are systematically eliminated using the nonlinear algebraic

constraint equations. Using the embedding technique, one can show that the two equations of

motion of the planar rigid body double pendulum shown in Fig. 7 can be written as

$$
\left.
\begin{aligned}
&\left(m^i (l^i)^2 + J^i + m^j (l^i)^2 \right) \ddot{\theta}^i + \left(2m^j l^i l^j \cos \theta^{ij} \right) \ddot{\theta}^j = \\
&\qquad - 2m^i g l^i \cos \theta^i - m^j g l^i \cos \theta^i - 2m^j l^i l^j \left(\dot{\theta}^j \right)^2 \sin \theta^{ij} \\
&\left(2m^j l^i l^j \cos \theta^{ij} \right) \ddot{\theta}^i + \left(m^j (l^j)^2 + J^j \right) \ddot{\theta}^j = \\
&\qquad - 2m^j g l^j \cos \theta^j + m^j l^i l^j \left(\dot{\theta}^i \right)^2 \sin \theta^{ij}
\end{aligned}
\right\} \tag{2.3}
$$

20

In this equation, m^k and l^k are, respectively, the mass and length of link k, $k = i, j$; $\ddot{\theta}^k$ is the angular acceleration of link k; $\theta^{ij} = \theta^i - \theta^j$; and g is the gravity constant. It is clear from Eq. 2.3 that the equations of motion for a simple planar rigid body double pendulum are highly nonlinear as the result of the nonlinear connectivity conditions. The resulting inertia coefficients are also highly nonlinear because of the geometric nonlinearities that result from the non-structural discontinuities. Such non-structural geometric discontinuities also lead to more geometric nonlinearities when the deformation of the links are considered using the FE/FFR formulation due to the dynamic coupling between the reference motion and the elastic deformations. In the FFR formulation, $\bar{\mathbf{u}}_P^k$ is expressed in terms of the elastic coordinates and the number of equations of motion increases by the number of these elastic coordinates.

2.2. <u>Computational Geometry and Knot Multiplicity</u>

The pin joint connectivity conditions used in the preceding section ensure C^0 continuity that allows for non-structural discontinuity due to the relative rotation. This non-structural discontinuity can be converted to structural discontinuity by imposing a constraint on the relative rotation between the two links. The degree of continuity in computational geometry methods is controlled using the concept of *knot multiplicity*. For example, in B-spline representation, any curve can be represented as a combination of several polynomial segments. Generally, B-spline curves can be defined using following equation (Piegl and Tiller, 1997):

$$\mathbf{r}(u) = N_{0,p}(u)\mathbf{P}_0 + N_{1,p}(u)\mathbf{P}_1 + \ldots\ldots + N_{n,p}(u)\mathbf{P}_n = \sum_{i=0}^{n} N_{i,p}(u)\mathbf{P}_i \qquad (2.4)$$

where $N_{i,p}(u)$ are the B-spline basis functions of degree p, u is the parameter, and $\mathbf{P}_i$ are the control points that define the control polygon. The basis functions can be defined as

21

$$N_{i,0}(u) = \begin{cases} 1 & \text{if } u_i \le u < u_{i+1} \\ 0 & \text{otherwise} \end{cases}$$

$$N_{i,j}(u) = \frac{u - u_i}{u_{i+j} - u_i} N_{i,j-1}(u) + \frac{u_{i+j+1} - u}{u_{i+j+1} - u_{i+1}} N_{i+1,j-1}(u) \tag{2.5}$$

where $u_i \le u_{i+1}$, and $\mathbf{U} = \{ u_0 \ u_1 \ .... u_{n+p+1} \}$ is called the *knot vector*. The elements of the knot

vector need not be distinct. Each nonzero span corresponds to a B-spline segment defined by two

knot points called in this case *breakpoints* that represent distinct knot values. The number of

equal knots at a point is referred to as the knot multiplicity. If the vector $\mathbf{U}$ takes the form

$\left\{ \underbrace{0....0}_{p+1} \ \underbrace{1....1}_{p+1} \right\}$, the B-spline reduces to a *p*-order Bezier curve, and therefore, Bezier curve can be

considered as a special case of B-spline. One may consider the knot multiplicity as a measure of

the degree of continuity. For example, in case of cubic B-spline curve ($p = 3$), one can always

define, at each knot point, the vectors $\mathbf{r}, \partial\mathbf{r}/\partial u, \partial^2\mathbf{r}/\partial u^2$, and $\partial^3\mathbf{r}/\partial u^3$. A knot multiplicity of

four at a knot point implies C^{-1} continuity, that is, the two segments at this point are not

connected and the coordinates and derivatives are discontinuous. A knot multiplicity of three

implies C^0 and only the vector $\mathbf{r}$ is continuous at that point. This is equivalent to imposing a set

of constraints similar to the pin joint constraints that allow for the elimination of one control

point and reducing the problem dimension. A knot multiplicity of two (C^1 continuity) ensures

that $\mathbf{r}$ and $\partial\mathbf{r}/\partial u$ are continuous at this point. This condition is equivalent to eliminating two

control points. A knot multiplicity of one (C^2 continuity) ensures the continuity of $\mathbf{r}, \partial\mathbf{r}/\partial u$, and

$\partial^2\mathbf{r}/\partial u^2$. Finally, knot multiplicity of zero in case of cubic polynomials ($p = 3$) implies

continuity of all the derivatives, and in this special case, two segments blend together forming

22

one larger segment. Note that the B-spline description is fundamentally different from the FE description since control points do not, in general, represent material points.

2.3. <u>ANCF Finite Elements and Derivative Continuity</u>

B-spline geometry can be converted to ANCF representation using a linear coordinate transformation. Nonetheless, the use of the gradients as nodal coordinates in the ANCF representation allows for defining element orientations and preserves the control point polygon structure when the mesh deforms. In the case of structural discontinuity, different coordinate lines can be systematically used with the ANCF representation, thereby allowing for modeling T and V junctions systematically. The standard ANCF assembly process ensures continuity of both position and gradient coordinates when two finite elements are rigidly connected. This is equivalent to a knot multiplicity of two in the cubic B-spline representation. Continuity of curvature and its derivative in B-Spline curves can be achieved by using knot multiplicity of one and zero, respectively. This degree of continuity can also be achieved in the ANCF representation using algebraic constraint equations that eliminate some nodal variables and reduce the model dimension. In order to demonstrate the use of ANCF finite elements in the formulation of linear connectivity conditions that ensure the continuity of higher derivatives, the planar two-node shear deformable beam element is used. Each of the element nodes has six degrees of freedom; two translational coordinates defined by the two-dimensional vector $\mathbf{r} = \begin{bmatrix} r_1 & r_2 \end{bmatrix}^T$, and four gradient coordinates defined by the two vectors $\mathbf{r}_x = \begin{bmatrix} r_{x1} & r_{x2} \end{bmatrix}^T$ and $\mathbf{r}_y = \begin{bmatrix} r_{y1} & r_{y2} \end{bmatrix}^T$. The vector of nodal coordinates $\mathbf{e}$ can then be written as

$$\mathbf{e} = \begin{bmatrix} \mathbf{r}^{AT} & \mathbf{r}_x^{AT} & \mathbf{r}_y^{AT} & \mathbf{r}^{BT} & \mathbf{r}_x^{BT} & \mathbf{r}_y^{BT} \end{bmatrix}^T$$

(2.6)

23

In this equation, A and B refer to the end points of the finite element. Using this vector of nodal coordinates, the ANCF displacement field is defined as

$$\mathbf{r}(x,y) = \mathbf{S}(x,y)\mathbf{e}(t) \tag{2.7}$$

where $\mathbf{S}$ is the element shape function matrix defined for the planar shear deformable element as

$$\mathbf{S} = \begin{bmatrix} s_1\mathbf{I} & s_2\mathbf{I} & s_3\mathbf{I} & s_4\mathbf{I} & s_5\mathbf{I} & s_6\mathbf{I} \end{bmatrix} \tag{2.8}$$

In this equation, $\mathbf{I}$ is the identity matrix, and $s_i, i = 1, 2, \ldots, 6$ are shape functions defined as

$$\left. \begin{aligned} s_1 &= 1 - 3\xi^2 + 2\xi^3, \quad s_2 = l\left(\xi - 2\xi^2 + \xi^3\right), \quad s_3 = l\eta\left(1 - \xi\right), \\ s_4 &= 3\xi^2 - 2\xi^3, \quad s_5 = l\left(-\xi^2 + \xi^3\right), \quad s_6 = l\xi\eta \end{aligned} \right\} \tag{2.9}$$

where l is the element length, $\xi = \dfrac{x}{l}$, and $\eta = \dfrac{y}{l}$.

Structural discontinuities can be systematically modeled using ANCF finite elements by using the proper gradient transformations. The gradient transformations, which are different from vector transformations, enter into the formulation of the element dynamic equations. Furthermore, constraints on higher derivatives can also be imposed at a preprocessing stage using linear algebraic equations; allowing for having a higher degree of continuity. For example, one can define the second derivative of the position vector at the two nodes of the element as

$$\left. \begin{aligned} \mathbf{r}_{xx}^{i-1,B} &= 6\left(\frac{1}{l^{i-1}}\right)^2 \mathbf{r}^{i-1,A} + 2\left(\frac{1}{l^{i-1}}\right)\mathbf{r}_x^{i-1,A} - 6\left(\frac{1}{l^{i-1}}\right)^2 \mathbf{r}^{i-1,B} + 4\left(\frac{1}{l^{i-1}}\right)\mathbf{r}_x^{i-1,B} \\ \mathbf{r}_{xx}^{i,A} &= -6\left(\frac{1}{l^i}\right)^2 \mathbf{r}^{i,A} - 4\left(\frac{1}{l^i}\right)\mathbf{r}_x^{i,A} + 6\left(\frac{1}{l^i}\right)^2 \mathbf{r}^{i,B} - 2\left(\frac{1}{l^i}\right)\mathbf{r}_x^{i,B} \end{aligned} \right\} \tag{2.10}$$

These equations can be used to develop linear constraint relationships that eliminate the gradient vector $\mathbf{r}_x$ at the interface of two elements. This is equivalent to reducing the number of independent B-spline control points by one, or equivalently decreasing the knot multiplicity by

24

one. Similarly, continuity conditions for the third derivative of the position vector can be achieved by equating $\partial^3 \mathbf{r} / \partial x^3$ at the node connecting two finite elements. In this case, since a cubic polynomial is used, the two elements blend together forming one longer finite element.

2.4. <u>Structural and Non-structural Discontinuities</u>

As previously mentioned, in the structural FE meshes developed using existing computer codes, the structural finite elements such as beams, plates and shells are assumed to be rigidly connected. That is, the finite elements are not allowed to have independent large relative rigid body displacements with respect to each other. This is mainly due to the fact that in most FE and rigid body dynamics formulations, relative rotations are source of geometric nonlinearities as explained in Section 2.1 using a simple planar double pendulum example. Relative rigid body rotations between the elements in a FE mesh lead to non-structural discontinuities since the gradients at the interface node are not continuous. Most existing formulations cannot be used to obtain linear connectivity conditions in the case of non-structural discontinuities. Nonetheless, ANCF finite elements allow for developing a kinematically linear mesh in which each finite element can have arbitrarily independent rotation. In ANCF/FE meshes, the element connectivity conditions in the case of non-structural discontinuities are formulated using linear algebraic constraint equations. This is an important ANCF feature since it can significantly reduce the number of nonlinear algebraic constraint equations and the associated Lagrange multipliers in many MBS applications including tracked vehicles. The development of such a kinematically linear ANCF mesh is demonstrated in this section using the pin joint as an example. The resulting modes of deformations of the new joint are also discussed in this section.

25

2.4.1. <u>Joint Formulation</u>

When two ANCF finite elements are connected by a pin joint, one has C^0 continuity that ensures only the continuity of the position coordinates. The two finite elements can have arbitrarily large rigid body rotation with respect to each other. In the case of a planar pin joint between two finite elements i and j, the algebraic joint constraint equations can be written as

$$\mathbf{r}^{i,A} = \mathbf{r}^{j,B} \tag{2.11}$$

where A and B refer to the joint node on the finite elements i and j, respectively. The preceding constraint equations eliminate the relative translation between the two finite elements. However, since ANCF structural finite elements can correctly describe arbitrary rigid body rotations, applying the linear algebraic equations of Eq. 2.11 at a preprocessing stage allows for developing a FE mesh in which each finite element can have an independent rotational displacement. Note that, while the pin joint constraints in the case of rigid body dynamics are highly nonlinear as demonstrated in Section 2.1, the ANCF pin joint constraints defined by Eq. 2.11 are linear. It will be shown in later chapters that similar linear equations can be developed for the spherical joint in the spatial analysis. Also, linear algebraic equations can be obtained for the spatial pin joint using ANCF finite elements by requiring two points on the two elements to coincide and two gradient vectors on the two elements to remain parallel and equal in magnitude.

2.4.2. <u>Deformation Modes</u>

The ANCF pin joint allows deformation modes at the joint definition point. The gradient vectors of the two elements can change their magnitude and orientation allowing for stretch and shear deformations at the joint node. Furthermore, when the fully parameterized beam element presented in the preceding section is used, the change in the cross section due to deformation can

be captured at the joint node. Because of the non-structural discontinuity, the strain field is not continuous. The modes of deformations at the joint nodes can be examined using the Green-Lagrange Strain tensor $\boldsymbol{\varepsilon}$ which can be written as

$$\boldsymbol{\varepsilon} = \frac{1}{2}\left(\mathbf{J}^{\mathbf{T}}\mathbf{J} - \mathbf{I}\right) \tag{2.12}$$

where $\mathbf{J}$ is the matrix of position vector gradients, and $\mathbf{I}$ is the identity matrix. Because the strain tensor $\boldsymbol{\varepsilon}$ is symmetric, one can define the strain vector $\boldsymbol{\varepsilon}_v = \begin{bmatrix} \varepsilon_{xx} & \varepsilon_{yy} & \varepsilon_{xy} \end{bmatrix}^{\mathbf{T}}$, where ε_{xx}, ε_{yy} and ε_{xy} are, respectively, the normal strain in the x direction, the normal strain in the y direction, and the shear strain. These strains components are defined in terms of the gradients as follows:

$$\varepsilon_{xx} = \frac{1}{2}\left(\mathbf{r}_x^{\mathbf{T}}\mathbf{r}_x - 1\right), \quad \varepsilon_{yy} = \frac{1}{2}\left(\mathbf{r}_y^{\mathbf{T}}\mathbf{r}_y - 1\right), \quad \varepsilon_{xy} = \frac{1}{2}\mathbf{r}_x^{\mathbf{T}}\mathbf{r}_y \tag{2.13}$$

These strain components are continuous inside the element and discontinuous at the joint nodes because of the discontinuity of the position vector gradients at these nodes.

The cross section deformation at the joint nodes can be captured using Nanson's formula which can be written as follows (Ogden, 1984; Shabana, 2008; Hussein et al., 2009):

$$ds = \frac{J}{\left(\mathbf{n}_n^{\mathbf{T}}\mathbf{J}\mathbf{J}^{\mathbf{T}}\mathbf{n}_n\right)^{\frac{1}{2}}} dS \tag{2.14}$$

In this equation, S and s are, respectively, the cross section area in the reference and current configurations, $\mathbf{n}_n$ is a unit vector in the direction normal to the cross section, and J is the determinant of the matrix of position vector gradients $\mathbf{J}$. In the case of the planar shear

27

deformable beam presented in the preceding section, one can show that Nanson's formula reduces to

$$ds = \left| \mathbf{r}_y \right| dS \tag{2.15}$$

Since the displacement gradients at the joint nodes are discontinuous, the preceding two equations show that the cross section areas of the two finite elements at the joint nodes can vary independently.

2.4.3. <u>Structural Discontinuities</u>

In the case of structural geometric discontinuities that include T- and V-junctions, rigid body displacements between the finite elements is not permitted. In this case, gradient transformations are used to assemble the finite elements of the flexible body mesh. Structural discontinuities can be modeled using fully parameterized and gradient deficient ANCF finite elements (Shabana, 2008). For both fully parameterized and gradient deficient ANCF finite elements, independent coordinate lines can always be defined and used to define the gradient transformation as described in the literature (Shabana and Mikkola, 2003; Shabana, 2010). In Section 2.6, a chain example that includes both structural and non-structural geometric discontinuities is presented. In this example, the entire chain system is described using one FE mesh.

2.5. <u>Equations of Motion</u>

The dynamic equations of motion of body i in a MBS can be written as follows (Roberson and Schwertassek, 1988; Schiehlen, 1997; Shabana, 1998):

$$\mathbf{M}^i \ddot{\mathbf{e}}^i + \mathbf{C}_\mathbf{e}^\mathrm{T} \boldsymbol{\lambda} = \mathbf{F}_e^i \tag{2.16}$$

where $\mathbf{M}^i$ and $\mathbf{F}_e^i$ are, respectively, the mass matrix and the generalized force vector that includes the nodal forces, $\mathbf{C}_e^T$ is the Jacobian matrix of the nonlinear kinematic constraint equations $\mathbf{C}(\mathbf{e},t) = \mathbf{0}$, $\boldsymbol{\lambda}$ is the vector of Lagrange multipliers, and $\ddot{\mathbf{e}}^i$ is the vector of ANCF nodal accelerations. Using ANCF finite elements, the mass matrix is constant, For an element k of the finite element mesh of body i, the mass matrix is defined as $\mathbf{M}^{ik} = \int_{V^{ik}} \rho^{ik} \, \mathbf{S}^{ik\mathbf{T}}\mathbf{S}^{ik} dV^{ik}$, where ρ^{ik} is the element density, V^{ik} is the element volume, and $\mathbf{S}^{ik}$ is the element shape function. Since the mass matrix of the ANCF finite elements is constant, the Coriolis and centrifugal force vector is identically equal to zero. As previously discussed, linear connectivity conditions between ANCF finite elements in the case of structural and non-structural discontinuities can be imposed during the finite element assembly process at a preprocessing stage. The use of this procedure allows for efficient elimination of the dependent nodal variables before the start of the dynamic simulation. Therefore, since joint constraints between ANCF finite elements are imposed at a preprocessing stage, these constraints are not included in the vector $\mathbf{C}(\mathbf{e},t) = \mathbf{0}$ which has only nonlinear constraint equations. If the body is not subjected to nonlinear constraint equations, the body equations of motion are defined as $\mathbf{M}^i\ddot{\mathbf{e}}^i = \mathbf{F}_e^i$. Furthermore, by using the large displacement ANCF Cholesky coordinates, one obtains an identity generalized mass matrix that leads to an optimum sparse matrix structure for the system dynamic equations. Therefore, a chain system, for example, in which the chain links can have independent rigid body displacements, can be represented by one FE mesh (one flexible body) in which the connectivity conditions are imposed at a preprocessing stage using linear algebraic equations. Such a FE mesh will have an identity inertia matrix if the large displacement ANCF

29

Cholesky coordinates are used. In fact, several chains can be represented by one FE mesh since ANCF finite elements correctly describe rigid body displacements, as previously mentioned.

2.6. Numerical Results

It will be demonstrated in this section that ANCF meshes that allow relative motion between the finite elements can be developed. In these ANCF meshes, the finite elements are connected using linear algebraic equations and the mesh mass matrix remains constant. Chain examples characterized by structural and non-structural discontinuities are considered. The links of the chains used are assumed to be flexible with mass density of 7200 kg/m^3, and a Poisson ratio of 0.3. Two different values of the modulus of elasticity, 2×10^8 and 2×10^{11} N/m^2, are used in the simulations. The elastic forces of the ANCF elements are formulated using a general continuum mechanics approach that employs a Hookean constitutive model. In all examples discussed in this section, the system is represented by one FE mesh (one flexible body).

2.6.1. Multi-Link Chain

Figure 8 shows a multi-link chain that has an overall length of 1 m. The chain consists of 8 links that are connected by pin joints. These pin joints ensure C^0 continuity and allow for independent relative rotations and deformation modes at the joint nodes. In computational geometry, this case of non-structural discontinuities at the joint nodes corresponds to knot multiplicity of 3 when cubic polynomials are used for the finite elements. Each link in this chain is represented by one planar shear deformable beam element. Therefore, the chain has 80 degrees of freedom; 8 degrees of freedom represent rigid body relative rotations, and the remaining 72 degrees of freedom represent deformation modes; with 9 deformation modes for each link. The chain is subjected to a base excitation defined by the function $X = -0.01\sin(0.1\pi t)$. All the

links of the chain are assumed to be initially horizontal. The effect of the link gravity is considered.
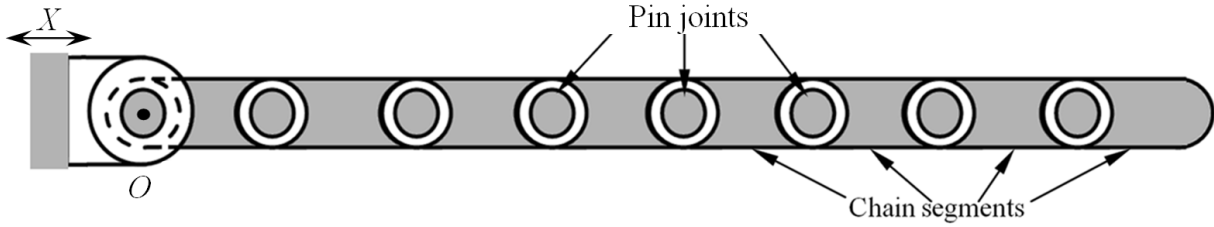
Figure 8 Eight-link chain system

In order to verify the obtained results, a simulation of a very stiff pendulum is carried out first, and the results are compared with the results of a rigid link chain model. For the very stiff chain, a modulus of elasticity of 2×10^{11} N/m^2 is used for the finite elements. Figure 9 shows the vertical position of the center of the last link as function of time for both cases of the rigid and stiff chains. Figure 10 shows the absolute rotation of the last link of the chain about an axis parallel to the pin joints axes. The results presented in Figs. 9 and 10 show a good agreement between the results obtained using the rigid and very stiff link chain models. For the rigid link chain model, nonlinear algebraic equations are used to define the pin joints and the resulting generalized mass matrix associated with the system degrees of freedom is highly nonlinear. For the flexible ANCF chain model, the chain is represented by one FE mesh (one flexible body), the pin joint constraints are linear, and the mass matrix is constant.
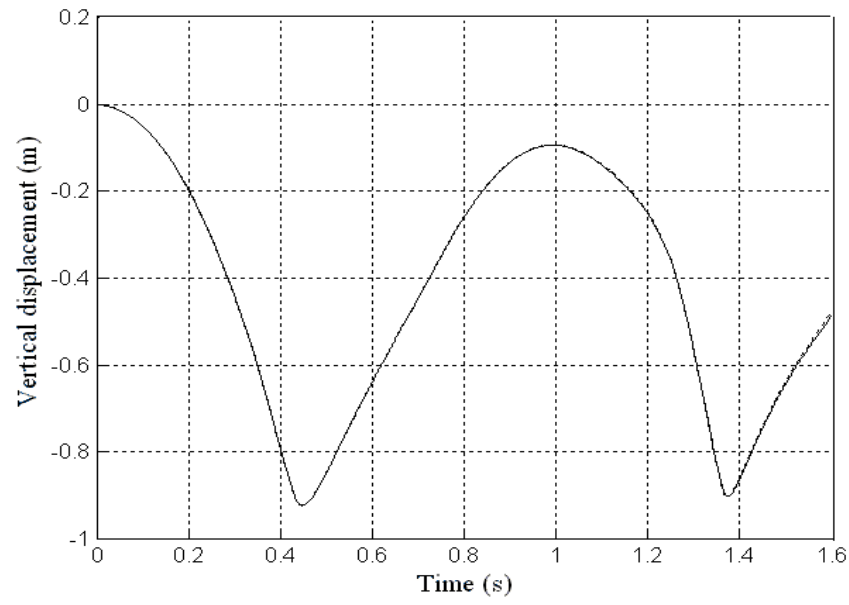
Figure 9 Vertical displacement of the center of link 8

(—— Flexible link chain, ---- Rigid link chain)
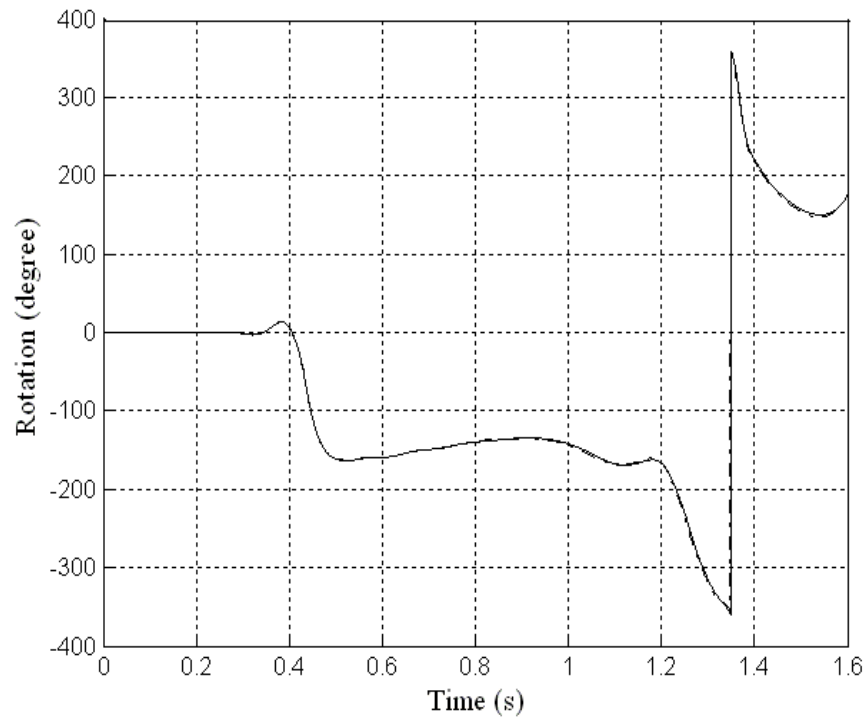
Figure 10 Rotation of link 8

(—— Flexible link chain, ---- Rigid link chain).

Figure 11 shows the vertical displacement of the tip point of link 8 of the chain when the modulus of elasticity is reduced to $2 \times 10^8 \text{ N/m}^2$. Figures 12 and 13 show the chain configurations at different time points. Figure 14 shows the relative rotation between links 7 and 8 of the flexible chain as function of time. Figures 15 and 16 show the distribution of the normal strain components ε_{xx} and ε_{yy}. It is clear from the results presented in these figures that the strains are discontinuous as the result of the non-structural discontinuities at the joints; the strains are continuous within the elements, and ε_{xx} decreases since the links at the beginning of the chain are subjected to higher gravity forces as compared to the links at the end of the chain. It is important, however, to point out that for fully parameterized ANCF finite elements, one can always define, at an arbitrary point inside the element, coordinate lines in which there are continuous strain components regardless of the shape of the structure.
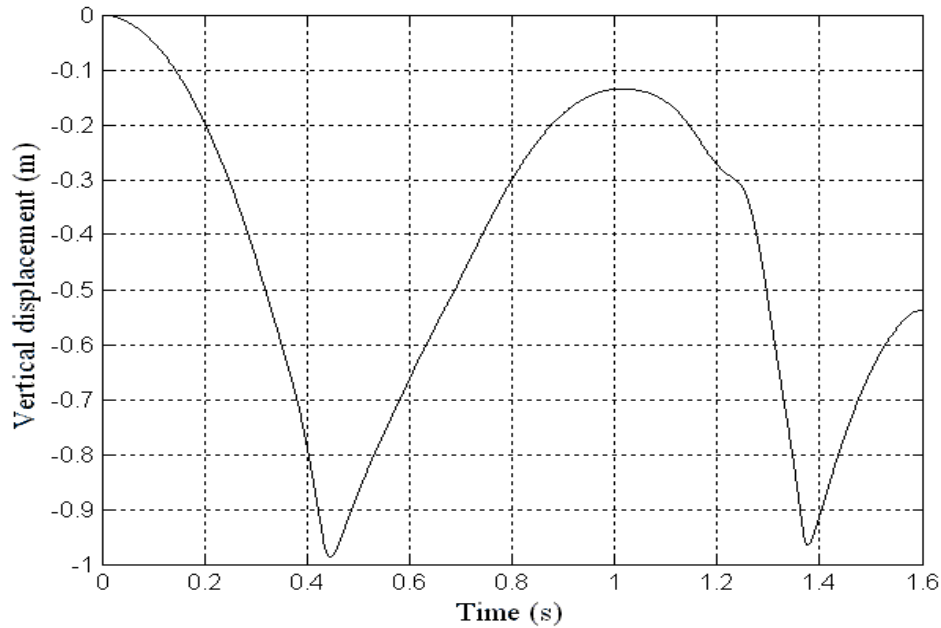
Figure 11 Vertical displacement of the tip point of link 8 of the flexible chain
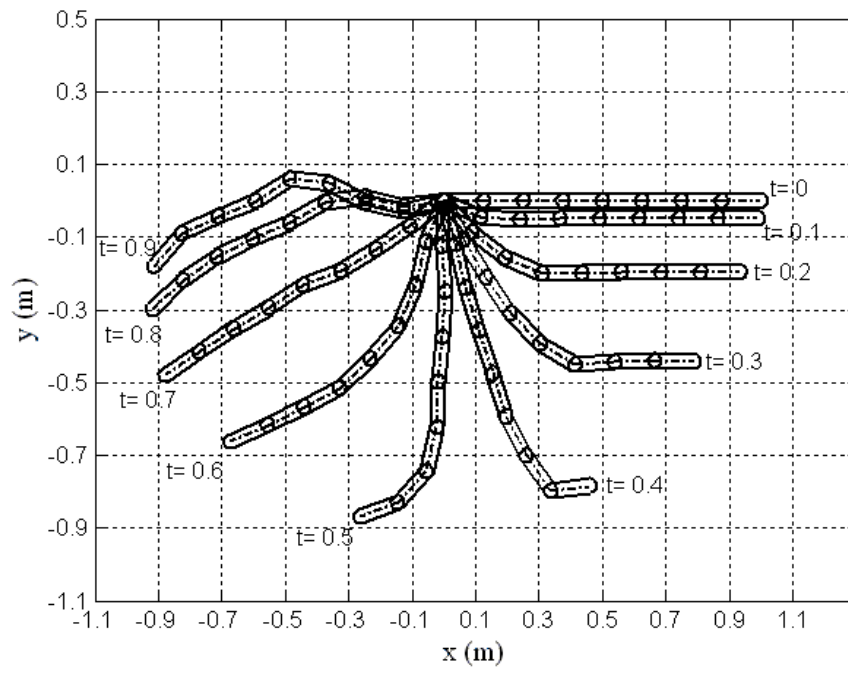
Figure 12 Chain configurations for $t = 0$ to $t = 0.9$ s
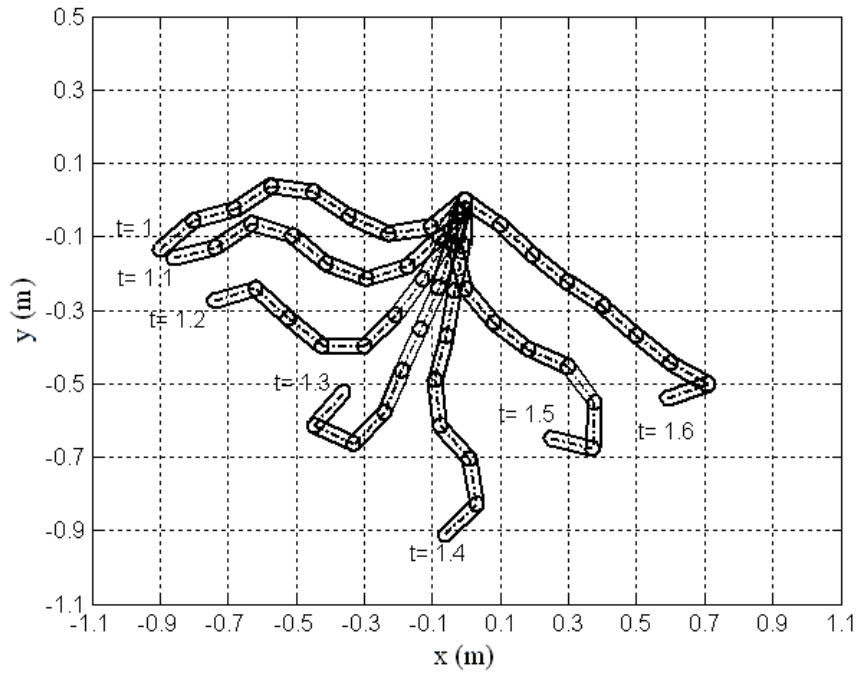
Figure 13 Chain configurations for $t = 1$ to $t = 1.6$ s

34
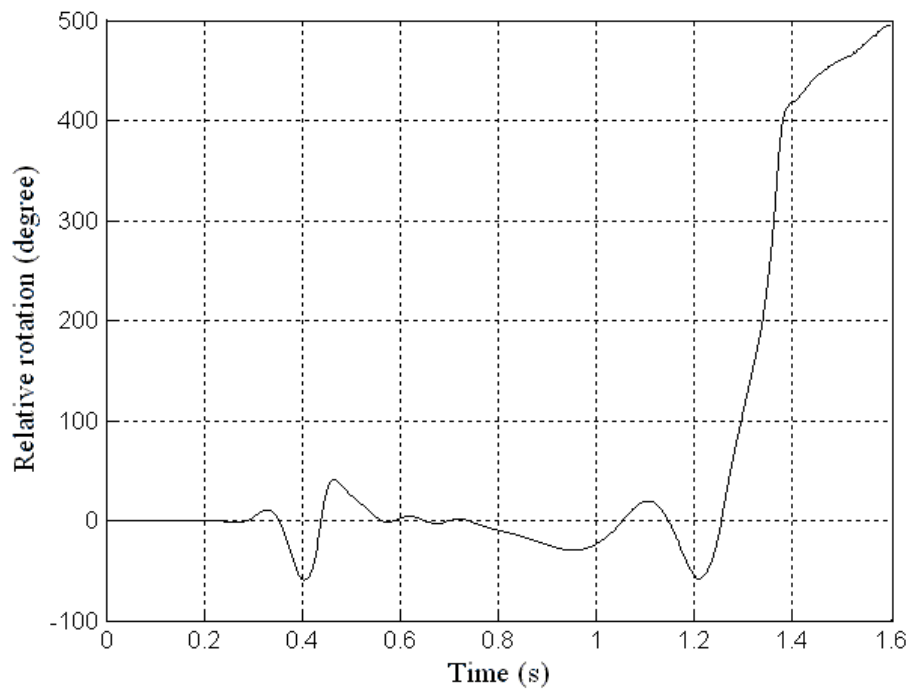
Figure 14 Relative rotation between last two chain links
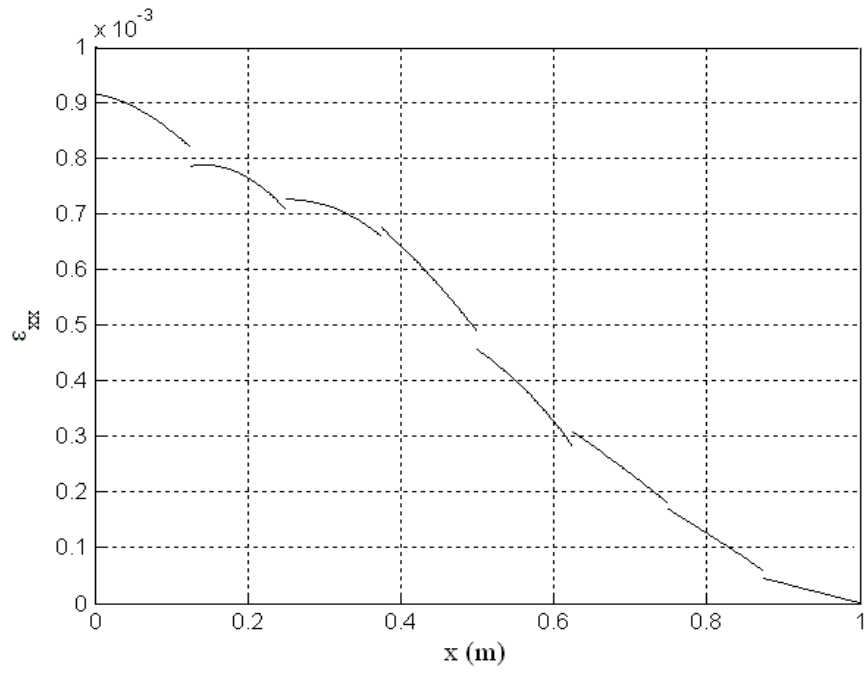
Figure 15 Distribution of the normal strain ε_{xx}
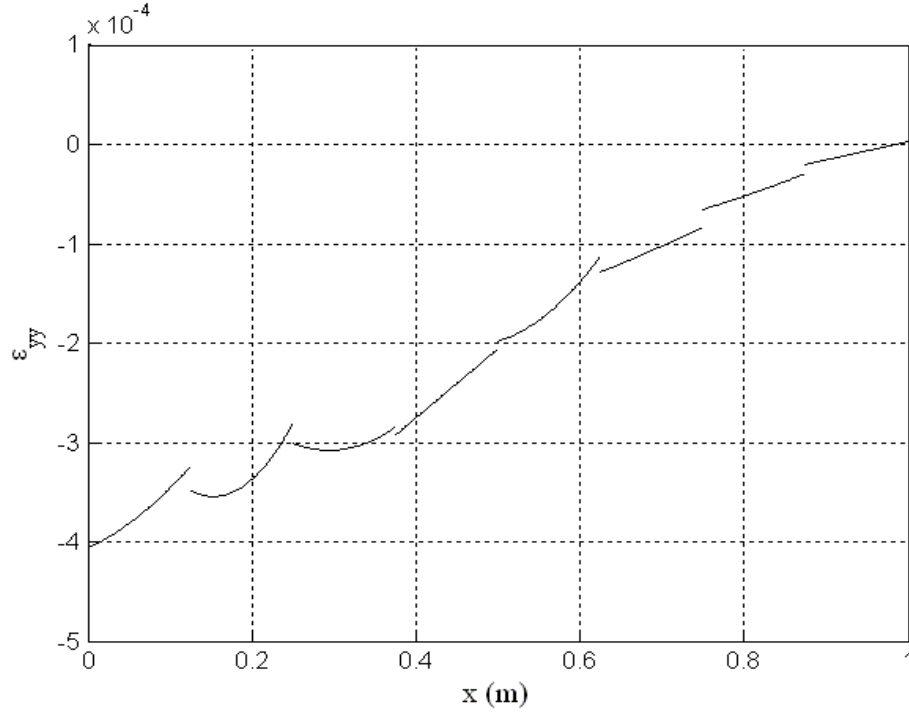
Figure 16 Distribution of the normal strain ε_{yy}

2.6.2. <u>**Structural and Non-Structural Discontinuities**</u>

Another example that includes both structural and non-structural geometric discontinuities is shown in Fig. 17. The system shown in this figure consists of 6 bodies including the ground. It has five pin joints that allow arbitrarily relative rotations between the links. The T-shaped section is modeled using three ANCF finite elements, while all other links in this chain system are modeled using one ANCF finite element. Therefore, the system which has 5 moving components is represented by one FE mesh (one flexible body) that has 7 ANCF beam elements. The pin joints in this example represent non-structural discontinuities, while the T-junction is an example of structural discontinuity. The cross-sectional area of all the finite elements is assumed to be 0.1×0.1 m^2, the length of each beam element is assumed to be 0.55 m, and the mass density is 7200 kg/m^3. The results obtained using very stiff beams with modulus

of elasticity equal to 2×10^{11} N/m^2 were found to be in a good agreement with the results obtained using the rigid body model. After this verification, the modulus of elasticity was reduced to 2×10^{8} N/m^2.
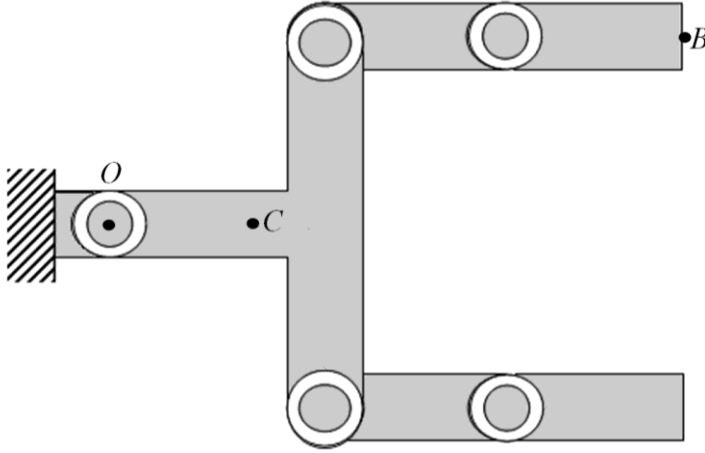
Figure 17 System with structural and non-structural discontinuities

Figure 18 shows motion simulation of the mechanism at different time points. The figure shows clearly the behavior of the structural and non-structural joints. The T-shaped section has structural geometric discontinuity that is described using ANCF gradient constraints (Shabana and Mikkola, 2003). This type of structural discontinuities is different from the non-structural discontinuities due to the pin joints that allow for arbitrary relative rotation between the chain links as demonstrated in Fig. 19. Figures 19 and 20 show, respectively, the trajectory of the centroid (Point C) of the T shaped beam and the trajectory of point B.

Time=0.00 s

Time=0.25 s

Time=0. 50 s

Time=0.75 s

Time=1.00 s

Time=1.25 s

Time=1.50 s

Time=1.75 s

Time=2.00 s
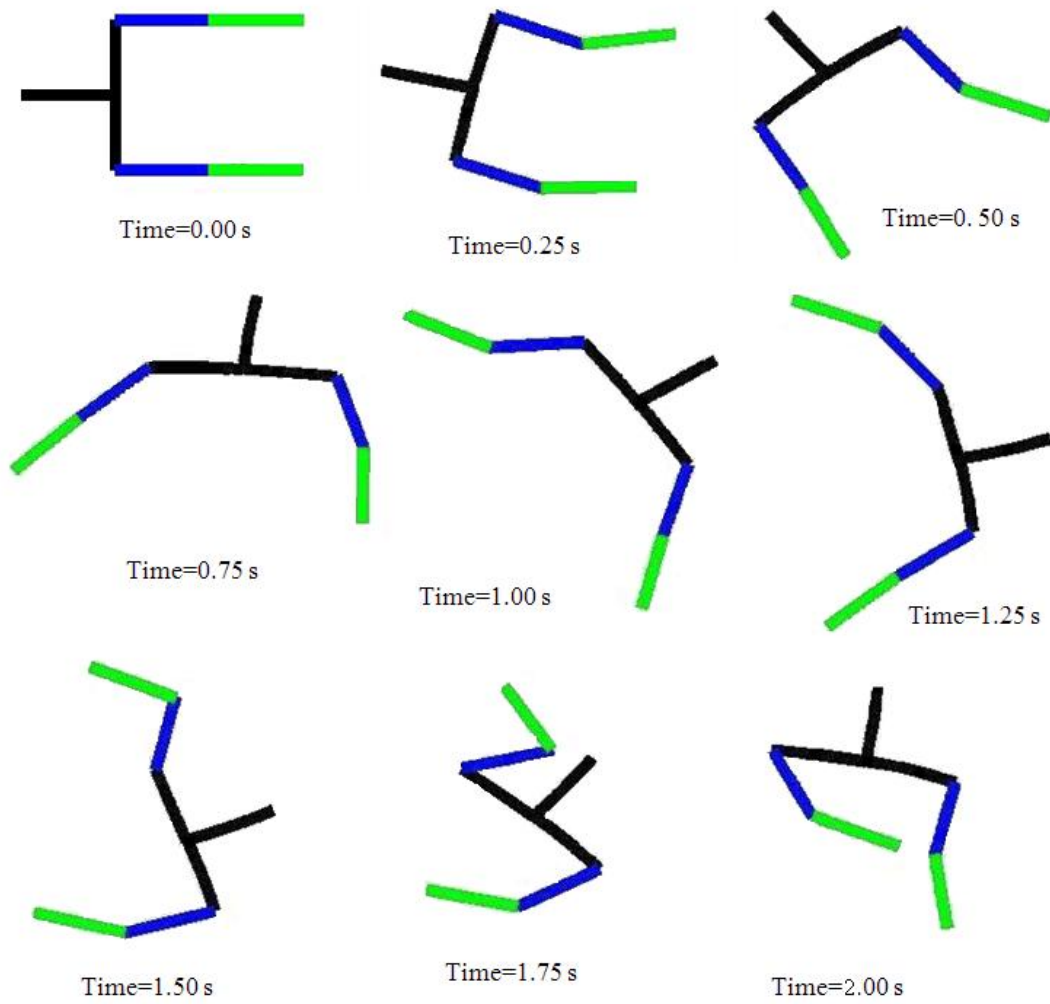
Figure 18 Dynamic simulation
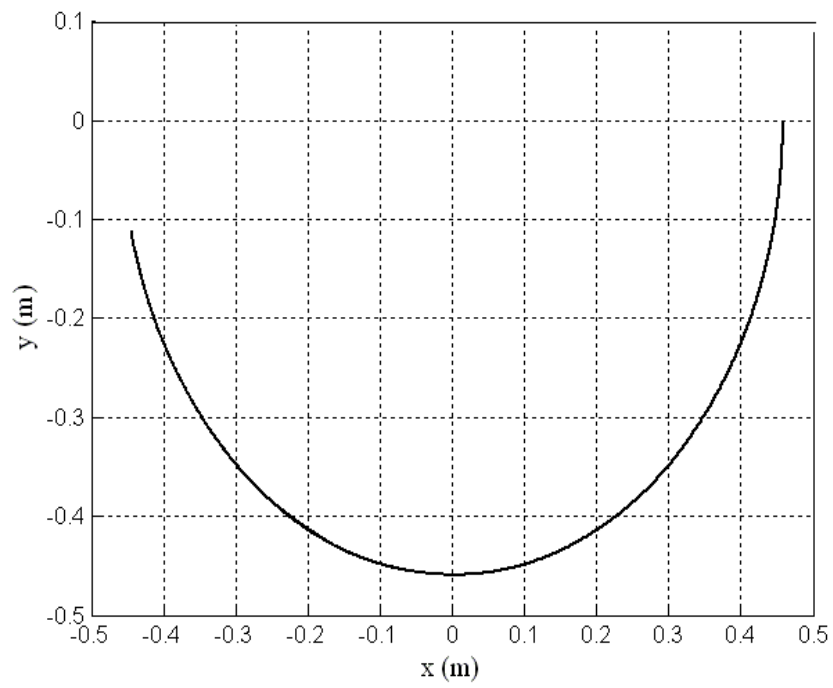
Figure 19 Trajectory of the centroid (point *C*) of the T shaped beam
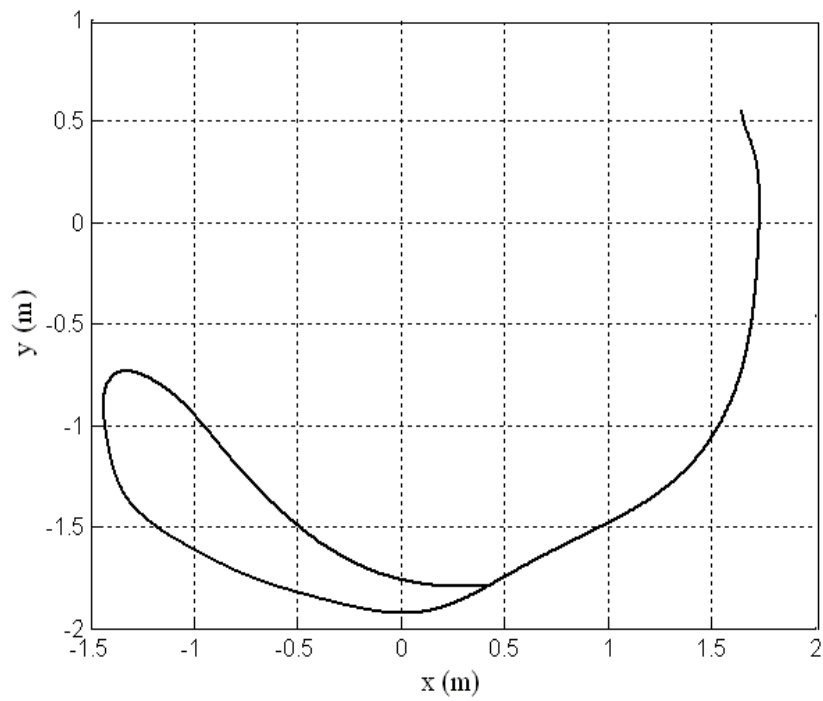
Figure 20 Trajectory of point *B*

2.7. <u>Concluding Remarks</u>

Existing MBS algorithms and computer programs do not allow structural finite elements (beams, plates, and shells) of a mesh to have arbitrarily large relative rigid body displacements that can introduce non-structural geometric discontinuities. Most algorithms and computer codes define structural FE meshes in which the elements are rigidly connected. In MBS algorithms, components which are not rigidly connected are treated as separate bodies, and nonlinear algebraic equations are used to define the joints that connect these bodies. Furthermore, the mesh inertia matrix becomes highly nonlinear in the case of rigid body rotations. Similarly, relative rigid body rotations lead to highly nonlinear kinematic constraint equations and inertia forces in the case of rigid body dynamics, as demonstrated in this chapter using a simple example. FE algorithms, on the other hand, employ co-rotational formulations that lead to highly nonlinear inertia matrix in the case of rigid body motion. For the most part, FE computer programs employ an incremental solution procedure that is not designed for solving MBS differential/algebraic equations. This thesis proposes the development of new FE meshes that can be effectively used in MBS dynamic analysis. The proposed ANCF procedure can be effectively used for modeling non-structural geometric discontinuities by allowing the structural finite elements of a mesh to have arbitrarily large relative rigid body displacements. Connectivity conditions between the finite elements are defined using linear algebraic constraint equations which can be introduced at a preprocessing stage before the dynamic analysis in order to eliminate redundant coordinates; thereby significantly reducing the number of algebraic equations and the associated Lagrange multipliers. Using ANCF finite elements that correctly describe rigid body displacements and do not require the use of the co-rotational formulation, one obtains a FE mesh that has rigid body degrees of freedom and at the same time has a constant mass matrix. The relationship between

these ANCF continuity conditions and the concept of knot multiplicity used in computational geometry methods such as B-splines and NURBS is discussed and demonstrated using several examples. The examples presented in this chapter show that ANCF finite elements can be used to systematically model non-structural discontinuities as well as structural discontinuities including T- and V-junctions.

CHAPTER 3

COMPARISON WITH COMPUTATIONAL GEOMETRY METHODS

*Materials presented in this chapter are taken from "Shabana, A.A., **Hamed, A.M.**, Mohamed, A. A., Paramsothy Jayakumar, Letherwood, D.M: Use of B-spline in the Finite Element analysis: Comparison with ANCF Geometry. Journal of Computational and Nonlinear Dynamics, 2012." Please refer to Appendix B for copyrights transfer.*

In previous chapter, it was shown that a linear formulation of the perfect plannar pin joints that allow for finite relative rotations between the connected elements can be systematically obtained using ANCF finite elements. This Chapter introduces a generalization of the proposed plannar joint formulation to the spatial analysis. It is shown that the constraints equations of the spherical and revolute (pin) joints will remain linear in the spatial analysis. This chapter also examines the limitations of using B-spline representation as an analysis tool by comparing its geometry with the nonlinear finite element *absolute nodal coordinate formulation* (ANCF) geometry. It is shown that while both B-spline and ANCF geometries can be used to model *non-structural discontinuities* using linear connectivity conditions, there are fundamental differences between B-spline and ANCF geometries. First, while B-spline geometry can always be converted to ANCF geometry, the converse is not true; that is, ANCF geometry cannot always be converted to B-spline geometry. Second, because of the rigid structure of the B-spline recurrence formula, there are restrictions on the order of the parameters and basis functions used in the polynomial interpolation; this in turn can lead to models that have significantly larger number of degrees of freedom as compared to those obtained using ANCF geometry. Third, in addition to the known fact that B-spline does not allow for straight forward modeling of T-junctions, B-spline representation cannot be used in a straight forward manner to model *structural discontinuities*. It is shown that ANCF geometric description can be used to develop

new spatial chain models governed by linear connectivity conditions which can be applied at a preprocessing stage allowing for an efficient elimination of the dependent variables. The modes of the deformations at the definition points of the joints that allow for rigid body rotations between ANCF finite elements are discussed. The use of the linear connectivity conditions with ANCF spatial finite elements leads to a constant inertia matrix and zero Coriolis and centrifugal forces. The fully parameterized structural ANCF finite elements used in this study allow for the deformation of the cross section and capture the coupling between this deformation and the stretch and bending. A new chain model that employs different degrees of continuity for different coordinates at the joint definition points is developed. In the case of cubic polynomial approximation, C^1 continuity conditions are used for the coordinate line along the joint axis; while C^0 continuity conditions are used for the other coordinate lines. This allows for having arbitrary large rigid body rotation about the axis of the joint that connects two flexible links. Numerical examples are presented in order to demonstrate the use of the formulations developed in this chapter.

3.1. <u>B-spline Surfaces</u>

B-spline surfaces are defined using the product of basis functions, two parameters, and two knot vectors. They can be defined in the following parametric form (Piegl and Tiller, 1997):

$$\mathbf{r}(u,v) = \sum_{i=0}^{n}\sum_{j=0}^{m} N_{i,p}(u)N_{j,q}(v)\mathbf{P}_{i,j} \tag{3.1}$$

where u and v are the parameters; $N_{i,p}(u)$ and $N_{j,q}(v)$ are B-spline basis functions of degree p and q, respectively; and $\mathbf{P}_{i,j}$ are a set of bidirectional control points. The B-spline basis functions $N_{i,p}(u)$ are defined as

$$N_{i,0}(u) = \begin{cases} 1 & \text{if } u_i \le u < u_{i+1} \\ 0 & \text{otherwise} \end{cases}$$

$$N_{i,j}(u) = \frac{u - u_i}{u_{i+j} - u_i} N_{i,j-1}(u) + \frac{u_{i+j+1} - u}{u_{i+j+1} - u_{i+1}} N_{i+1,j-1}(u)$$

(3.2)

where u_i, $i = 0, 1, 2, \ldots, n + p + 1$ are called the *knots*; and $u_i \le u_{i+1}$. The vector

$\mathbf{U} = \{u_0 \quad u_1 \quad \cdots \quad u_{n+p+1}\}$ is called the *knot vector*. Similar definitions can be introduced for

$N_{j,q}(v)$ with another knot vector $\mathbf{V} = \{v_0 \quad v_1 \quad \cdots \quad v_{m+q+1}\}$. Note that the orders of the

polynomials in the u and v directions can be different; for example, a cubic interpolation can be

used along u while a linear interpolation can be used along v. As in the case of B-spline curves,

the knots of B-spline surfaces do not have to be distinct; distinct knots are called *breakpoints* and

define surface segments with non-zero dimensions. The number of the non-distinct knots in $\mathbf{U}$

and $\mathbf{V}$ at a point is referred to as the knot multiplicity associated, respectively, with the

parameters u and v at this point. At a given breakpoint, the multiplicity associated with u can

be different from the multiplicity associated with v; allowing for different degrees of continuity

for the derivatives with respect to u and v. For cubic $N_{i,p}$ ($p = 3$), C^0, C^1, or C^2 conditions

correspond, respectively, to knot multiplicity of three, two, and one; while in the case of linear

interpolation of $N_{j,q}$, the highest continuity degree that can be demanded is continuity of the

gradients. When zero multiplicity is used at a breakpoint, the segments blend together at this

point.

In B-spline surface representation, there is a relationship between the polynomial degree,

the number of knots, and the number of control points. This relationship must be fully

understood if B-spline geometry will be used as an analysis tool. If $r+1$ is the number of knots in $\mathbf{U}$ and $s+1$ is the number of knots in $\mathbf{V}$, then in B-spline geometry, one must have

$$r = n + p + 1, \quad s = m + q + 1 \tag{3.3}$$

These formulas imply that, for a given polynomial order, if the number of knots decreases, the number of control points (degrees of freedom used in the analysis) must also decrease. A decrease in the knot multiplicity by one is equivalent to eliminating one control point. This can also be equivalent to increasing the degree of continuity since eliminating a control point can be the result of imposing algebraic equations that relates the derivatives at a certain breakpoint. From the bidirectional structure used in Eq. 3.1, a surface which has cubic interpolation along u ($p=3, n=3, r+1=8$) and a linear interpolation along v ($q=1, m=1, s+1=4$), should have $(n+1) \times (m+1) = 8$ control points; this is regardless of whether the surface is two- or three-dimensional. Manipulation of the B-spline surface of Eq. 3.1 shows that these eight control points are the result of using the alternate basis set $1, u, v, uv, u^2, u^2v, u^3, u^3v$. That is, B-spline representation and the formulas of Eq. 3.3 do not allow for the use of the basis set $1, u, v, uv, u^2, u^3$ which can be effectively used to develop a shear deformable beam model. If a cubic interpolation is used for both u and v (thin plate), the B-spline representation will require 16 control points because the expansion must include all terms $u^k v^l$; $k, l = 0, 1, 2, 3$ regardless of whether the shape of deformation of the plate is simple or complex; one must strictly follow the B-spline rigid structure. This can be of disadvantage in the analysis since such a geometric representation can unnecessarily increase the dimension of the analysis model and leads to the loss of the flexibility offered by the FE method or modal analysis techniques. As the degree of the polynomial interpolation increases, the problem gets even worse. Another important and

interesting issue with regard to the use of B-spline as an analysis tool is capturing discontinuities; this is discussed in the following section.

3.2. <u>Generality of ANCF Geometry</u>

While B-spline geometry can always be converted to ANCF geometry, the converse is not true. ANCF geometry does not impose restriction on the basis functions that must be included in the interpolating polynomials. This allows for developing finite elements that have less coordinates as compared to those developed using the B-spline representation. Furthermore, ANCF geometry can be used to model both structural and non-structural discontinuities (Shabana and Mikkola, 2003; Shabana, 2010; Hamed et al., 2010), while the rigid recurrence B-spline representation cannot be used to model structural discontinuities in a straightforward manner. The basic differences between ANCF and B-spline geometries are demonstrated in this section using a planar beam example. The displacement field of the shear deformable beam used in this section can be written as $\mathbf{r}(x, y) = \mathbf{S}(x, y)\mathbf{e}(t)$, where x and y are the element spatial coordinates, t is time, $\mathbf{S}$ is the element shape function matrix, and $\mathbf{e}$ is the vector of the element nodal coordinates. The shape function matrix for the element considered in this section is defined as

$$\mathbf{S}^j = \begin{bmatrix} s_1\mathbf{I} & s_2\mathbf{I} & s_3\mathbf{I} & s_4\mathbf{I} & s_5\mathbf{I} & s_6\mathbf{I} \end{bmatrix} \tag{3.4}$$

where the shape functions s_i, $i = 1, 2, \ldots, 6$ are defined as (Omar and Shabana, 2001)

$$\left.\begin{aligned} s_1 &= 1 - 3\xi^2 + 2\xi^3, & s_2 &= l\left(\xi - 2\xi^2 + \xi^3\right), & s_3 &= l\eta\left(1 - \xi\right), \\ s_4 &= 3\xi^2 - 2\xi^3, & s_5 &= l\left(-\xi^2 + \xi^3\right), & s_6 &= l\xi\eta \end{aligned}\right\} \tag{3.5}$$

46

In this equation, $\xi = x/l$, $\eta = y/l$. ANCF finite elements employ gradient vectors as nodal coordinates. For the element used in this section, the vector of nodal coordinates is defined as

$$\mathbf{e} = \left[(\mathbf{r})_1^T \quad (\partial \mathbf{r}/\partial x)_1^T \quad (\partial \mathbf{r}/\partial y)_1^T \quad (\mathbf{r})_2^T \quad (\partial \mathbf{r}/\partial x)_2^T \quad (\partial \mathbf{r}/\partial y)_2^T \right]^T \qquad (3.6)$$

where $(\ )_k$, $k = 1, 2$ indicates variables evaluated at node k of the element. Note that the element defined by the preceding equations is based on a cubic interpolation for x and a linear interpolation for y. This element has been widely used in the analysis of large deformation problems.

The finite element described in this section is an example of ANCF elements that cannot be converted to B-spline representation. This element is based on a polynomial expansion that does not have the two basis functions $x^2 y$ and $x^3 y$. These terms can be systematically included in ANCF geometry by adding nodal coordinates allowing for converting B-spline representation to ANCF representation. Similar comments apply to ANCF thin plate elements that do not have to include all the basis functions $x^k y^l$; $k, l = 0, 1, 2, 3$. This flexibility offered by ANCF geometry allows for developing finite elements that have smaller number of coordinates compared to those elements developed by B-spline geometry.

As mentioned earlier in Chapter 2, one can also show that ANCF finite elements can describe structural and non-structural discontinuities. Non-structural discontinuities that allow for large rigid body rotations can be described using a C^0 model obtained by imposing constraints on the position coordinates only. For example if two elements i and j are connected

by pin joint at a node, one can apply the algebraic equations $\mathbf{r}^i = \mathbf{r}^j$ at this node. These algebraic equations can be imposed at a preprocessing stage to eliminate the dependent variables and define FE mesh that has a constant mass matrix and zero Coriolis and centrifugal forces despite the finite rotations allowed between the finite elements of the mesh. As previously mentioned, non-structural discontinuities can also be described using B-spline geometry by reducing the knot multiplicity at the joint node by one. Note that in the case of non-structural discontinuities, no constraints are imposed on the gradient vectors, and therefore, the state of strain is not unique at the joint node. Each of the Lagrangian strains $\varepsilon_{xx} = \left(\mathbf{r}_x^T \mathbf{r}_x - 1 \right)/2$, $\varepsilon_{yy} = \left(\mathbf{r}_y^T \mathbf{r}_y - 1 \right)/2$, and $\varepsilon_{xy} = \mathbf{r}_x^T \mathbf{r}_y / 2$ have two values at the joint node; one defined on element i and the other is defined on element j.

The concept of degrees of freedom widely used in mechanics is not considered in developing the recurrence relationships on which B-spline and NURBS geometry are based. This represents another serious limitation when these computational geometry methods are used as analysis tools; as evident by the fact that B-spline geometry cannot describe structural discontinuities. This type of discontinuities, while it remains of the C^0 continuity type, requires imposing additional constraints on the gradients; these constraints cannot be captured by the B-spline recurrence formula since they require the elimination of additional vectors. In the case of B-spline, C^0 continuity is achieved by reducing the knot multiplicity by one, and this eliminates one control point leading to the definition of a pin joint (non-structural discontinuity). ANCF geometry, on the other hand, allows for imposing constraints on the gradients using the tensor transformation $\left(\partial \mathbf{r}/\partial \mathbf{x}_1 \right) = \left(\partial \mathbf{r}/\partial \mathbf{x}_2 \right) \mathbf{A}$, where $\mathbf{x}_1 = \begin{bmatrix} x_1 & y_1 \end{bmatrix}^T$ and $\mathbf{x}_2 = \begin{bmatrix} x_2 & y_2 \end{bmatrix}^T$ are two sets of

coordinate lines, and **A** is the matrix of coordinate line transformation. Using this tensor gradient transformation, the structural discontinuities can be systematically modeled using ANCF finite elements (Shabana and Mikkola, 2003; Shabana, 2010). For example, if the axis of a beam element j makes an angle α with the axis of another element i and the two elements are rigidly connected at a node, the structural discontinuity conditions that eliminate all the relative rigid body displacements can be written at the joint node as

$$\mathbf{r}^i = \mathbf{r}^j, \qquad \begin{bmatrix} \dfrac{\partial \mathbf{r}^i}{\partial x^i} & \dfrac{\partial \mathbf{r}^i}{\partial y^i} \end{bmatrix} = \begin{bmatrix} \dfrac{\partial \mathbf{r}^j}{\partial x^j} & \dfrac{\partial \mathbf{r}^j}{\partial y^j} \end{bmatrix} \begin{bmatrix} \cos\alpha & \sin\alpha \\ -\sin\alpha & \cos\alpha \end{bmatrix} \qquad (3.7)$$

where, α is the angle between the two connected bodies.

These six scalar algebraic equations can be used to eliminate a position coordinate vector and two gradient vectors, defining a unique strain state at the node of connectivity between the ANCF finite elements. The algebraic conditions of Eq. 3.7 that allow ANCF finite elements to describe two types of C^0 discontinuity cannot be automatically captured by the B-spline recurrence formula. Note that, these algebraic conditions are linear in the ANCF finite element coordinates, and therefore, they can be applied using a standard FE assembly procedure at a preprocessing stage of the analysis. These conditions lead to a relative motion, between the finite elements, that is pure deformation displacement.

It is important to point out that the coordinate line transformation of Eq. 3.7 need to be applied only in the case of structural discontinuities. Such a transformation is not required in the case of non-structural discontinuities despite the fact that the elements can have arbitrary orientation relative to each other. This is due to the facts that non-structural discontinuity does

not impose constraints on the gradient vectors, ANCF geometry is invariant under an arbitrary rigid body displacement, and each ANCF finite element has its own independent parameters. Similarly, in the case of curved shapes as in belt applications, the coordinate transformation used in Eq.3.7 is not required since there are no structural discontinuities and the gradients at all points on the belt can be defined with respect to the same coordinate lines. In the curved sections of the belt, one must provide the appropriate values of the gradient vectors that define the correct shape. Recall that a curve, regardless of its shape, requires only one parameter; while a surface, regardless of its shape, requires only two parameters.

3.3. <u>Three-Dimensional Non-structural Discontinuities</u>

In this section, it is shown how fully parameterized ANCF three-dimensional finite elements can be used to develop spatial joint models that allow large relative rigid body rotation between the finite elements. ANCF finite elements connected by this joint can be assembled using linear connectivity conditions leading to FE mesh that has a constant mass matrix and zero Coriolis and centrifugal forces. The fully parameterized three-dimensional ANCF beam element is used in this investigation to demonstrate the development of such joint models. The displacement field of the element can be written as $\mathbf{r}(x, y, z) = \mathbf{S}(x, y, z)\mathbf{e}(t)$ where x, y, and z are the element spatial coordinates. The shape function matrix of this element is defined as (Yakoub and Shabana, 2001; Shabana, 2008)

$$\mathbf{S} = \begin{bmatrix} s_1\mathbf{I} & s_2\mathbf{I} & s_3\mathbf{I} & s_4\mathbf{I} & s_5\mathbf{I} & s_6\mathbf{I} & s_7\mathbf{I} & s_8\mathbf{I} \end{bmatrix} \tag{3.8}$$

where the shape functions s_i, $i = 1, 2, \dots, 8$ are defined as

$$
\left.
\begin{aligned}
s_1 &= 1 - 3\xi^2 + 2\xi^3, \quad s_2 = l\left(\xi - 2\xi^2 + \xi^3\right), \\
s_3 &= l(\eta - \xi\eta), \quad s_4 = l(\varsigma - \xi\varsigma), \quad s_5 = 3\xi^2 - 2\xi^3, \\
s_6 &= l\left(-\xi^2 + \xi^3\right), \quad s_7 = l\xi\eta, \quad s_8 = l\xi\varsigma
\end{aligned}
\right\}
\tag{3.9}
$$

In this equation, $\xi = x/l, \eta = y/l, \varsigma = z/l$. The element has two nodes; each node has 12 nodal coordinates defined by the vector $\mathbf{e}^k = \begin{bmatrix} \mathbf{r}^{kT} & \mathbf{r}_x^{kT} & \mathbf{r}_y^{kT} & \mathbf{r}_z^{kT} \end{bmatrix}^T$, where k is the node number. The ANCF finite element defined by Eqs. 3.8 and 3.9 captures the cross section deformation and its coupling with extension and bending. Therefore, this element can be used to develop general models for belt drives and rubber tracked vehicles.

The three-dimensional beam element presented in this section is another example that can be used to demonstrate the generality of the ANCF geometry. This element is based on cubic interpolation in x and linear interpolation in y and z. Nonetheless, one can show that the four basis functions $x^2 y, x^3 y, x^2 z, x^3 z$ are not used in developing the displacement field of this widely used ANCF beam element. Therefore, the geometry of this element cannot be converted to B-spline volume geometry. These missing basis functions can be systematically included in the development of another ANCF finite element that can be converted to B-spline volume geometry. However, such an element will lead to 50% increase in the number of the element nodal coordinates.

A planar pin joint between rigid or flexible bodies is an example of C^0 continuity, as previously discussed. A pin joint between two rigid bodies in the spatial analysis also allows for only one degree of freedom, which is a relative rotation about the joint axis. Since the pin joint eliminates five degrees of freedom in the rigid body analysis, its formulation requires five

51

algebraic constraint equations that eliminate three relative translation displacements and two relative rotations between the two bodies. In the case of flexible bodies, an infinitesimal volume can have 12 modes of displacements; three rigid body translations, three rotations, and six deformation modes. In this section, a new model of pin joint between ANCF finite elements is introduced. The formulation of this pin joint between elements i and j employs the following six scalar equations defined at the joint node:

$$\mathbf{r}^i = \mathbf{r}^j, \qquad \mathbf{r}_\alpha^i = \mathbf{r}_\alpha^j \tag{3.10}$$

Here α is the coordinate line that defines the joint axis; α can be x, y, or z or any other coordinate line as discussed later in this section. The six scalar equations of Eq. 3.10 eliminate six degrees of freedom; three translations, two rotations, and one deformation mode. This joint model ensures C^1 continuity with respect to the coordinate line α and C^0 continuity with respect to the other two parameters. It follows that the Lagrangian strain component $\varepsilon_{\alpha\alpha} = \left(\mathbf{r}_\alpha^T \mathbf{r}_\alpha - 1\right)/2$ is continuous at the joint definition point, while the other five strain components can be discontinuous.

While the algebraic constraint equations of a pin joint between two rigid bodies are highly nonlinear, the algebraic constraint equations of Eq. 3.10 are linear. Therefore, these equations can be applied at a preprocessing stage to systematically eliminate the dependent variables. Using these equations, one can develop a new kinematically linear FE mesh for flexible-link chains in which the links can have arbitrarily large relative rotations. The use of this pin joint model with ANCF finite elements leads to a constant mass matrix and zero Coriolis and centrifugal forces.

As previously mentioned, B-spline geometry can describe the type of non-structural discontinuity discussed in this section. Nonetheless, if an arbitrary axis of a pin joint is to be used in the analysis, the use of B-spline geometry can be difficult given the rigid structure of the B-spline recurrence formula. In order to be able to choose an arbitrary axis of rotation for the pin joint, one must be able to define the gradient vector in the direction of a coordinate line along this axis of rotation. Such a definition can be easily made using ANCF geometry using the gradient tensor transformation. Let u, v, and w be another set of parameters; one of them can be used to define the joint axis. It follows that $\begin{bmatrix} \mathbf{r}_u & \mathbf{r}_v & \mathbf{r}_w \end{bmatrix} = \begin{bmatrix} \mathbf{r}_x & \mathbf{r}_y & \mathbf{r}_z \end{bmatrix} \mathbf{A}$, where $\mathbf{A}$ is the constant matrix of coordinate transformation defined as

$$\mathbf{A} = \begin{bmatrix} \dfrac{\partial x}{\partial u} & \dfrac{\partial x}{\partial v} & \dfrac{\partial x}{\partial w} \\ \dfrac{\partial y}{\partial u} & \dfrac{\partial y}{\partial v} & \dfrac{\partial y}{\partial w} \\ \dfrac{\partial z}{\partial u} & \dfrac{\partial z}{\partial v} & \dfrac{\partial z}{\partial w} \end{bmatrix} \tag{3.11}$$

The fact that this matrix is constant allows having linear pin joint connectivity conditions when ANCF finite elements are used (Shabana and Mikkola, 2003; Shabana, 2010).

3.4. <u>Numerical Examples</u>

In this section, three-dimensional belt drive and chain examples are used to demonstrate the implementation of the concepts discussed in this chapter. The degree of continuity at the element interfaces can be applied at a preprocessing stage in order to eliminate the dependent variables leading to a finite element mesh that has a constant mass matrix and zero Coriolis and centrifugal forces. The fully parameterized three-dimensional ANCF beam element discussed

53

earlier is used in modeling the belt and the chain used in this section. The following three different models are considered:

1. A finite element belt model with C^1 continuity. The geometry of this model can be defined in the initial configuration using a smooth curve that defines the centerline of the belt. This model, referred to in this section as the C^1 belt model, leads to continuous gradients and strains at the element interfaces.

2. A finite element belt model that ensures continuity of $\mathbf{r}_y$ (C^1 continuity along y), but it has C^0 continuity along x and z. In the initial configuration, the centerline of the belt is continuous. This model is referred to as the C^0/C^1 belt model.

3. A finite element flexible-link chain model that ensures continuity of $\mathbf{r}_y$ (C^1 continuity along y), but it has C^0 continuity along x and z. This model differs from the previous two models due to the fact that the chain centerline is not continuous at the initial configuration because $\mathbf{r}_x$ and $\mathbf{r}_z$ are not continuous. This model will be referred to in this section as the chain model.

The belt and chain drive mechanisms considered in this section are assumed to consist of two pulleys and a flexible belt or a chain as shown in Figs. 21 and 22. Figure 22 shows the discontinuity of the gradients at the joints in the initial configuration. The pulleys are connected to the ground using revolute joints.
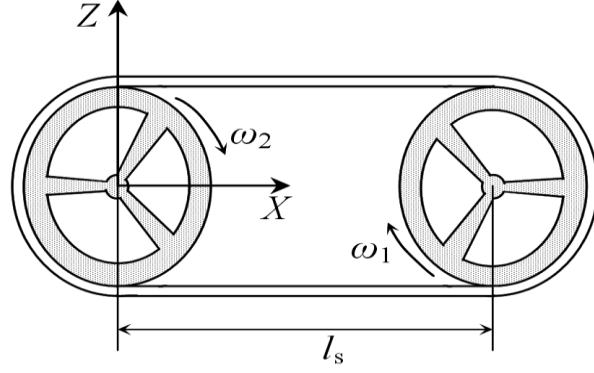
Figure 21 Initial configuration of the belt drive mechanism for both C^0/C^1 and C^1 models
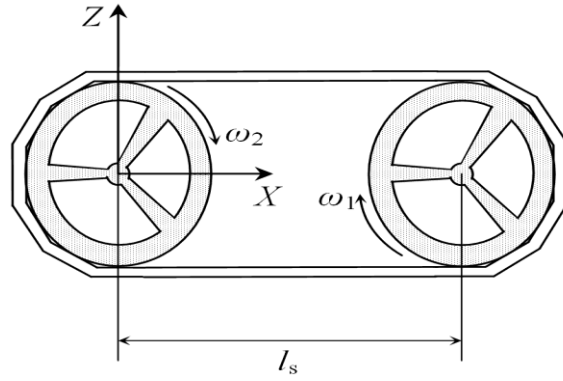
Figure 22 Initial configuration of the chain model

The span length in the reference configuration is assumed to be 0.12 m in the case of the belt model and 0.128 m in the case of the chain model. In the examples considered in this section, the angular velocity of the driving pulley is specified by the following equation:

$$\omega_1 = \begin{cases} 0 & t \le 0.3 \\ 100\dfrac{(t-0.3)}{0.7} & 0.3 < t \le 1.0 \\ 100 & t > 1.0 \end{cases} \tag{3.12}$$

where ω_1 is expressed in rad/s, and t is the time expressed in seconds. The mass moment of inertia of the driven pulley about its axis of rotation is 0.0075 kg/m^2. In order to introduce

55

tension in the system, the driving pulley is displaced in the X direction until the span length reaches 0.18 m for the three models. In order to avoid oscillations at the beginning of the simulation, this pulley displacement is achieved over a period of 0.2 s. A resistance moment defined by the following equation is applied to the driven pulley:

$$M = \begin{cases} 0 & t \le 0.3 \\ -1.1\dfrac{(t-0.3)}{0.7} & 0.3 < t \le 1.0 \\ -1.1 & t > 1.0 \end{cases} \tag{3.13}$$

The two pulleys are assumed to have the same radius and width of 0.058 and 0.01 m, respectively. A compliant force model is used to describe the belt/pulley interaction. The stiffness and damping coefficients used in the belt/pulley contact force model are given respectively by 9×10^7 N/m^3 and 2×10^3 N.s/m^3. Tangential friction forces are also introduced using a coefficient of dry friction of 1.2 (Leamy and Wasfy, 2002). The friction parameter that defines the slope in the transition region is assumed to be 10^6 N.s/m^3 (Maqueda et al, 2008). The belt is modeled using 20 ANCF three-dimensional beam elements. Incompressible Neo-Hookean constitutive model with nonlinear damping model is used to model the flexible belt. The belt is assumed to have a rectangular cross-section of dimensions 0.01×0.004 m and density of 3500 kg/m^3. The incompressible Neo-Hookean model constant is assumed to be $\mu_s = 2 \times 10^6$ N/m^2, the incompressibility constant is assumed to be $k = 10^8$ N/m^2, and the dilatation and deviatoric dissipation factors used for the damping model are assumed to be 10^{-4} and 5×10^{-5}, respectively.

Figure 23 shows the angular velocity of the driving and driven pulleys for both the C^1, C^0/C^1, and chain models. The results presented in this figure show that the angular velocity of

56

the driven pulley in the case of the C^1 belt model is higher than that of C^0/C^1 belt and chain models. This can be attributed to the fact that in the case of the C^0/C^1 and chain models, some of the loads such as bending moment about Y axis are not transferred between elements.
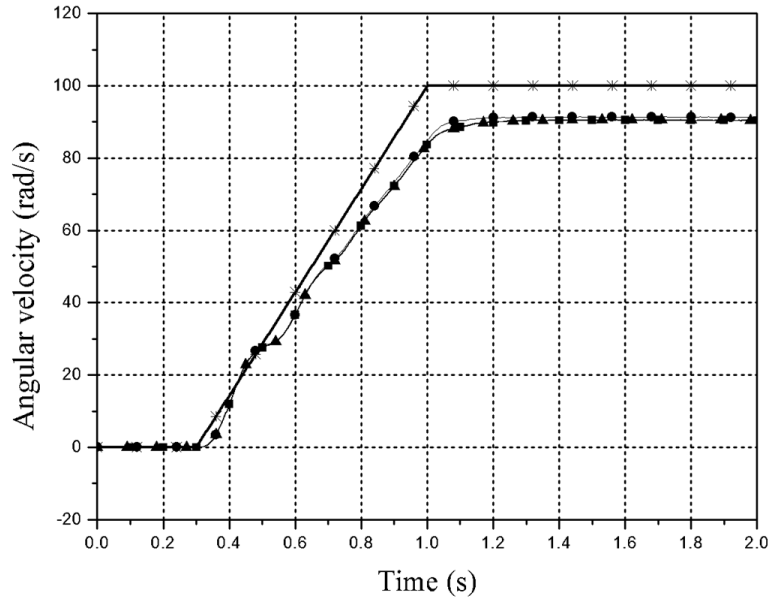
Figure 23 Angular velocity of the driving and driven pulleys
($\ast$ Driving pulley, $\bullet$ C^1 belt (driven pulley), $\blacktriangle$ C^0/C^1 belt (driven pulley),
- $\blacksquare$ - chain (driven pulley))

Figures 24-26 show the configurations of the belt centerline for the three models at time 1 s. These figures show that the gradients $\mathbf{r}_x$ and $\mathbf{r}_z$ are discontinuous in case of the C^0/C^1 belt and chain models and they are continuous in case of the C^1 belt model.
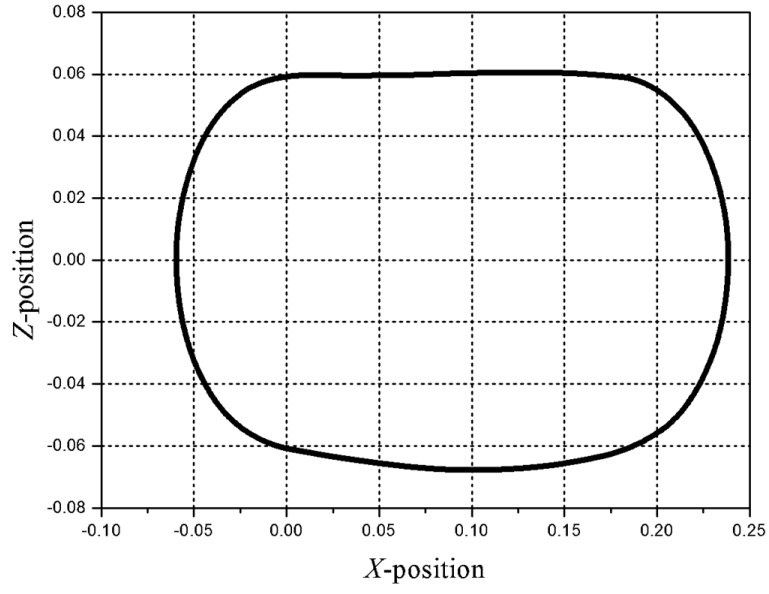
Figure 24 Centerline of the C^1 belt model at time 1s
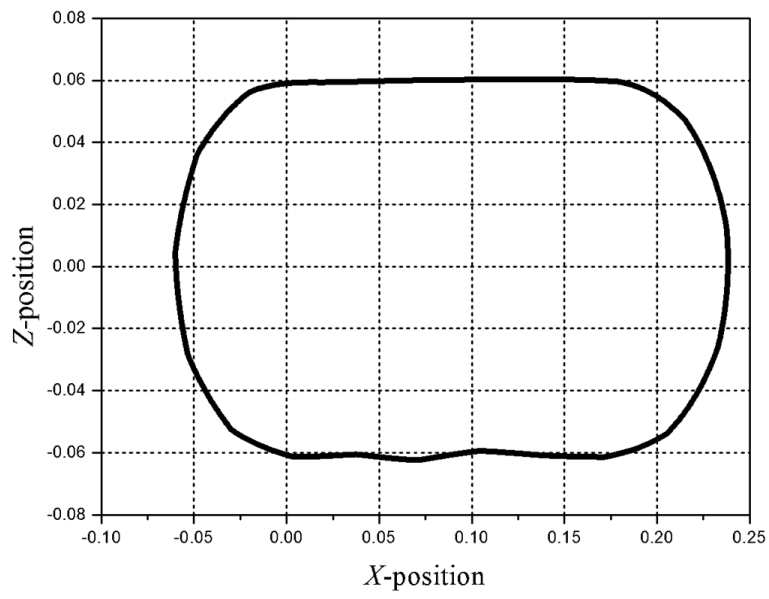
Figure 25 Centerline of the C^0/C^1 belt model at time 1s

58
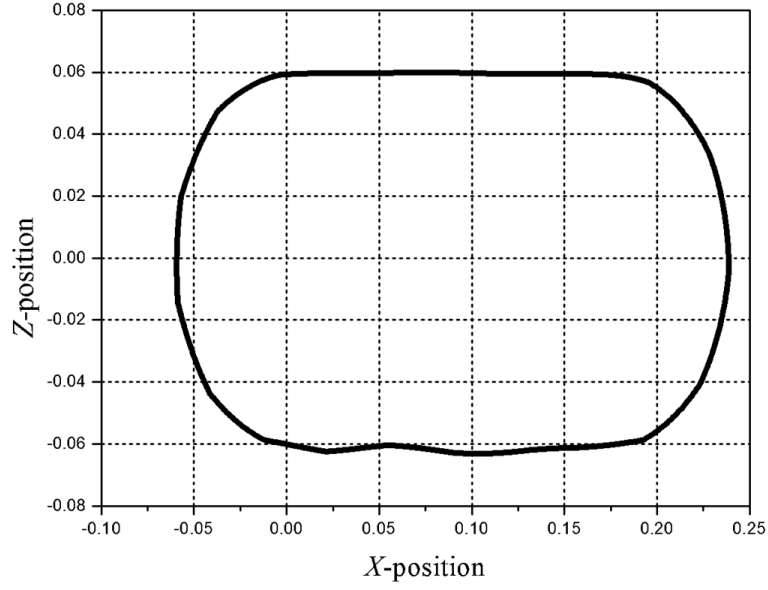
Figure 26 Centerline of the chain model at time 1s

Figure 27 shows a measure of the cross section deformation along the belt centerline at time 2s. This measure is defined by Nanson's formula that can be used to calculate the ratio between the areas in the current and reference configurations. Nanson's formula is defined as (Ogden, 1984; Shabana, 2008)

$$\frac{da}{dA} = \frac{J}{\left(\mathbf{n}_n^T \mathbf{J} \mathbf{J}^T \mathbf{n}_n\right)} \tag{3.14}$$

where a and A are, respectively, the area in the current and the reference configurations, J is the determinant of the matrix of position vector gradients $\mathbf{J}$, and $\mathbf{n}_n$ is the unit vector normal to the area. The results of Fig. 27 show that the area ratio is continuous in the case of the C^1 belt model while it is not continuous in case of the C^0/C^1 and chain models.

59
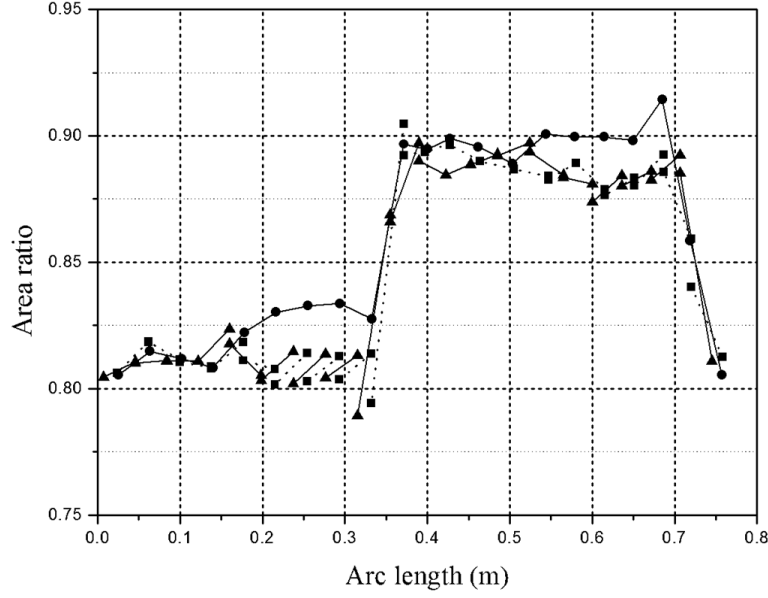
Figure 27 Area ratio along the belt centerline at time 1.9s
(—●— C^1 belt, —▲— C^0/C^1 belt, - -■- - chain)

Figures 28-30 show comparison of the normal strains at the element interface points along the belt centerline for the three models. The results obtained in this investigation show that all the strain components, which are functions of the gradient vectors, are continuous in the case of the C^1 belt model; while in the case of the C^0/C^1 and chain models only ε_{yy} is continuous. Figure 31 shows the Lagrangian shear strain component ε_{xz} along the belt centerline. The results of this figure show ε_{xz} to be discontinuous in the case of the C^0/C^1 and chain models because it is function of both the gradient vectors $\mathbf{r}_x$ and $\mathbf{r}_z$, which are discontinuous when these models are used.

60
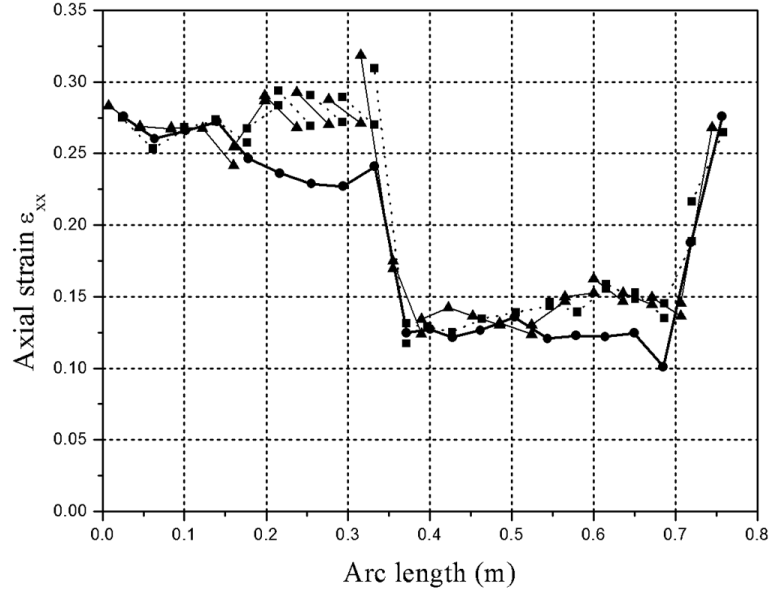
Figure 28 The axial strain ε_{xx} along the belt centerline at time 1.9s

(—●— C^1 belt, —▲— C^0/C^1 belt, - -■- - chain)
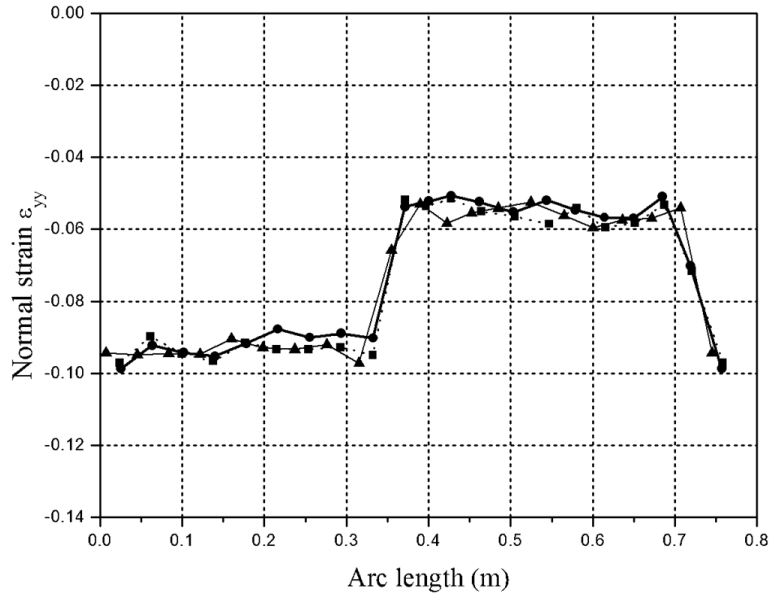
Figure 29 Normal strain ε_{yy} along the belt centerline at time 1.9s

(—●— C^1 belt, —▲— C^0/C^1 belt, - -■- - chain)
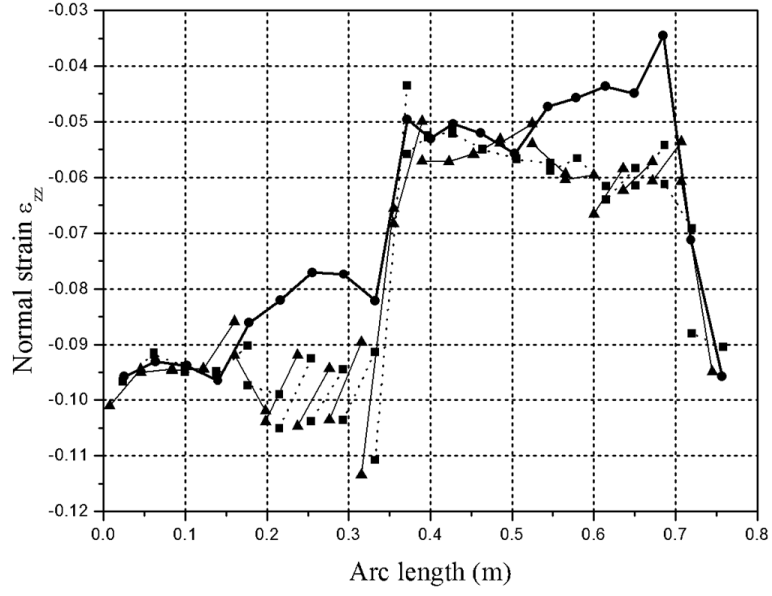
Figure 30 Normal strain ε_{zz} along the belt centerline at time 1.9s

(—●— C^1 belt, —▲— C^0/C^1 belt, - ■ - chain)
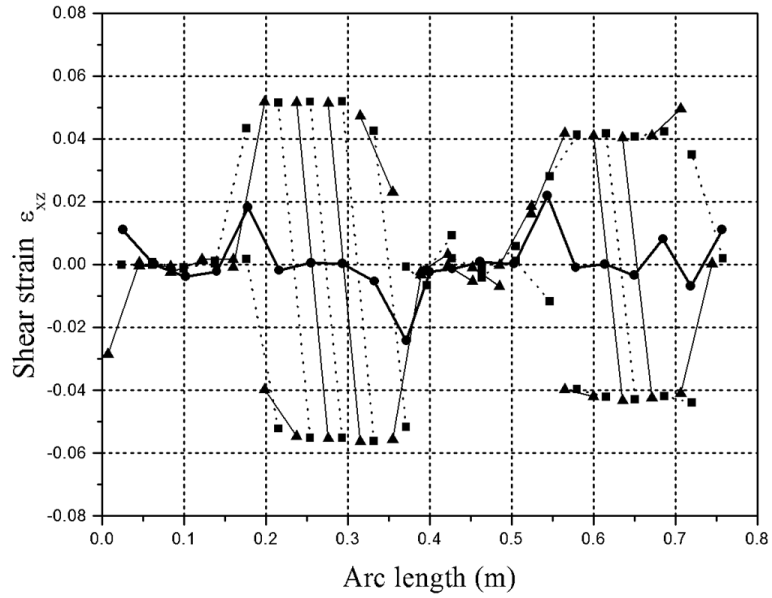
Figure 31 Shear strain ε_{xz} along the belt centerline at time 1.9s

(—●— C^1 belt, —▲— C^0/C^1 belt, - ■ - chain)

3.5. <u>Concluding Remarks</u>

This chapter addresses the important issue of using computational geometry methods such as B-spline and NURBS as analysis tools. B-spline and NURBS employ recurrence formulas that allow changing the degree of continuity at a breakpoint by adjusting the knot multiplicity at this point. As demonstrated, the recurrence formula has several drawbacks when B-spline representation is used as an analysis tool. Because the recurrence formula does not provide flexibility for choosing the basis functions, B-spline representation can lead to significantly larger number of coordinates and a higher dimensional model. This fact was used to demonstrate the generality of the ANCF geometry. While B-spline geometry can always be converted to ANCF geometry, the converse is not true. It is also shown that the B-spline recurrence formula cannot be used to model structural discontinuity in a straight forward manner. While structural discontinuities are of the C^0 type, they cannot be captured in the B-spline representation by reducing the knot multiplicity by one. This reduction of the knot multiplicity is equivalent to elimination of the relative translation only; and such a reduction in the knot multiplicity leads to a rigid body mode that defines the conditions of a pin joint. In the case of structural discontinuities, on the other hand, the C^0 B-spline representation does not eliminate the rigid body mode since additional algebraic constraint equations are required in order to eliminate the relative rotations between two segments. This chapter also presents a new three-dimensional pin joint model that leads to linear connectivity conditions and constant mass matrix when used with ANCF finite elements. The implementation of this new model is demonstrated using a flexible-link chain example. The limitations identified in this chapter when B-spline geometry is used as analysis tool suggest the use of the I-CAD-A approach in which a constant transformation can be developed to convert CAD geometry to FE mesh. It should be also clear

63

that NURBS geometry has the same limitations as B-spline representation when used as an analysis tool.

CHAPTER 4

COMPLIANT CONTINUUM JOINTS

Some of the limitations of using B-spline surfaces as analysis tool were compared to ANCF geometry in the preceding chapter. This chapter will continue this discussion by extensively examining the new class of *ideal compliant joints* which accounts for the distributed inertia and elasticity. The ANCF degrees of freedom are used in order to capture modes of deformation that cannot be captured using existing formulations. *The ideal compliant joints* developed can be formulated, for the most part, using linear algebraic equations, allowing for the elimination of the dependent variables at a preprocessing stage, thereby significantly reducing the problem dimension and array storage needed. Furthermore, the constraint equations are automatically satisfied at the position, velocity, and acceleration levels. When using the proposed approach to model large scale chain systems, differences in computational efficiency between the augmented formulation and the recursive methods are eliminated, and the CPU times resulting from the use of the two formulations become similar regardless of the complexity of the system. The elimination of the joint constraint equations and the associated dependent variables also contribute to the solution of a fundamental singularity problem encountered in the analysis of closed loop chains and mechanisms by eliminating the need to repeatedly change the chain or mechanism independent coordinates. It is shown that the concept of the knot multiplicity used in computational geometry methods, such as B-spline and NURBS (**N**on-**U**niform **R**ational **B**-**S**pline), to control the degree of continuity at the breakpoints is not suited for the formulation of many ideal compliant joints. This issue is closely related to the inability of B-spline and NURBS to model structural discontinuities. This chapter also demonstrates that large deformation ANCF finite elements can be effective, in some MBS

application, in solving small deformation problems. This is demonstrated using a heavily constrained tracked vehicle with flexible link chains. Without using the proposed approach, modeling such a complex system with flexible links can be very challenging. The analysis presented in this chapter also demonstrates that adding significant model details does not necessarily imply increasing the complexity of the MBS algorithm.

4.1. <u>Background</u>

Several FE/MBS formulations have been developed for the deformation analysis of mechanical systems. Some of these formulations are suited for the analysis of large rotation small deformation problems, while the others can be used in the analysis of large rotation and large deformation problems. An example of the large rotation and small deformation formulations is the FE/FFR formulation which employs mixed set of reference and elastic coordinates (Shabana, 2014). This formulation leads to a highly nonlinear inertia matrix that has a strong coupling between the reference and deformation coordinates. In addition to the high nonlinearity of the inertia forces, the joint constraints equations developed using the FFR formulation are also highly nonlinear because of the use of orientation parameters (Korkealaakso et al, 2009). Furthermore, rigid triads and unit vectors are often used in the formulation of the joints in the rigid body and FFR algorithms, and as a result, these ideal joint formulations do not capture modes of deformation.

While the FFR formulation will remain an effective approach for modeling small deformation problems because it allows for filtering out high frequency modes, the more general large rotation large deformation finite element *absolute nodal coordinate formulation* (ANCF) can be effective in solving a class of small deformation problems (Shabana et al, 2012; Hamed et

al, 2011; Shabana, 2010, 2012; Dimtrochenko and Pogorelov, 2003; Abbas et al, 2010; Dufva et al, 2005, 2007; Schwab and Meijaard, 2010; Shabana and Mikkola, 2003; Tian et al, 2009; Yakoub and Shabana, 2001; Omar and Shabana, 2001). As mentioned earlier, ANCF finite elements can be used to model both structural and nonstructural discontinuities in a straightforward manner (Shabana et al, 2012; Hamed et al, 2011). Using ANCF finite elements, the absolute position vectors and their gradients are considered nodal coordinates. The global position of an arbitrary point on an element k of body i can be defined in a global coordinate system as $\mathbf{r}^{ik} = \mathbf{S}^{ik}(x^{ik}, y^{ik}, z^{ik})\mathbf{e}^{ik}(t)$, where $\mathbf{S}^{ik}(x^{ik}, y^{ik}, z^{ik})$ is the space-dependent matrix that defines the element shape functions, and $\mathbf{e}^{ik}$ is time-dependent vector of nodal coordinates. An example of ANCF finite elements is the three-dimensional gradient deficient Euler-Bernoulli beam element shown in Fig. 32. For this element, the vector of nodal coordinates $\mathbf{e}^{ik}$, which contains position and position gradient vectors, can be defined as $\mathbf{e}^{ik} = \left[\mathbf{r}^{ik1\mathrm{T}} \ \dfrac{\partial \mathbf{r}^{ik1\mathrm{T}}}{\partial x^{ik}} \ \mathbf{r}^{ik2\mathrm{T}} \ \dfrac{\partial \mathbf{r}^{ik2\mathrm{T}}}{\partial x^{ik}} \right]^{\mathrm{T}}$

(Gerstmayr and Shabana, 2006; Shabana, 2012), where $\mathbf{r}^{ikj}$ and $\left(\partial \mathbf{r}^{ikj} / \partial x^{ik} \right)$ refer to the displacement and displacement gradient vectors at node j of element k.
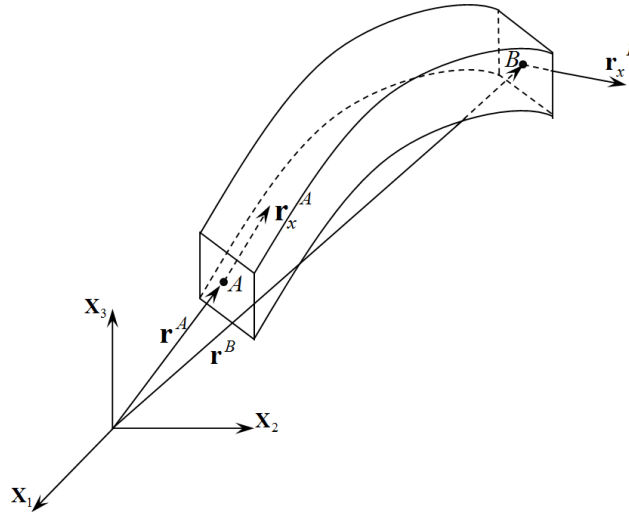
Figure 32 Euler-Bernoulli beam element

While ANCF finite elements were introduced for large deformation problems of very flexible bodies, these elements can be very effective in the analysis of small deformation in complex flexible multibody systems containing a large number of joints and flexible links. As demonstrated in this chapter using a large scale tracked vehicle that has flexible-link chains, ANCF finite elements can be used to capture model details that cannot be captured using small deformation and rigid body formulations.

A number of approaches have been proposed in the literature for developing tracked vehicle models. Galaitsis (1984) introduced a comprehensive model incorporating the dynamics of independent rigid track shoes. In this model, the equations of motion for the track chain were developed for a tracked vehicle traveling on a flat ground. Bando et al (1991) developed a procedure for the design and analysis of small-size rubber tracked bulldozers. They presented a computer simulation which was used in the evaluation of the vehicle behavior. Nakanishi and Shabana (1994) introduced a model for the nonlinear dynamic analysis of two dimensional

tracked vehicle systems. They used both the augmented and the velocity transformation techniques. In their investigation, it was shown that the singularity problem, which can be encountered if one set of independent coordinates is used throughout the simulation, can be avoided by either repeatedly changing the set of independent coordinates or by using a penalty function approach. In this latter approach, a cut is made at a selected secondary joint in the track in order to form an open loop structure, and the chain is closed using a spring with high stiffness coefficient. Choi et al (1998A; 1998B) developed a three dimensional contact force model that represents the interaction between the track links and the vehicle components. In their work, track links were connected using perfect pin joints. The highly nonlinear joints constraint equations were adjoined to the equations of motion using the augmented formulation. Maqueda et al (2010) developed a three-dimensional tracked vehicle model with rubber chains modeled using ANCF finite elements which allows for a straightforward implementation of general linear and nonlinear material models. The cross section deformation results obtained using ANCF finite elements were verified by comparing with the results obtained using solid finite elements in the case of a simple tension test. In previous chapters (Hamed et al, 2011; Shabana et al, 2012), an ANCF C^0/C^1 continuity flexible-link chain mesh was developed. This new ANCF mesh can be used in the efficient modeling of flexible-link chains. The C^0/C^1 ANCF chain model leads to linear connectivity conditions, thereby allowing for an efficient elimination of the dependent joint variables at a preprocessing stage. Using this approach, the ANCF mesh mass matrix remains constant in the case of articulated systems.

4.2. <u>**Modelling Discontinuities in Multibody System Analysis**</u>

Structural and nonstructural discontinuities have been fundamental issues in the development of MBS formulations. Understanding these types of discontinuities will also shed light on the fundamental differences between the approaches currently being developed for the integration of computer aided design and analysis. Structural discontinuities refer to the type of joints that do not allow relative rigid body displacements, while nonstructural discontinuities refer to the types of joints that allow for relative rigid body displacements. The joints used in flexible-link chains are example of joints that lead to nonstructural discontinuities.

Structural discontinuity was the main issue in the development of the large displacement small deformation FE/FFR formulation. In the classical finite element formulations, beams, plates, and shells, which employ infinitesimal rotations as nodal coordinates, are considered nonisoparametric elements. Rigid body motion of such elements does not lead to zero strains and rigid body inertia cannot, in general, be exactly modeled (Shabana, 2014). Therefore, before introducing the FE/FFR formulation in the early eighties, an incremental approach was needed when these elements are used in the analysis of large rotation problems. Because the incremental solution of linearized system of equations eventually deviates from correct solution, there was a need to develop a new FE formulation that correctly describes rigid body motion when nonisoparametric elements are used. For this reason, the FFR formulation was introduced. In this formulation, a floating body coordinate system which shares the large displacement and rotation of the body is introduced. The large displacement of the body can be described using the global position of the floating frame origin and a set of orientation parameters that can be used to define the FFR transformation matrix. The use of these independent *reference coordinate*s is sufficient

70

to describe correctly the rigid body motion. Nonetheless, the introduced body coordinate system allows only modeling simple geometries that do not have any slope discontinuities as the one shown in Fig. 33. On the other hand, complex geometries that consist of elements with different orientations as shown in Fig. 34 can be modeled using the concept of the *intermediate element coordinate system*. This coordinate system has an origin that is rigidly attached to the origin of the body coordinate system and has axes that are initially parallel to the axes of the finite element coordinate system as shown in Fig. 35. Using this coordinate system, the finite elements that have different orientations can be connected rigidly using linear algebraic constraint equations at a preprocessing stage. Therefore, the FE/FFR formulation provides a general solution for accurately modeling structural geometric discontinuities using linear connectivity conditions. This leads to an FE mesh that is locally linear allowing for the use of coordinate reduction techniques to filter out high frequency modes of vibration.
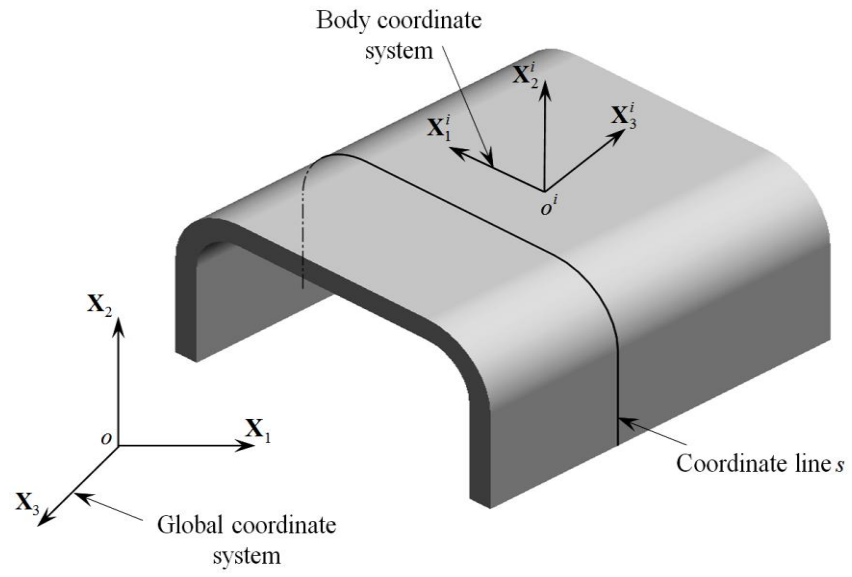
Figure 33 Structure without slope discontinuity
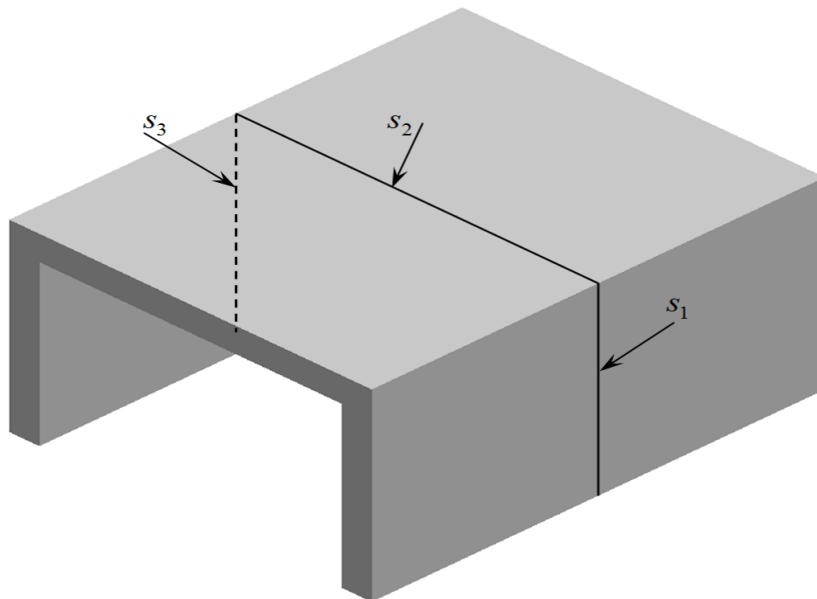
Figure 34 Structure with slope discontinuity
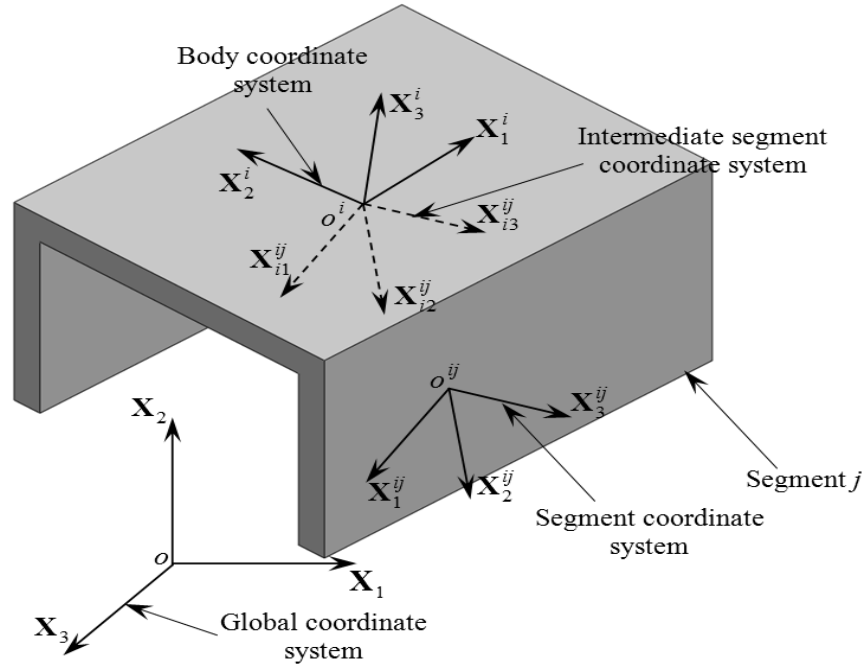
Figure 35 Intermediate coordinate system

Another type of slope discontinuity is the nonstructural discontinuity which permits the relative rigid body displacements between the segments connected. Example of which is a chain of links connected by pin joints as the one shown in Fig. 36. In the case of large relative rotation between the connected links, the dynamics of these chains, even for a planar rigid-link chain, is governed by highly nonlinear equations as the result of the geometric nonlinearities due to the finite relative rotations (Korkealaakso et al, 2009). For this type of joints, the FFR or rigid body formulations lead to a highly nonlinear connectivity conditions as the result of using orientation parameters. Furthermore, the resulting joint formulations do not include any deformation modes since the resulting joint degrees of freedom define only relative rigid body displacements.
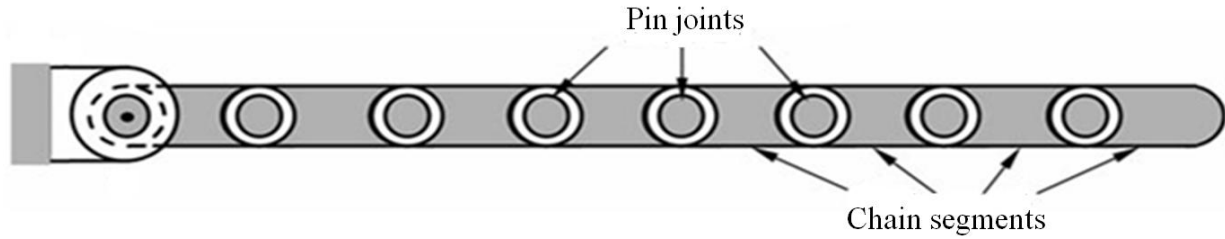
Figure 36 Eight-link chain

A systematic approach for modeling joints between flexible bodies using ANCF finite elements was introduced by Sugiyama et al (2003). In their work, tangent frames were used to define transformation matrices at the joint definition points. This approach leads to complex nonlinear constraints that are adjoined to the system equations of motion using the technique of Lagrange multipliers. Nonetheless, as demonstrated in previous chapters, a linear finite element mesh of chains that consist of flexible links can be developed in many MBS applications (Vallejo et al., 2003; Hamed et al, 2011; Shabana et al, 2012). This can be achieved using ANCF finite elements which allow for developing an FE mesh that includes one or more chains with flexible links, and each of the links can have independent relative finite rotations. The connectivity conditions between the ANCF finite elements can be described using linear algebraic constraint equations that can be used at a preprocessing stage to eliminate redundant variables. The use of this new concept can lead to significant simplification of the MBS algorithm and can eliminate the distinction between the augmented and recursive methods. Both the augmented and recursive methods will converge to approximately the same CPU time. Figure 37 shows two flow charts that describe the steps of the dynamic analysis of two different ANCF chains defined using the conventional nonlinear constraint approach and the new linear ANCF constraint approach.

74
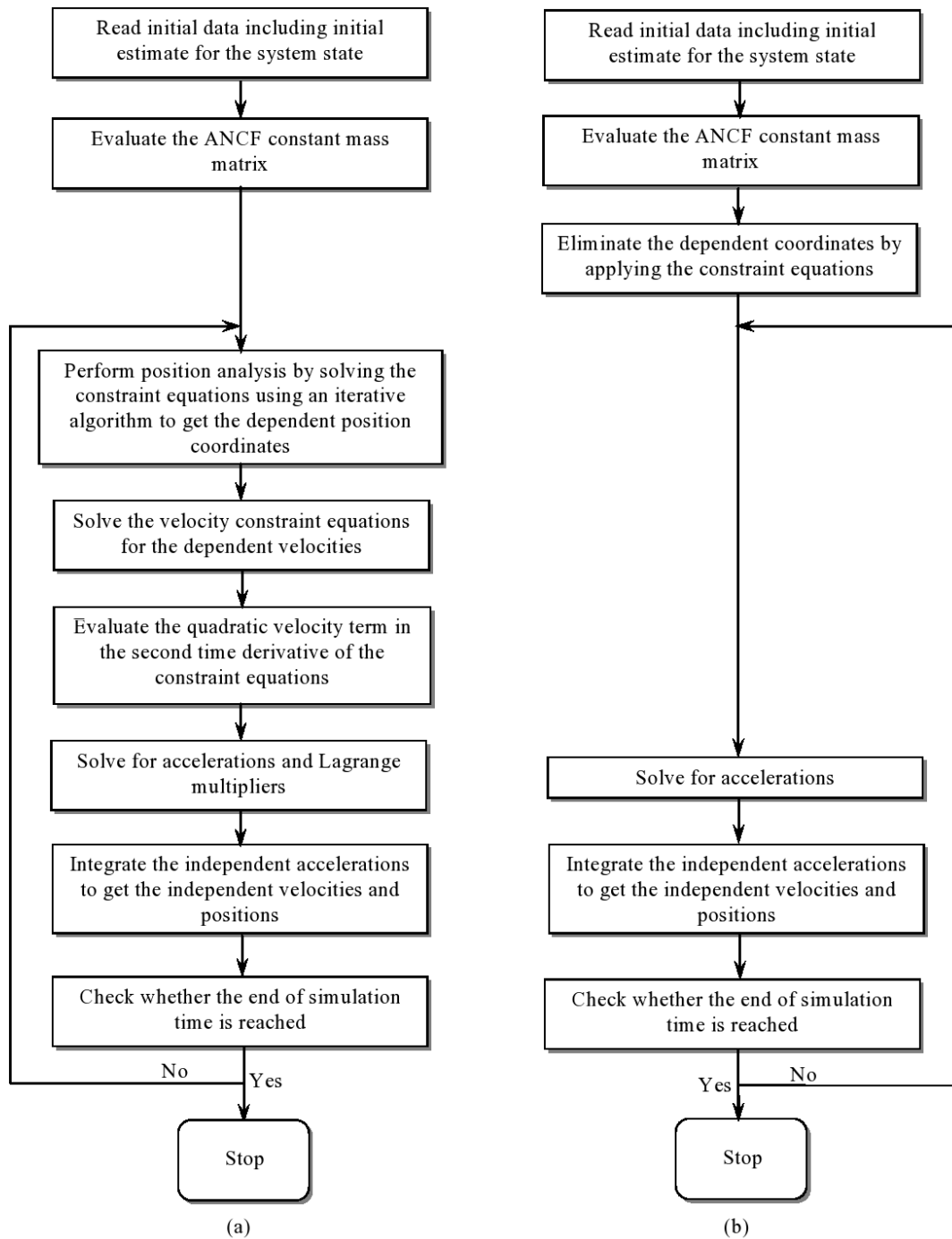
Figure 37 Flow chart of the dynamic analysis of ANCF chains
(a)Nonlinear constraints   (b) New linear constraints

It is clear that using the new ANCF linear constraint approach is more efficient since it eliminates many of the time-consuming steps of the conventional approach. For instance, when the new approach is used, there is no need to solve the constraint equations at the position, velocity or acceleration levels. Furthermore, the dimension of the system differential/algebraic equations will be significantly reduced as a result of the elimination of dependent variables and the associated Lagrange multipliers.

4.3. <u>ANCF Joint Formulations and Deformation Modes</u>

As mentioned in previous chapters, using ANCF finite elements, mechanical joints between finite elements can be formulated using linear connectivity conditions (Vallejo et al., 2003; Hamed et al, 2011; Shabana et al, 2012). This is an important feature that can be exploited to significantly reduce the number of nonlinear algebraic constraint equations and the associated Lagrange multipliers in many MBS applications. Several flexible bodies can be modeled as one FE mesh consisting of elements that have relative translations and finite rotations with respect to each other. This section expands the discussion of the ANCF linear joints using several examples, and shows how ANCF finite elements can also reduce the degree of nonlinearity when linear joint formulations cannot be obtained for some joints. The modes of the deformation of the new ANCF joints are also discussed in this section. Before discussing different ANCF joint formulations, it is important to point out that not all joints can be formulated using linear ANCF connectivity conditions. More research on this important topic will provide the answers to the question of which joints can have linear connectivity conditions that allow for the elimination of the dependent variables at a preprocessing stage. In fact, there can be also hybrid joints that have both linear and nonlinear constraint equations. The linear constraint equations can be eliminated

at a preprocessing stage, while the nonlinear equations can be coupled to the system differential

equations and treated during the dynamic simulation.

4.3.1. Spherical Joint

When two bodies or finite elements are connected by a spherical joint, one has C^0

continuity that ensures only the continuity of the position coordinates. The two connected bodies

can arbitrarily rotate with respect to each other. For a spherical joint between two finite elements

i and j, the algebraic spherical joint constraint equations can be written as

$$\mathbf{r}^{i,B} = \mathbf{r}^{j,A},\qquad\qquad (4.1)$$

where A and B refer to the joint node on the finite elements i and j, respectively. The preceding

constraint equations eliminate the relative translation between the two finite elements. However,

since ANCF structural finite elements can correctly describe arbitrary rigid body rotations,

applying the linear algebraic equations of Eq. 4.1 at a preprocessing stage allows for developing

a FE mesh in which each finite element can have an independent rotational displacement. Note

that the above spherical joint constraints are linear in the ANCF coordinates. The same constraint

equations are highly nonlinear in the case of the rigid body or the FFR formulation (Shabana,

2001).

4.3.2. Pin Joint

The formulation of the three-dimensional ANCF linear pin joint will be discussed using

two different ANCF finite elements. The first element is the three-dimensional Euler-Bernoulli

beam element. This element has only one gradient vector tangent to the element center line and

considers only the axial and bending deformations. It employs one parameter in the longitudinal

direction which does not allow measuring the rotation of the beam about its axis in the straight undeformed reference configuration. Such an element is not suited for capturing certain shear modes resulting from torsion. Consequently, four constraint equations are sufficient to define the pin joint when this simple ANCF element is used. The first set of conditions is the continuity of the position coordinates at the joint definition point. This set of conditions can be imposed at a preprocessing stage by using the same position degrees of freedom for the two elements at the joint node. The second set of conditions constrain the normal to the gradient vectors at the joint point to be parallel to each other. This second set of conditions can also be introduced at a preprocessing stage by applying continuity on the component of the gradient vector in the direction of the joint axis. The constraint equations of a pin joint between two ANCF Euler-Bernoulli beam elements i and j can thus be written as follows:

$$\mathbf{r}^{i,B} = \mathbf{r}^{j,A}, \quad \left(\frac{\partial \mathbf{r}^{i,B}}{\partial x} \right)_{\alpha} = \left(\frac{\partial \mathbf{r}^{j,A}}{\partial x} \right)_{\alpha} \tag{4.2}$$

where $\alpha = 1, 2, \text{or } 3$ denotes the direction of the joint axis. The preceding equations represent a set of four scalar equations. The second equation in Eq. 4.2 is a scalar equation that equates the α th component of element i gradient vector along the joint axis to the corresponding α th component of element j gradient vector. For example, if the joint axis is the element y axis, then in this case $\alpha = 2$. Note that the second set of algebraic equations can be formulated at a preprocessing step and can be used to eliminate dependent variables before the start of the dynamic simulation. Using the preceding equations, one can develop one linear FE mesh for flexible-link mechanisms in which the links can have arbitrarily large relative rotations and large deformations without the need to include nonlinear algebraic constraint equations in the

78

formulation since these conditions can be eliminated at a preprocessing stage. Note that for the gradient deficient Euler-Bernoulli beam element, the joint axis needs to be one of the finite element axes in order to obtain the linear relationships of Eq. 4.2. This restriction, which can be relaxed when using fully parameterized ANCF finite elements, does not represent a serious limitation when chain models are developed.

Another example of ANCF finite elements is the three-dimensional shear deformable beam element. A node on this fully parameterized ANCF element has 12 degrees of freedom. These degrees of freedom include three rigid body translations, three rotations, and six deformation modes. In order to define linear connectivity conditions for the pin joint, it is assumed that the normal strains of the two bodies in the direction of the joint axis are equal at the joint definition point. This condition implies that the joint axis does not stretch. If this condition is relaxed, the pin joint can be represented by three linear algebraic equations and two nonlinear algebraic equations. The three linear constraint equations can be imposed at a preprocessing stage, allowing for the elimination of a subset of the dependent variables. One may then introduce a pin joint formulation that uses the following six scalar equations defined at the joint node between elements i and j (Shabana et al, 2012).

$$\mathbf{r}^{i,B} = \mathbf{r}^{j,A} \ , \ \frac{\partial \mathbf{r}^{i,B}}{\partial \beta} = \frac{\partial \mathbf{r}^{j,A}}{\partial \beta} \ . \tag{4.3}$$

In the above equations, β is the coordinate that defines the joint axis. It can be either x, y, z, or any other coordinate line since the use of ANCF finite elements allows for a straightforward application of the gradient tensor transformation. The six scalar equations represented by Eq. 4.3 define a pin joint with six degrees of freedom: one rotation and five

79

deformation degrees of freedom. Consequently, the joint leads to C^1 continuity for the gradient vector along the coordinate line β and C^0 continuity for the remaining gradient vectors.

4.3.3. **Sliding Joint**

Sliding joints between flexible bodies are examples of variable boundary conditions joints. Developing the kinematic equations of these joints using the FFR formulation that employs linear modes can be difficult because of the change of the boundary conditions. On the other hand, these joints can be systematically formulated using ANCF finite elements as explained in the literature (Sugiyama et al, 2003). Using ANCF finite elements, a procedure was introduced to model the sliding joints using local frames defined at the joint definition point. A tangent frame can be used to define a joint local coordinate system whose transformation matrix at the joint definition point can be evaluated. In order to define the time derivative of the constraint equations, the time derivatives of the columns of the transformation matrices are written as function of the generalized coordinates and velocities. This procedure leads to complex constraint equations that are difficult to implement. The same joint constraints can be formulated using a simple and straightforward approach by introducing two *non-generalized coordinates*. The first non-generalized coordinate u defines the local position of the joint definition point on the base element as shown in Fig. 38, while the second one m defines the ratio between lengths of the two element position gradient vectors in the direction of the sliding axis. The following equations can be used to define the constraint equations of the sliding joint:

$$\mathbf{C}(\mathbf{e}^i, \mathbf{e}^j, u^i) = \mathbf{r}_p^i(\mathbf{e}^i, u^i) - \mathbf{r}_p^j(\mathbf{e}^j) = \mathbf{0}, \quad \frac{\partial \mathbf{r}^i}{\partial \zeta} = m \frac{\partial \mathbf{r}^j}{\partial \gamma} \quad . \tag{4}$$

80

In the above equations, ζ and γ are the coordinate lines in the direction of the joint axis on each element, and, $\mathbf{e}^i$ and $\mathbf{e}^j$ are the nodal coordinates of the two finite elements. These constraint equations can be applied to constrain 4 of the joint degrees of freedom: 2 rigid rotations, and 2 rigid translations. The sliding is ensured by requiring continuity of the gradient along the sliding axis and preventing the joint definition point from moving normal to the direction of the sliding axis. This guarantees the freedom of sliding without the need to define local frames which lead to complex constraint equations required to ensure the parallelism of the sliding axes.

Figure 38 Sliding joint

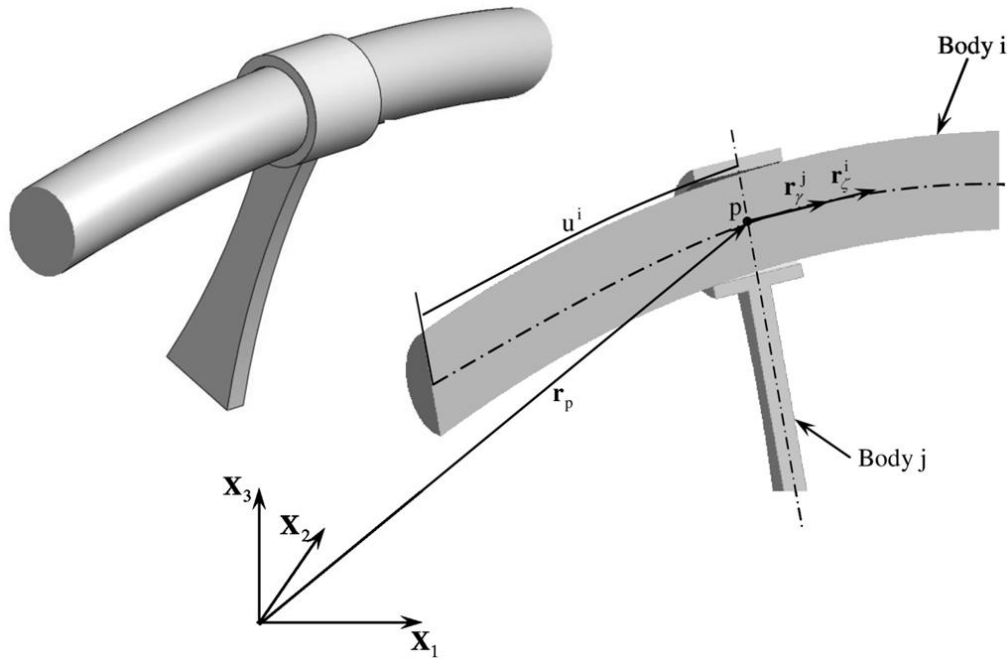### 4.3.4. ANCF Joint Deformation Modes

In rigid body and small deformation FFR MBS algorithms, joint formulations allow for only relative rigid body degrees of freedom that describe the relative displacements between two rigid triads attached to the two bodies connected by the joint. The ANCF joint formulations, on the other hand, allow for deformation modes at the joint definition point. This leads to a new

class of *ideal compliant joints* defined using algebraic equations. The gradient vectors of the two elements can change their magnitude and orientation allowing for stretch and shear deformations at the joint node. Depending on the element type and the number of algebraic equations used in the formulation of the joint, different deformation modes can be captured. As an example, the gradient deficient Euler-Bernoulli beam element allows for only the axial, bending, and twist. Therefore, such an element does not capture shear and cross section deformations. On the other hand, the fully parameterized beam element which has a complete set of gradient vectors can be used to capture the change in the cross section due to deformation at the joint node. For the fully parameterized beam element, the modes of deformations at the joint nodes can be examined using the Green-Lagrange strain tensor $\boldsymbol{\varepsilon}$ which can be written as $\boldsymbol{\varepsilon} = \frac{1}{2}\left(\mathbf{J}^T \mathbf{J} - \mathbf{I}\right)$, where $\mathbf{J}$ is the matrix of position vector gradients, and $\mathbf{I}$ is the identity matrix. Because the strain tensor $\boldsymbol{\varepsilon}$ is symmetric, one can define the strain vector $\boldsymbol{\varepsilon}_v = \begin{bmatrix} \varepsilon_{xx} & \varepsilon_{yy} & \varepsilon_{zz} & \varepsilon_{xy} & \varepsilon_{yz} & \varepsilon_{zx} \end{bmatrix}^T$, where ε_{xx}, ε_{yy} and ε_{zz} are the normal strains, and ε_{xy}, ε_{yz} and ε_{zx} are the shear strains. The strain components are continuous inside the element and some of the strain components can be discontinuous at the joint nodes because of the discontinuity of position vector gradients at these nodes. Figure 39 shows some of the deformation modes of the three-dimensional fully parameterized beam element. These modes are the stretch mode, the bending mode, and one of the cross section deformation modes. The stretch mode is a result of changing the magnitude of the gradient $\mathbf{r}_x$ at the joint point. The bending mode is due to the change of the orientation of the gradient vector $\mathbf{r}_x$ with respect to the line connecting the two nodes of the element. Finally, the cross section deformation mode defines the change of the cross section dimensions which is the result of the

change in the magnitude of the gradient vectors along the cross section fibers. Furthermore, the

second condition of Eq. 4.3, $\left(\partial \mathbf{r}^{i,B}/\partial\beta\right)=\left(\partial \mathbf{r}^{j,A}/\partial\beta\right)$, allows for the stretch of the joint pin.
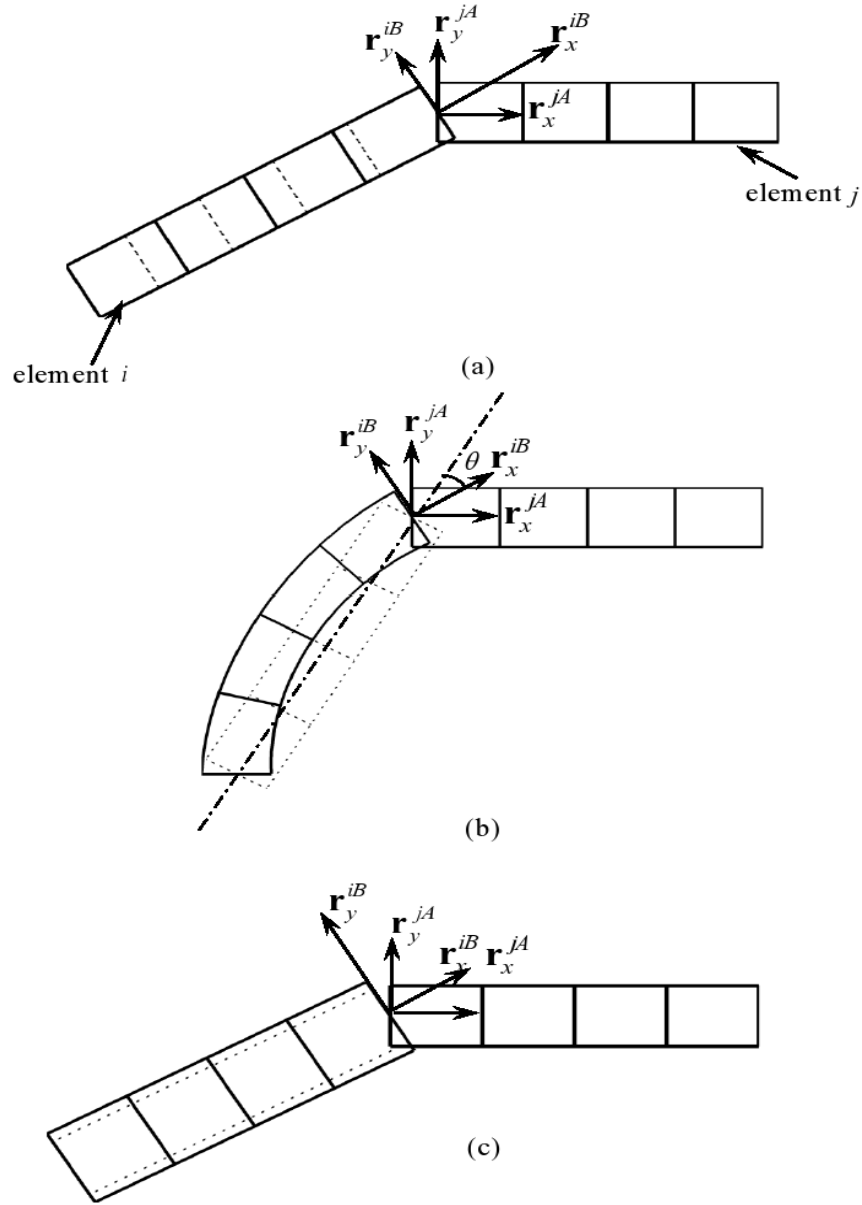
Figure 39 Deformation modes
(a) Stretch mode   (b) Bending mode   (c) Cross section deformation

4.4. <u>Comparison with the Iso-geometric Approach</u>

Computational geometry methods such as B-spline and NURBS (Non-Uniform Rational B-Splines) use control points as coordinates. The control points do not necessarily represent material points. This is one of the fundamental differences between computational geometry methods and the finite element method. The *isogeometric analysis* is a concept aims at unifying the two fields of *computer aided design* (CAD) and *finite element analysis* (FEA) by using the same basis for the geometry description and analysis (Hughes et al, 2005). This concept, which has been used in computer science for many years to build physics based models, has recently received attention from the computational mechanics community. The increasing interest in isogeometric analysis is motivated by the desire to deal with the difficulties and cost associated with the conversion of solid models to FE analysis models. This conversion process leads to distortion of the geometry of the analysis model because existing structural elements such as beams, plates and shells cannot describe correctly arbitrary geometry.

As discussed earlier, while the use of the isogeometric analysis can be considered as a step in the right direction, the use of computational geometry methods as analysis tool can lead to fundamental implementation problems which can be avoided by using ANCF geometry. This section expands on the discussion of some of the limitations of computational geometry methods when used as analysis tools. The discussion will focus on the limitations associated with the joint formulations which is the subject of the thesis.

4.4.1. <u>Basis Functions</u>

ANCF geometry does not impose restrictions on the number of basis functions used in the interpolating polynomials. In contrast, B-spline rigid recurrence formula restricts the number

of basis functions depending on the degree of the interpolating functions; there is a relationship between the polynomial degree, the number of knots, and the number of control points. If $r+1$ is the number of knots in $\mathbf{U}$ and $s+1$ is the number of knots in $\mathbf{V}$, then in B-spline geometry, one must have

$$r = n + p + 1, \quad s = m + q + 1 \tag{4.7}$$

Using Eq. 4.7, one can show that if a cubic interpolation is used for both u and v, as in the case of a thin plate, the B-spline representation requires 16 control points regardless of whether the shape of deformation of the plate is simple or complex (Shabana et al, 2012). This can be a disadvantage in the analysis since such a geometric representation can unnecessarily increase the dimension of the analysis model and leads to a loss of the flexibility offered by the FE method. As the degree of the polynomial interpolation increases, this drawback of B-spline becomes more serious.

4.4.2. Knot Multiplicity

In computational geometry methods, a decrease in the knot multiplicity by one leads to elimination of one control point and to an increase in the degree of continuity by one. The knot multiplicity cannot be used to impose continuity condition on only one element of a position vector or a gradient vector. In three-dimensional analysis, a minimum of three scalar equations are automatically imposed when the knot multiplicity is decreased by one. Some ideal compliant joints, as discussed in this chapter, may require imposing only one or two algebraic equations to obtain a certain degree of continuity for one or two elements of a position or gradient vector. Such ideal compliant joint constraints cannot be formulated using the rigid B-spline and NURBS knot multiplicity concept.

4.4.3. <u>Structural Discontinuities</u>

Structural discontinuities, such as T-, L-, and V-sections, which can be thought of as a sudden change in geometry, represent discontinuities in gradients as the result of the discontinuities of the coordinate lines (directions). Modeling this type of discontinuity, which characterizes both mechanical and structural systems, requires the use of gradient transformation which is fundamental in the implementation of the ANCF geometric representation (Hamed et al, 2011). Using C^0 continuity in B-spline analysis is equivalent to having a pin joint in the planar analysis and to a spherical joint in the spatial analysis. The case of structural discontinuity, which is also of the C^0 type, requires additional algebraic equations in order to eliminate the relative rotation at the joint definition point. Therefore, there are important geometric configurations where the degree of continuity does not change by eliminating degrees of freedom or equivalently control points. These important geometric configurations cannot be covered by the rigid structure of the B-spline and NURBS which relates the number of degrees of freedom or the control points to the degree of continuity (knot multiplicity).

4.4.4. <u>Sliding Joints</u>

Another important geometric scenario associated with the ideal compliant constraints is the sliding joint. This type of joint requires continuity of the gradients, but not continuity of all position coordinates. In the B-spline representation, C^1 requires first C^0 continuity. As previously discussed, ANCF representation does not require this sequence, and for this reason, such an ANCF representation can be used to model the sliding joint in a straightforward manner. Modeling the same joint using B-spline geometry is not as straight forward: at a given breakpoint, the multiplicity associated with a knot can be used to change the continuity of the

derivatives. For example, in the case of cubic interpolation, C^0, C^1, and C^2 conditions correspond, respectively, to knot multiplicity of three, two, and one. Applying higher degree of continuity implies all lower degree continuity. In other words, a knot multiplicity of one which corresponds to C^2 implies C^0 and C^1 continuity. Similarly, applying C^1 implies C^0 continuity. Therefore, B-spline structure does not allow applying continuity on position gradients without position continuity. Therefore, two sliding bodies must be modeled as two separate meshes and additional algebraic constraint equations must be added to guarantee the sliding motion.

4.5. <u>Use of ANCF for Small Deformation Problems</u>

Chains are used in many important MBS applications, and therefore, it is important to be able to develop efficient and accurate chain models, particularly when the link flexibility is considered. For example, chains are critical in defining the mobility of tracked vehicles that consist of a large number of components interconnected by joints and force elements. The dynamics of such systems are governed by complex relationships as result of the relative motions and joint forces. Furthermore, considering the flexibility of the track links increases the system complexity, model dimension, and degree of nonlinearity. For this reason, it is necessary to carefully select the procedure used to model the flexible links and the joints connecting them in a chain structure.

As previously discussed, an efficient formulation that can be used to model complex chain systems is the ANCF which allows for the elimination of the joint constraint equations at a preprocessing stage, allowing for the elimination of the joint dependent variables before the dynamic simulation starts and leading to a chain mesh that has a constant inertia matrix and zero Coriolis and centrifugal forces. Furthermore, the ANCF geometry description, in contrast to

conventional finite elements, is consistent with the descriptions used in computational geometry methods (Lan and Shabana, 2010; Mikkola et al, 2013).

While ANCF allows for the use of a general continuum mechanics approach, special elastic force models can be derived and implemented in ANCF/MBS algorithms for the solution of specific applications. In the case of the tracked vehicle model considered in subsequent sections, the deformation of the track links is small. Nonetheless, the development of an FFR model to study the flexible link chain dynamics is not recommended because of the following specific reasons:

1. The FFR formulation leads to a highly nonlinear mass matrix and complex non-zero Coriolis and centrifugal forces. On the other hand, ANCF leads to a constant inertia matrix and zero Coriolis and centrifugal forces. ANCF Cholesky coordinates can be used to obtain an identity generalized inertia matrix, leading to an optimum sparse matrix structure.

2. The FFR formulation leads to highly nonlinear constraint equations for the joints between the chain links. These constraint equations must be satisfied at the position, velocity, and acceleration levels, and as discussed before, contribute to increasing the problem dimensionality and the array storage needed. In the case of flexible-link chains, the overhead can be significant. On the other hand, ANCF finite elements allow for the formulation of linear connectivity conditions, and therefore, the dependent variables can be eliminated systematically at a preprocessing stage. The use of the new ANCF meshes can lead to significant simplification of the solution algorithm and significant reductions in the array storage as previously discussed.

3. In both rigid and FFR chain models, the use of closed chains can lead to singular configurations if one set of independent coordinates is used. This is not the case when the new ANCF models are used. No singularities are encountered because the joint constraint equations and the joint dependent variables are eliminated at a preprocessing stage.

4. In the case of simple geometry, one chain link can be modeled using one finite element. Therefore, the FFR coordinate reduction methods will not be advantageous, particularly if the high frequency axial modes need to be included in the model in order to capture the link tension forces. Furthermore, in tracked vehicle applications, the contact forces have very high frequency contents that can be comparable to the frequencies that results from the elastic forces.

Because of these reasons, the large deformation ANCF finite elements can be effectively used to efficiently solve small deformation problems. ANCF finite elements allow for implementing small deformation elastic forces models as described in the following section.

4.6. Small Deformation ANCF Elastic Force Model

In this section, a simple force model, which can be used in the analysis of small deformation based on a three-dimensional ANCF Euler-Bernoulli beam, is introduced. The developed force model accounts for the coupling between bending and axial deformations. The model can be considered as a generalization of the two-dimensional force model developed by Berzeri et al (2001). Despite the simplicity of the proposed force model, it accounts for the elastic nonlinearity in the strain-displacement relationship.

4.6.1. Generalized Elastic Forces

The strain energy of the Euler-Bernoulli beam element can be written as a function of longitudinal strain ε_x and curvature κ as (Gerstmayr and Shabana, 2006; Shabana, 2012)

89

$$U = \frac{1}{2} \int_0^l [EA\varepsilon_x^2 + EI\kappa^2]dx \ . \tag{4.8}$$

In the preceding equation, x is the longitudinal coordinate, l is the length of the element, E is the modulus of elasticity, A is the cross section area, and I is the second moment of area. The expression for the vector of elastic forces can be determined by differentiating the strain energy with respect to the ANCF coordinates as

$$\mathbf{Q}_e = \left(\frac{\partial U}{\partial \mathbf{e}}\right)^{\mathrm{T}} = \int_0^l [EA\varepsilon_x \frac{\partial \varepsilon_x}{\partial \mathbf{e}} + EI\kappa \frac{\partial \kappa}{\partial \mathbf{e}}]dx \ . \tag{4.9}$$

In the computer implementation, it is possible to derive the expressions for the derivatives in Eq. 4.9 by means of a symbolic computer program, or to derive them analytically in order to minimize the number of mathematical operations. Closed form expressions for the derivatives of both the axial strain and the curvature can be written as shown in (Gerstmayr and Shabana, 2006). The elastic force expressions were modified based on the curvature definition given in (Gerstmayr and Irschik, 2008) as

$$\left. \begin{aligned} &\frac{\partial \varepsilon_x}{\partial \mathbf{e}} = \mathbf{S}_x^T \mathbf{r}_x, \qquad \frac{\partial k}{\partial e_i} = \frac{1}{g^2}\left(g\frac{\partial f}{\partial e_i} - f\frac{\partial g}{\partial e_i}\right), \quad f = \left|\mathbf{r}_x \times \mathbf{r}_{xx}\right|, \\ &\frac{\partial f}{\partial e_i} = \left((\mathbf{r}_x \times \mathbf{r}_{xx})^{\mathrm{T}}(\mathbf{r}_x \times \mathbf{r}_{xx})\right)^{-1/2}\left((\mathbf{r}_x \times \mathbf{r}_{xx})^{\mathrm{T}}\left(\frac{\partial}{\partial e_i}\mathbf{r}_x \times \mathbf{r}_{xx} + \mathbf{r}_x \times \frac{\partial}{\partial e_i}\mathbf{r}_{xx}\right)\right), \\ &g = \left|\mathbf{r}_x\right|^2, \qquad \frac{\partial g}{\partial e_i} = 2\left(\mathbf{r}_x \frac{\partial \mathbf{r}_x}{\partial e_i}\right) \end{aligned} \right\} \tag{4.10}$$

The computation of these complex expressions can be time consuming, especially, for models containing a large number of elements. Berzeri et al (2001) introduced a simple model for the elastic forces of the planar Euler-Bernoulli beam element. Their model can be extended to

the spatial Euler-Bernoulli beam element assuming small longitudinal deformation, which is the

case for the steel track links used in the chains of the tracked vehicle model considered in the

next section. The expression for the elastic forces due to longitudinal forces can be written as

$$\mathbf{Q}_{e,l} = \int_0^l EA\varepsilon_x \frac{\partial \varepsilon_x}{\partial \mathbf{e}} dx = \int_0^l EA\varepsilon_x \mathbf{S}_x^T \mathbf{S}_x \mathbf{e} dx.$$ (4.11)

By assuming small variation of the strain over the length of the beam, the strain ε_x can be

factored out from the expression of the elastic forces, allowing writing the preceding equation as

$$\mathbf{Q}_{e,l} = EA\bar{\varepsilon}_x \int_0^l \mathbf{S}_x^T \mathbf{S}_x dx \mathbf{e} = \mathbf{K}_{e,l} \mathbf{e},$$ (4.12)

where $\mathbf{K}_{e,l} = EA\bar{\varepsilon}_x \int_0^l \mathbf{S}_x^T \mathbf{S}_x dx$. The average axial strain can be simply calculated as $\bar{\varepsilon}_x = (d-l)/l$

where d is the current length of the beam.

The expression of the elastic forces due to bending can be written as

$$\mathbf{Q}_{e,t} = \int_0^l EI\kappa \frac{\partial \kappa}{\partial \mathbf{e}} dx.$$ (4.13)

In the case of small longitudinal deformation, the curvature can be defined as $|\mathbf{r}_{xx}|$.

Hence, the transverse elastic forces can be written as

$$\mathbf{Q}_{e,t} = EI \int_0^l \mathbf{S}_{xx}^T \mathbf{S}_{xx} dx \mathbf{e} = \mathbf{K}_{e,t} \mathbf{e},$$ (4.14)

91

where $\mathbf{K}_{e,t} = EI \int_0^l \mathbf{S}_{xx}^T \mathbf{S}_{xx} dx$.

Finally, the elastic force vector can be written as

$$\mathbf{Q}_e = (\mathbf{K}_{e,l} + \mathbf{K}_{e,t})\mathbf{e}, \tag{4.15}$$

where $\mathbf{K}_{e,l}$ and $\mathbf{K}_{e,t}$ are constant stiffness matrices associated with longitudinal and bending elastic forces, respectively.

4.6.2. <u>Generalized Damping Forces</u>

The internal damping characteristics of most known materials lead to energy dissipation when the materials are subjected to initial disturbances or shock loadings. Therefore, developing realistic flexible MBS models requires the inclusion of the effect of internal damping. One of the advantages of ANCF finite elements is the ability of capturing modes of deformations that cannot be captured using existing structural finite elements (Mohamed and Shabana, 2011). In some applications, some of these ANCF modes, which can have high frequencies, may not have significant effect on the solution. In such cases, explicit numerical integration schemes are forced to select very small time steps to capture the high frequencies. Therefore, for such applications, it is desirable to damp out these high frequency modes by using an appropriate visco-elastic constitutive model. This subsection introduces a suitable damping model that can be used with the simple elastic force model introduced in the previous section. The damping model introduced is also based on the assumption of small deformation.

The proposed visco-elastic model applies damping to the deformation associated with the gradient vector $\mathbf{r}_x$ and the curvature vector $\mathbf{r}_{ss}$ where s is the arc length. In order to properly define the deformation and avoid damping out rigid body displacement modes, a tangent frame

can be used to define an orthogonal matrix using the vectors $\mathbf{r}_x$ and $\mathbf{r}_{ss}$ as

$\mathbf{R} = \begin{bmatrix} \dfrac{\mathbf{r}_x}{|\mathbf{r}_x|} & \dfrac{\mathbf{r}_x \times \mathbf{r}_{ss}}{|\mathbf{r}_x \times \mathbf{r}_{ss}|} & \dfrac{\mathbf{r}_{ss}}{|\mathbf{r}_{ss}|} \end{bmatrix}$. The power dissipated can be written as a function of the damping

stress $\boldsymbol{\sigma}_d$ and the strain rate $\dot{\boldsymbol{\varepsilon}}$ as (Vallejo et al, 2005)

$$P_d = \frac{1}{2}\int_V \boldsymbol{\sigma}_d^{\mathrm{T}}\,\dot{\boldsymbol{\varepsilon}}\,dV\,. \tag{4.16}$$

Following a procedure similar to the one given in (Mohamed and Shabana, 2011; Mohamed, 2011), the power dissipated can be rewritten in the case of the Euler-Bernoulli beam element as

$$P_d = \frac{1}{2}\int_0^l \boldsymbol{\sigma}_d^{\mathrm{T}} \begin{bmatrix} A & 0 \\ 0 & I \end{bmatrix} \begin{bmatrix} \dot{\varepsilon}_x & \dot{\kappa} \end{bmatrix} dx\,, \tag{4.17}$$

where $\dot{\varepsilon}_x$ and $\dot{\kappa}$ are the longitudinal strain rate and curvature rate. By differentiating the dissipated energy with respect to the absolute nodal velocities, the generalized damping force can be written as

$$\mathbf{Q}_d = \int_0^l (A(\frac{\nu_1 \dot{\varepsilon}_x}{1 + 2\varepsilon_x})\frac{\partial \varepsilon_x}{\partial \mathbf{e}} + I\nu_2 \dot{\kappa}\frac{\partial \kappa}{\partial \mathbf{e}})dx\,, \tag{4.18}$$

where ν_1 and ν_2 are two damping constants.

Using the assumption of small variation of the strain over the length, both the longitudinal strain and strain rate can be assumed constant through the length. Hence, the longitudinal damping force can be written as

$$\mathbf{Q}_{\mathrm{d,l}} = A \frac{v_1 \dot{\varepsilon}_x}{1 + 2\varepsilon_x} \int_0^l \mathbf{S}_x^{\mathrm{T}} \mathbf{S}_x \mathbf{e}\, dx = \mathbf{K}_{d,l} \mathbf{e} \tag{4.19}$$

where, $\mathbf{K}_{d,l} = A \left(v_1 \dot{\varepsilon}_x / \left(1 + 2\varepsilon_x\right)\right) \int_0^l \mathbf{S}_x^{\mathrm{T}} \mathbf{S}_x dx$. Using the same assumption, the curvature and

curvature rate can be assumed constant through the length. Therefore, the transverse damping

force can be written as

$$\mathbf{Q}_{d,t} = I \frac{\gamma_2 \dot{\kappa}}{\kappa} \int_0^l \mathbf{S}_{xx}^{\mathrm{T}} \mathbf{S}_{xx} \mathbf{e}\, dx = \mathbf{K}_{d,t} \mathbf{e}, \tag{4.20}$$

where. $\mathbf{K}_{d,t} = I \left(v_2 \dot{\kappa} / \kappa \right) \int_0^l \mathbf{S}_{xx}^{\mathrm{T}} \mathbf{S}_{xx} \mathbf{e} dx$. Then, the generalized internal damping force vector can be

written as

$$\mathbf{Q}_d = (\mathbf{K}_{d,l}(\mathbf{e}, \dot{\mathbf{e}}) + \mathbf{K}_{d,t}(\mathbf{e}, \dot{\mathbf{e}}))\mathbf{e} \tag{4.21}$$

These generalized damping forces can be introduced to the ANCF element equations.

The generalized damping forces associated with the ANCF Cholesky coordinates can also be

obtained using the Cholesky transformation.

4.7. <u>Numerical Results</u>

A flexible-link chain three-dimensional tracked vehicle example is used in this section to

demonstrate the implementation of the concepts discussed in this chapter. This example

represents a complex system with large number of bodies connected by large number of revolute

(pin) joints. Furthermore, the mathematical models of such vehicles represent a stiff numerical

integration problem due to high frequencies of the contact forces. Such vehicle models can be

used to test the robustness of the MBS algorithm developed.

4.7.1. <u>Model Description</u>

The tracked vehicle used is an armored personnel carrier that consists of a chassis and two track chains. Each track system consists of an idler, one sprocket, 5 road-wheels, and 64 track links. A schematic drawing of the selected tracked vehicle is shown in Fig. 40.
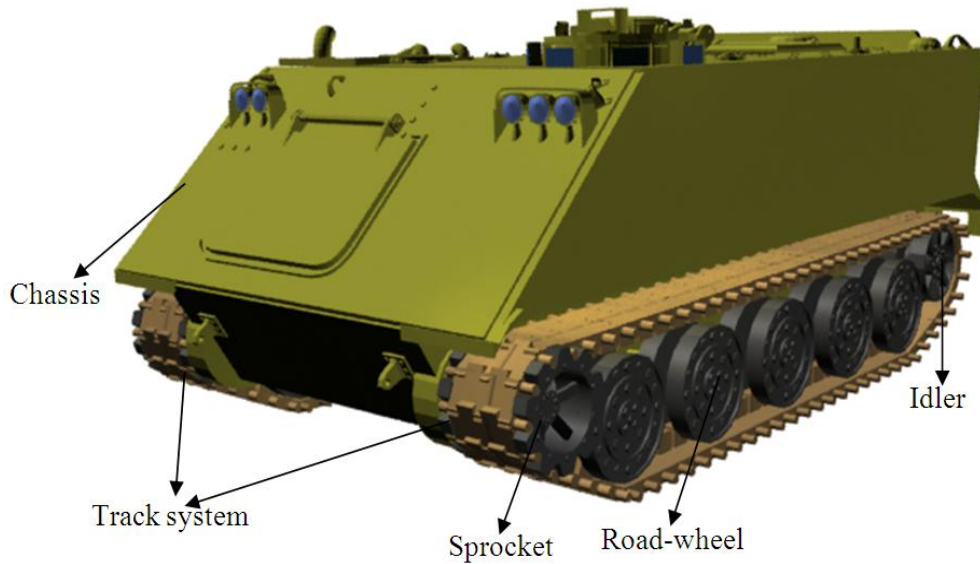
Figure 40 Tracked vehicle model

Table I shows the inertia properties for all the tracked vehicle model components used in this simulation. The vehicle has a suspension system that consists of a road arm, placed between each road wheel and the chassis, and a shock absorber that consists of a spring and a damper connecting each road arm to the chassis. In order to control the tension of the two tracks, each idler is connected to the chassis through a tensioner. Table II shows the stiffness coefficients k and the damping coefficients c of the contact models, the suspension system, and the tensioner; as well as the friction coefficient μ of the contact models. Ideal pin joints are used to connect the road arms and the sprockets to the chassis, and the road-wheels to the road arms. The normal

contact forces are calculated based on a linear dissipative contact force model (Choi et al, 1998; Maqueda et al, 2010; Dufva et al, 2007).

Table I. Tracked vehicle components inertia properties

Part	Mass (kg)	I_{XX} (kg m^2)	I_{YY} (kg m^2)	I_{ZZ} (kg m^2)	I_{XY}, I_{YZ}, I_{XZ} (kg m^2)
Chassis	5489.24	1786.92	10449.67	10721.22	0
Sprocket	436.67	13.87	12.22	12.22	0
Idler	429.57	14.70	12.55	12.55	0
Road Wheel	561.07	26.06	19.82	19.82	0
Road Arm	75.26	0.77	0.37	0.77	0
Track link	18.02	0.04	0.22	0.25	0

Table II. Tracked vehicle contact and suspension parameters

Parameters	Sprocket-Track Contact	Roller-Track Contact	Ground-Track Contact	Suspension	Tensioner
k (N/m)	2×10^6	2×10^6	2×10^6	1×10^6	1×10^6
c (N·s/m)	5×10^3	5×10^3	5×10^3	1.5×10^4	1.4×10^4
μ	0.15	0.10	0.30	-	-

The models discussed in this section are assumed to have flexible track links. The flexible links are defined as three-dimensional steel Euler-Bernoulli beam elements with a modulus of rigidity of 76.9 GPa, a Young's modulus of 200 GPa, and a mass density of 7800 kg/m^3. The flexible chain links are connected to each other using ANCF ideal compliant pin

joints, which define a linear ANCF mesh. As previously mentioned, one of the advantages of using this ANCF definition of joints is having linear joint constraints which allow for the elimination of the dependent joint variables at a preprocessing stage. As a result, this procedure avoids the computational cost required to formulate the nonlinear pin joint constraint equations at the position, velocity, and acceleration levels. In the case of the tracked vehicle used in this study, the proposed approach allows for the elimination of 126 pin joints which is equivalent to 630 highly nonlinear constraint equations at a preprocessing stage. In conventional MBS algorithms, this large number of highly nonlinear constraint equations must be satisfied at position, velocity, and acceleration levels. If ANCF joints are used, all these constraints become linear and can be eliminated at a preprocessing stage.

Three different tracked vehicle models are used to demonstrate the effectiveness of using the ANCF linear ideal compliant joint model. In the first vehicle, the chain links are modeled as rigid bodies. In order to solve the singularity problem encountered in the case of closed chain (Nakanishi and Shabana, 1994), the first and last links of the chain are connected through a very stiff spring. The links of the second and third tracked vehicle models are modeled as flexible links connected using ANCF continuum-based joints. The chain of the second model has a secondary joint by making a cut and using a very stiff spring to close the chain as in the case of the rigid-link chains. In the case of the third model, on the other hand, an ANCF closed loop chain is used. The third model is used to demonstrate the fact that using the new linear ANCF joint model does not lead to any singularity problems as in the case of conventional MBS nonlinear joint algorithms. An explicit Adams-Bashforth predictor-corrector method was used for the numerical solution of the system differential equations.

97

4.7.2. <u>**Rigid Body Motion**</u>

The angular velocities of the two sprockets of all the three tracked vehicle models were specified
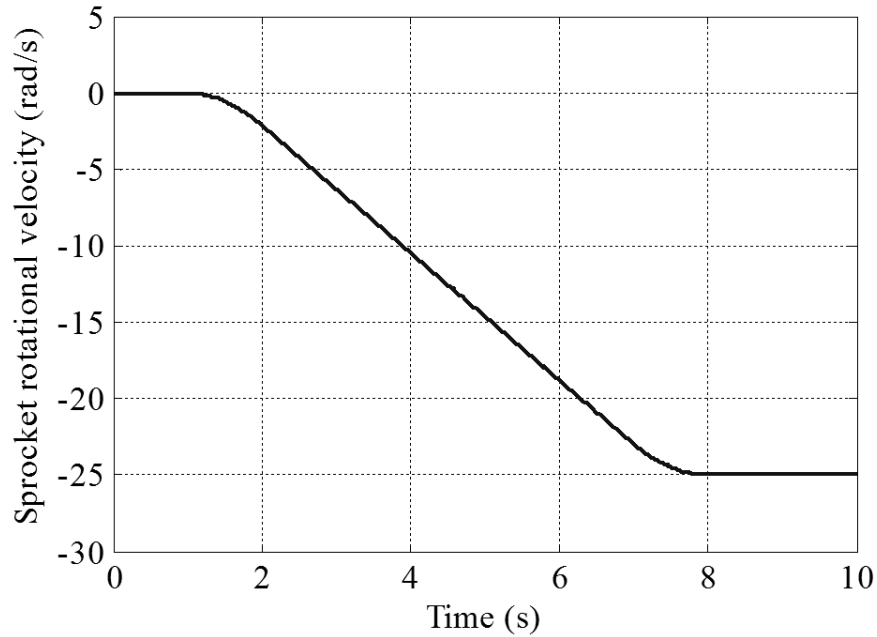
to follow the pattern shown in Fig. 41.

Figure 41 Sprocket rotational velocity

The response of the chassis to this input sprocket velocity is shown in Figs. 42-44. Figure

42 shows the forward velocity of the chassis. As expected, the velocity of the chassis follows the

same pattern as the sprocket velocity. The results of Fig. 43 and 44 show the forward and vertical

positions of the chassis center of mass. It can be noticed from the results presented in Fig. 44 that

the chassis has 0.03m downward displacement as a consequence of an initial settlement of the

suspension springs. These springs, in addition to the contact forces, deform under the effect of

the weight of the vehicle components until equilibrium positions are reached.

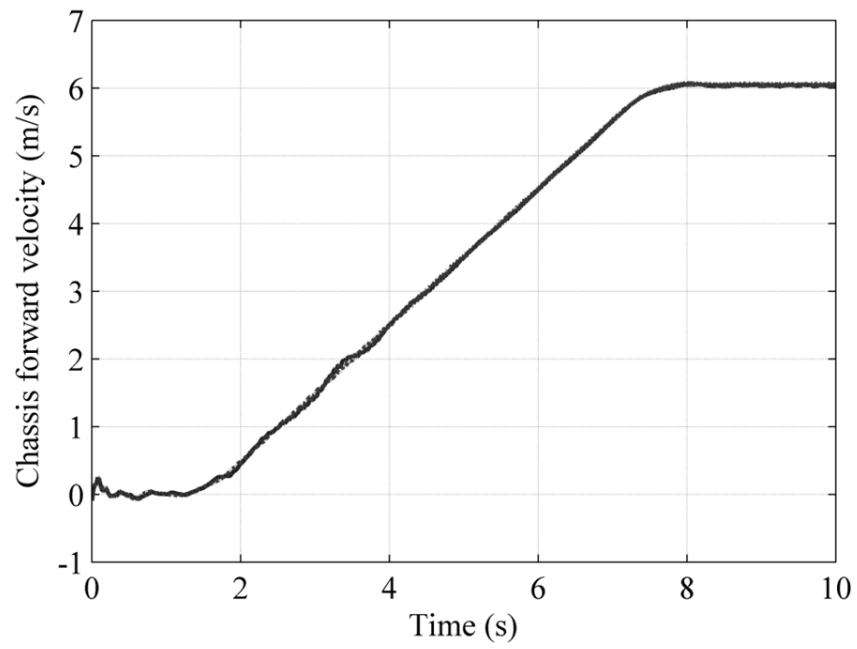Figure 42 Chassis forward velocity
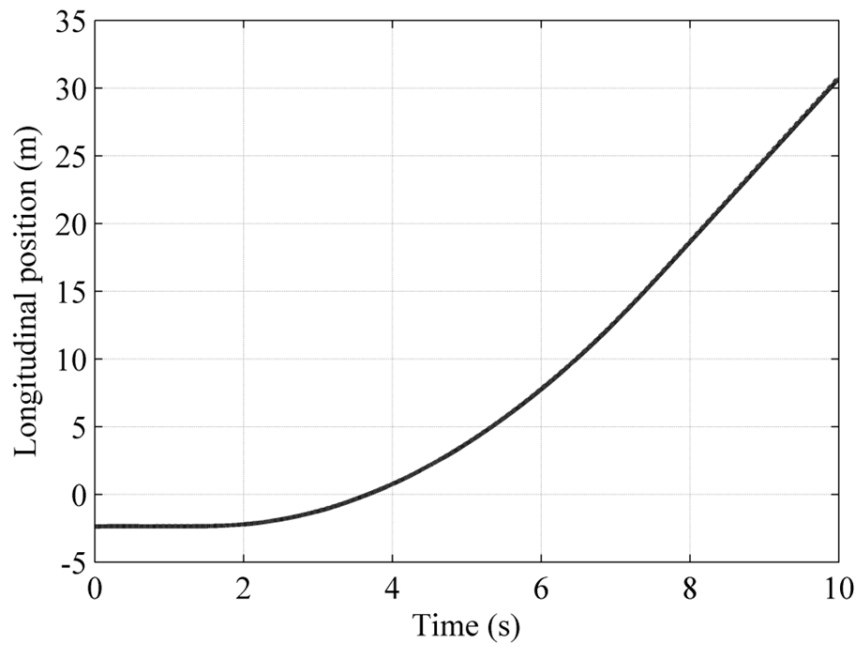(-·--·- Rigid model, ———— Closed loop flexible model, ------- Open loop flexible model)

Figure 43 Forward displacement of the chassis
(-·--·- Rigid model, ———— Closed loop flexible model, ------- Open loop flexible model)
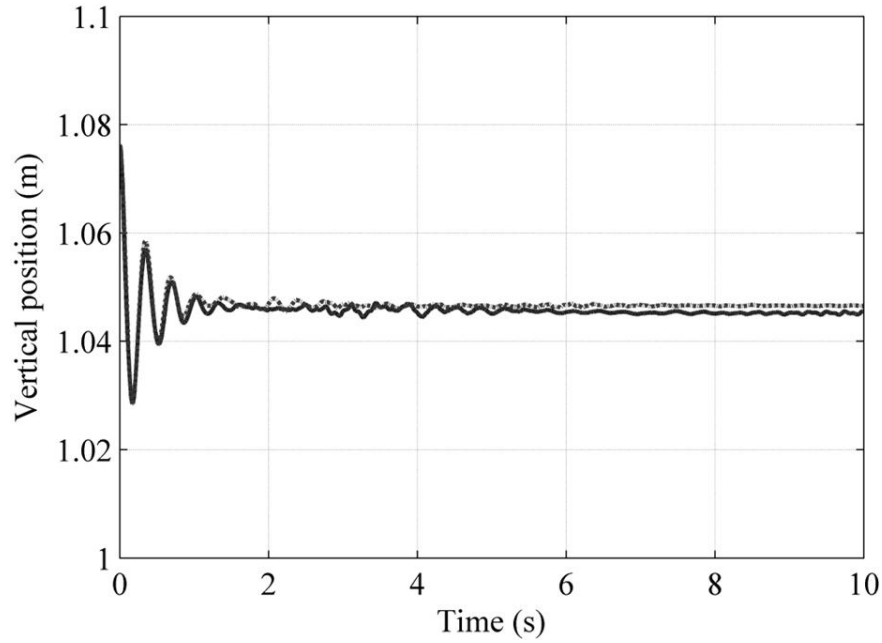
Figure 44 Vertical displacement of the chassis
(-·-·-·- Rigid model, —— Closed loop flexible model, ------- Open loop flexible model)

From the results presented in Figs. 42 to 44, it is clear that the rigid body motion results of the two flexible chain models are in a good agreement with the results of the rigid body model. Figure 45 shows the forward position of an arbitrarily selected point (end point of link 31). At the beginning of the simulation, this node is in contact with the ground. After that, the vehicle starts moving, and this point moves and comes into contact with the idler. It continues moving until it comes again into contact with the ground. This motion is repeated as the vehicle continues to move forward. Figure 46 shows the motion trajectory of the same node defined in the chassis coordinate system.
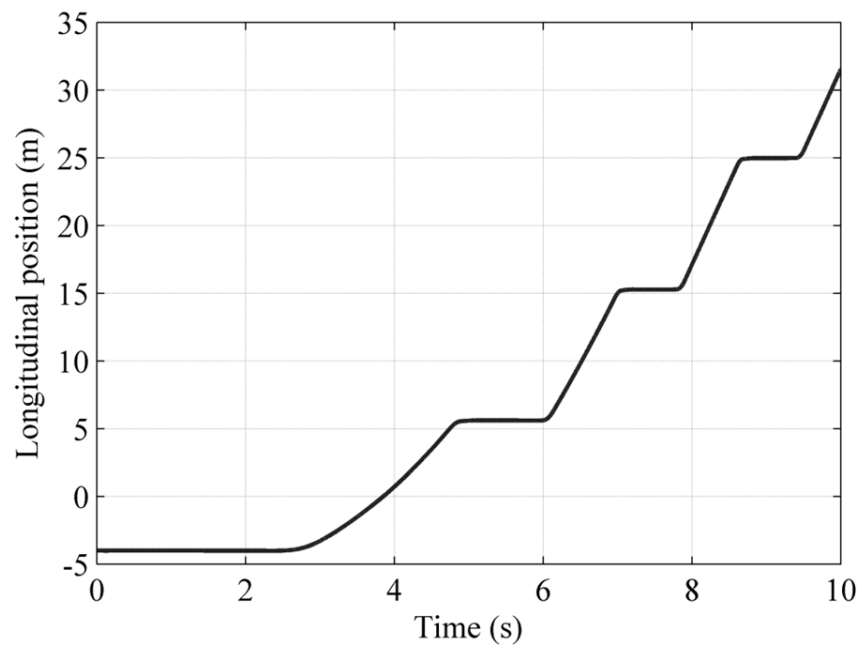
Figure 45 Node-32 forward position
(——— Rigid model, ------- Flexible models)
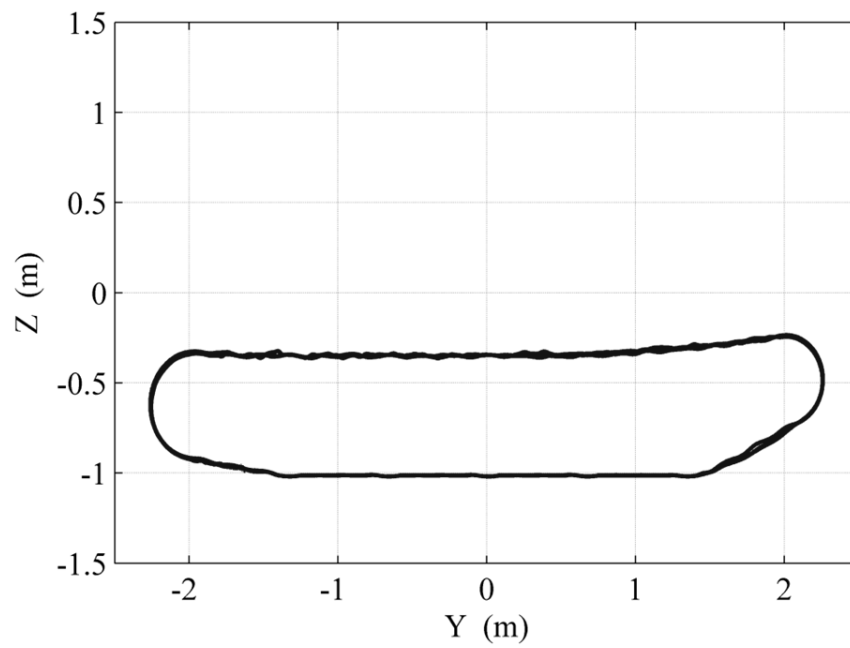
Figure 46 Motion trajectory of a flexible track link point

101

4.7.3. Forces and Deformations

In tracked vehicle dynamics, it is important to study the reaction forces at the pin joints. These forces can be used to further analyze the strain and stress state of the chain and determine whether or not the chain can sustain the forces without failure. Figures 47 and 48 show the joint constraint forces of the first joint (marked in Fig. 52) in the longitudinal and the vertical directions for the rigid and ANCF joint models.
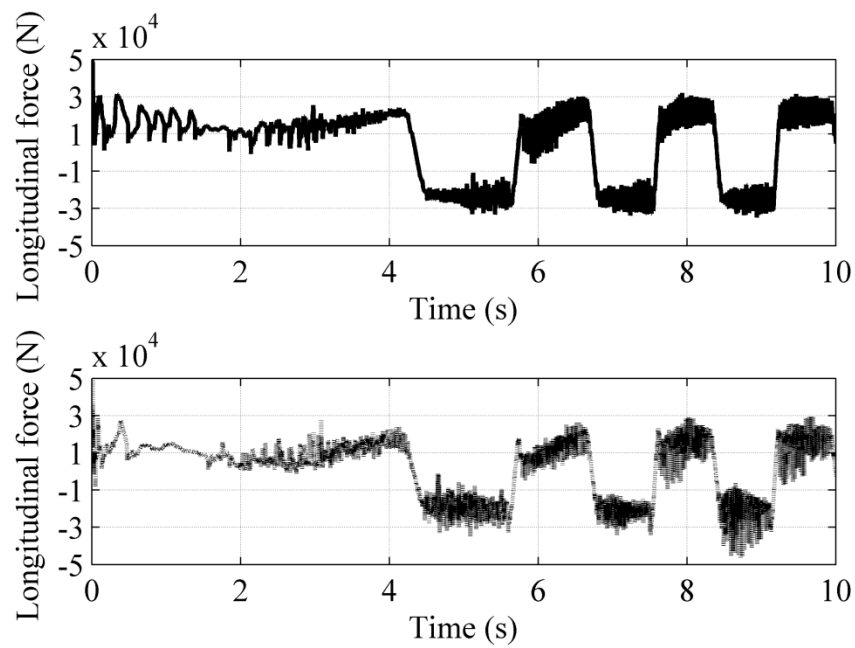
Figure 47 First joint longitudinal forces
(———— Rigid model, ------- Flexible models)
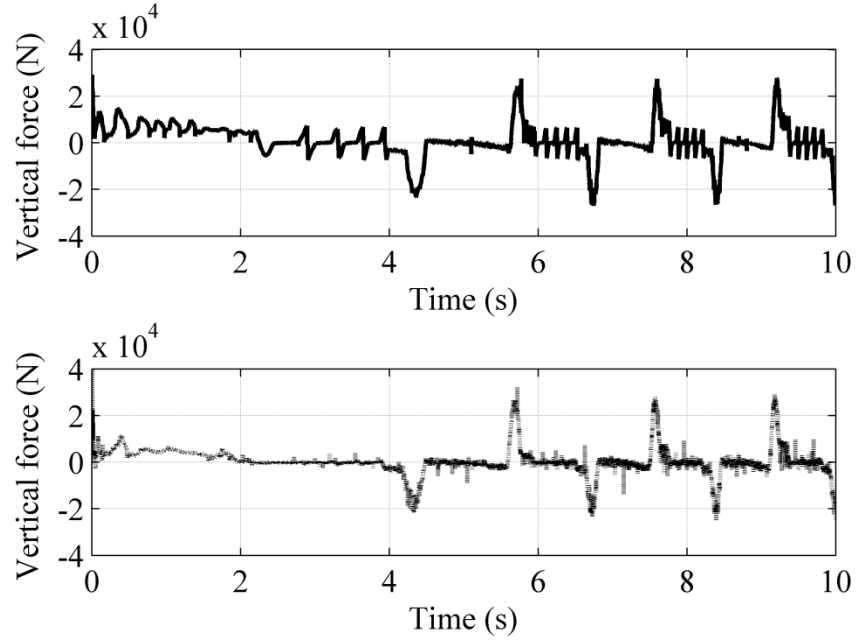
Figure 48 First joint vertical forces
(—— Rigid model, ------- Flexible models)

One advantage of including the flexibility of the track links is to be able to calculate the strains and stresses online. The online computation of the track link deformation leads to a more realistic prediction of the system dynamics, this is due to a nature of the coupling between different displacement modes and simulation parameters. Figures 49 and 50 show the axial and transverse deformations of the first link of the right chain at $t = 5s$. In these figures, the deformation is magnified by a factor of 10^5. The deformation of this link was calculated using a local tangent frame that has its longitudinal axis parallel to the first node position gradient vector.
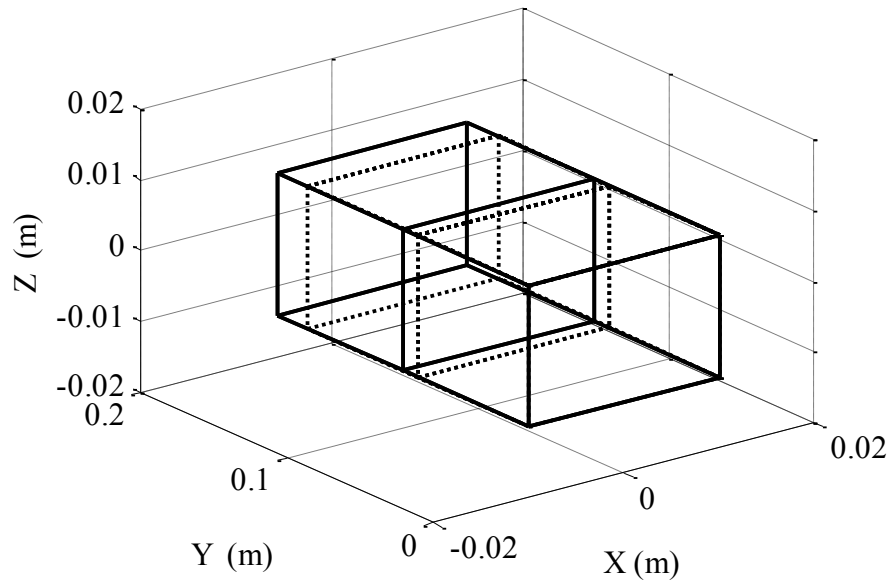
Figure 49 Axial deformation of first link of the right chain at $t = 5\text{s}$ magnified by a factor of 10^5

(------- Initial configuration, ——— deformed configuration)
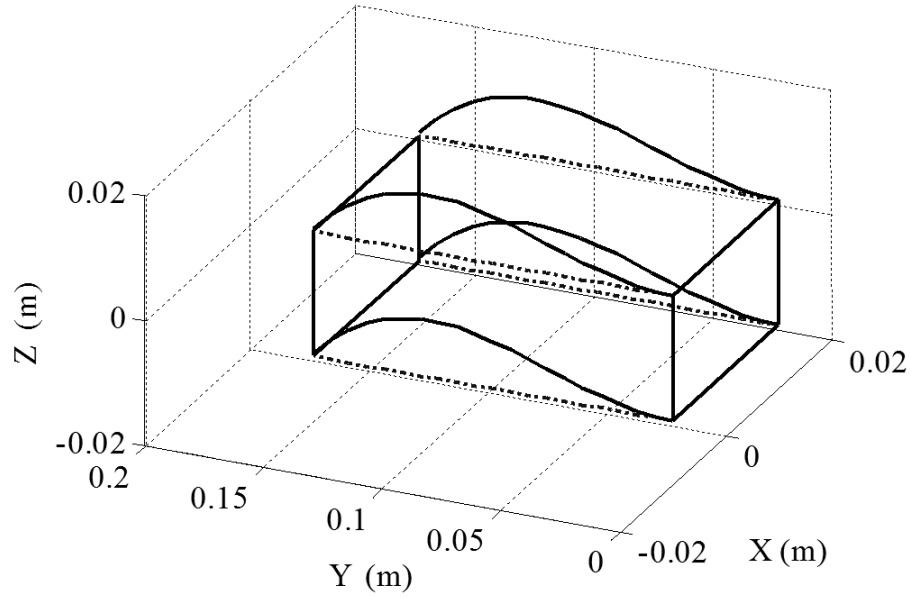
Figure 50 Transverse deformation of first link of the right chain at $t = 5\text{s}$ magnified by a factor of 10^5

(------- Initial configuration, ——— deformed configuration)

Figure 51 shows the axial stress of the right track chain at $t = 5s$, while Fig. 52 shows the configuration of the chain at $t = 5s$. It is clear from the results of Figs. 51 and 52 that the chain span can be divided into three sections. First section, which is located before the sprocket and is directly affected by the sprocket forces, is the tight section which has the highest tension. The second section is the slack section located after the sprocket and has the lowest degree of tension. The third section is a transition section between the tight and slack sections of the chain.
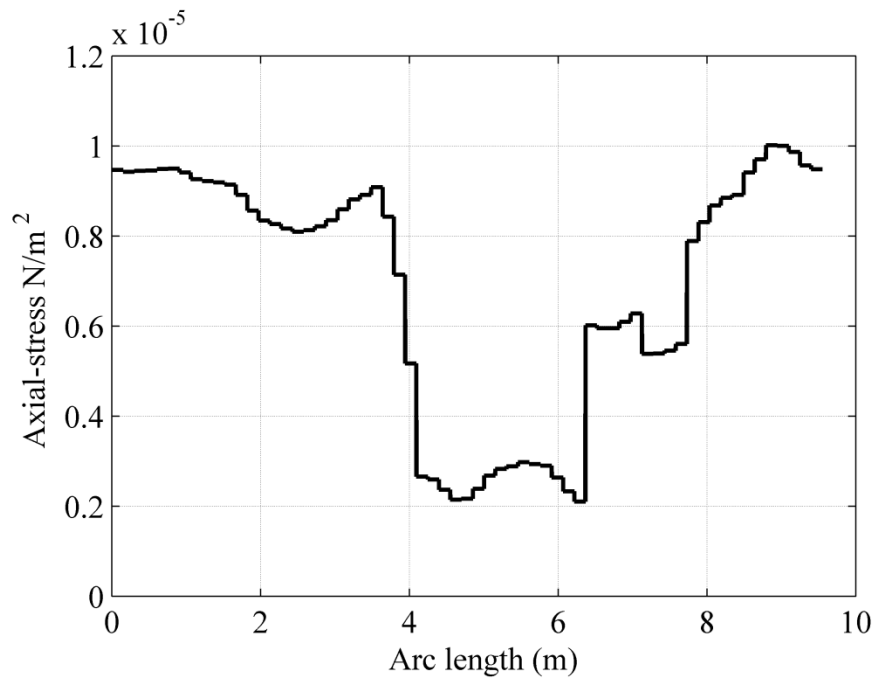
Figure 51 Right chain axial stress at $t = 5s$
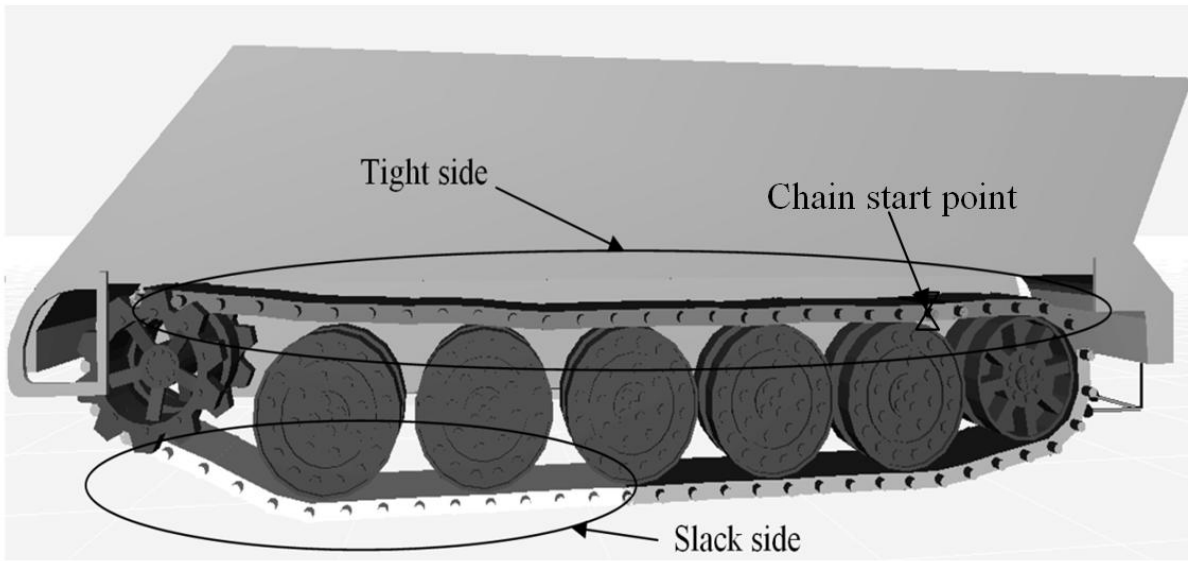
Figure 52 Right chain axial force distribution at $t = 5$s

While all the results of rigid body motion of the different models presented show good agreement, the computational time of the flexible model is almost four times the computational time of the rigid tracked vehicle model. This can be justified because of the high frequencies associated with the track link deformation. The presence of high frequencies can be confirmed by considering the number of function evaluations of the flexible and the rigid tracked vehicle models. The ratio between the numbers of function evaluations for the rigid and flexible tracked vehicle is approximately $1:8.5$. Considering both the simulation time and the number of function evaluations, it can be concluded that using the new ANCF linear mesh in modeling the flexible link tracked vehicles leads to significant computational saving. This computational saving is the result of the elimination of the joint constraints and the corresponding dependent coordinates and Lagrange multipliers. Furthermore, numerical experimentation showed that when a low modulus

of elasticity is used, flexible-link tracked vehicle models become more efficient than the rigid-link tracked vehicle model as the result of using the new ANCF finite element mesh.

4.7.4. <u>Augmented and Recursive Formulations.</u>

As previously mentioned, the proposed chain model allows for the elimination of dependent variables at a preprocessing stage resulting in a significant reduction in the number of joints constraints equations that need to be considered during the dynamic simulation. In the chain model considered in this investigation, the number of joints is reduced from 152 joints (760 equations) to 26 joints (130 equations). This amounts to 83% reduction in the number of algebraic equations. The elimination of these joint constraint equations and the associated dependent variables contributed to the solution of a fundamental singularity problem encountered in the analysis of the closed loop chains. Both the augmented and recursive formulations were used in the simulation of the rigid and flexible tracked vehicles. The recursive simulation was more efficient in the simulation of the rigid tracked vehicle compared to the augmented formulation. The CPU time of the recursive formulation was 75% of the augmented formulation CPU time. While, in the case of the flexible tracked vehicle, the CPU time of the recursive formulation was 95% of the augmented formulation CPU time.

4.7.5. <u>Physical and Numerical Damping</u>

For stiff systems of differential equations, explicit integration methods can be inefficient because of the small time steps selected. In some applications, the high stiffness can be attributed to insignificant high frequency modes (Hussein et al, 2008), which can be damped out using an appropriate visco-elastic constitutive model (Mohammed and Shabana, 2011). Another alternative is to use implicit integration methods which include numerical damping (Hussein et

al, 2008). In order to test the effectiveness of the proposed visco-elastic model in the numerical simulation of the flexible tracked vehicle, explicit Adams-Bashforth predictor-corrector and implicit HHT (Hilber et al, 1977) methods were used. The proposed physical damping model was used with Adams-Bashforth explicit integrator. The parameters of the HHT were assumed as reported in the literature (Hussein et al, 2008). In both cases, the undesired high frequencies were successfully damped out. The use of the two integration methods leads to approximately 30% reduction in the simulation time compared to using Adams-Bashforth without physical damping. Therefore, in some applications, the use of physical damping with explicit integration methods can lead to the same computational efficiency achieved by using the implicit integration methods that have numerical damping.

4.8. <u>Concluding Remarks</u>

A new class of ideal compliant joints that account for the distributed inertia and elasticity is introduced and used to discuss fundamental issues related to the integration of computer aided design and analysis (I-CAD-A). Additional degrees of freedom are introduced in order to capture modes of deformation that cannot be captured using existing formulations that employ rigid triads or unit vectors to formulate the joint equations. The ideal compliant joints developed, while more general and capture more modes of displacements, can be, for the most part, formulated using linear algebraic equations. These linear connectivity conditions allow for the elimination of the dependent variables at a preprocessing stage, thereby significantly reducing the problem dimension and array storage needed. Consequently, the constraint equations are automatically satisfied at the position, velocity, and acceleration levels. Therefore, when using the proposed approach to model large scale chain systems, differences in computational

108

efficiency between the augmented formulation and the recursive methods are eliminated, and the CPU times resulting from the use of the two formulations become similar regardless of the complexity of the system. Furthermore, the elimination of the joint constraint equations and the associated dependent variables contribute to the solution of a fundamental *singularity problem* encountered in the analysis of closed loop chains and mechanisms, and there is no need to repeatedly change the chain or mechanism independent coordinates.

Using the concept of the ideal compliant joints, the fundamental problems that can be encountered when using computational geometry methods, can be explained. The concept of the knot multiplicity used in computational geometry methods is not suited for the formulation of ideal compliant joints that may require different degrees of continuity for different variables or elements of the gradient vector or require imposing constraints on the gradient vectors along directions that differ from the B-spline and NURBS coordinate lines. As explained, this issue is closely related to the inability of B-spline and NURBS to model *structural discontinuities*.

This chapter also demonstrates that large deformation ANCF finite elements can be effective in solving small deformation problems. The necessity of using the new concepts developed in modeling complex systems is demonstrated using a heavily constrained tracked vehicle with flexible link chains. Without using the proposed approach modeling such a complex system with flexible links can be a challenging task. The analysis presented in this chapter also demonstrates that adding significant model details does not necessarily imply increasing the complexity of the MBS algorithm. In fact, including significant details such as body flexibility and joint deformations can be accomplished using MBS algorithms that are much simpler than the algorithms currently used for rigid body system analysis.

CHAPTER 5

VERIFICATION OF THE PROPOSED ELASTIC FORCE MODEL

In the previous chapter, a simplified Euler-Bernoulli beam elastic force model was proposed. This proposed force model can be used in the case of small deformations and only accounts for bending and axial modes. The model employs constant stiffness matrices that can be calculated at a preprocessing stage. This contributes to reducing the computational effort needed to evaluate the elastic forces. In this chapter, the new simplified Euler-Bernoulli beam elastic force model is compared to the elastic line and continuum mechanics approaches. This comparison serves as a verification of the proposed model. The comparison is made using a heavily constrained flexible link tracked vehicle model. The track chain links are connected using linear ANCF revolute joints. It is shown that the Euler-Bernoulli beam force model results are in a good agreement with the results obtained using the elastic line and continuum mechanics approaches. It is also shown that the proposed force model is computationally very efficient compared to both the elastic line and continuum mechanics approaches.

5.1. Continuum Mechanics Approach

In the continuum mechanics theory, the most general displacement of an infinitesimal volume is described using twelve independent modes; six of them for the rigid body and the other six for the deformation. For this reason, the coordinate representation used in the fully parameterized ANCF finite elements is in general sufficient to describe the rigid body motion and deformation of a continuum. In the ANCF fully parameterized elements, three position vector gradients are used to define the three independent rigid body rotations and strain modes. Such a coordinate representation, when used for beams, accounts for the deformation of the cross

section and allows using the more general continuum mechanics beam model that relaxes the assumptions of the Euler–Bernoulli and Timoshenko beam theories (Yakoub and Shabana, 2001). The simplicity of the continuum mechanics beam model makes it the dominating approach in the definition of the ANCF elastic forces (Mikola and Matikainen, 2006). In this approach, the elastic forces can be formulated using the Green–Lagrange strain and the second Piola–Kirchhoff stress tensors. The Green-Lagrange strain tensor can be calculated as function of the matrix of position vector gradients $\mathbf{J}$ as

$$\boldsymbol{\varepsilon} = \frac{1}{2}(\mathbf{J}^{\mathrm{T}}\mathbf{J} - \mathbf{I}) \tag{5.1}$$

In the preceding equation, $\mathbf{I}$ is the identity matrix. The matrix of the position vector can be written as

$$\mathbf{J} = \frac{\partial \mathbf{r}}{\partial \mathbf{X}} = \frac{\partial \mathbf{r}}{\partial \mathbf{x}}\left[\frac{\partial \mathbf{X}}{\partial \mathbf{x}}\right]^{-1} = \frac{\partial \mathbf{r}}{\partial \mathbf{x}}\mathbf{J}_0^{-1} \tag{5.2}$$

where, $\mathbf{X}$ is the vector of the global parameters (coordinate lines), $\mathbf{x}$ is the vector of the local element spatial coordinates, and $\mathbf{J}_0$ is the matrix of position vector gradients in the initial configuration. The constant matrix $\mathbf{J}_0$ must be considered in formulating the elastic forces if the beam has an arbitrary initial configuration. Note that $\mathbf{J}_0$ is the identity matrix in the case of initially horizontal beams.

Using the principle of virtual work, the vector of the generalized elastic forces $\mathbf{Q}_k$ is defined as (Vallejo et al, 2003)

111

$$\mathbf{Q}_k = -\int_v (\frac{\partial \boldsymbol{\varepsilon}}{\partial \mathbf{e}})^{\mathrm{T}} \mathbf{E} \boldsymbol{\varepsilon} \, \mathrm{d}v \tag{5.3}$$

where $\mathbf{E}$ is the matrix of elastic coefficients, and $\mathbf{e}$ is the nodal coordinates vector.

The simplicity of the continuum mechanics approach comes at the expense of having several locking problems (Mikkola et al., 2013). As a consequence, for some elements with certain interpolating polynomials, the results may not converge to the correct solution in the case of a Poisson's ratio larger than zero. The locking problems may lead to elements with poor numerical performance as a consequence of an inefficient bending strain description and shear and curvature thickness locking. Several methods were proposed in the literature to solve the locking problems associated with the continuum mechanics approach. The first strategy used to prevent Poisson locking was to employ local frames to define a linearized form of the elastic forces (Sopanen, and Mikkola, 2003). In other investigations, Poisson ratio was simply assumed to be zero (Gerstmayr, and Matikainen, 2006). In a later investigation, reduced integration was applied to the part of elastic forces that is function of Poison ratio (Gerstmayr et al., 2008; Nachbagauer et al., 2013). Another approach to remove the Poisson locking is to employ an elastic line approach, in which the strain tensor is defined at the beam center line and curvatures are used to define the bending elastic forces (Sugiyama et al., 2006; Schwab and Meijaard, 2010). The elastic line approach will be explained in details in the following subsection.

5.2. <u>Elastic Line Approach</u>

As previously mentioned, one approach to eliminate the Poisson locking is to use an elastic line approach that employs the beam kinematical quantities of classical nonlinear rod theories (Mikkola et al, 2013). In this approach, all the Green-Lagrange strains are defined at the

beam centerline, while the curvature expression is used to define the bending strains. The vectors

of position gradients at the beam centerline are written as (Dmitrochenko et al, 2009)

$$\mathbf{r}_{0x} = \mathbf{r}_x(x,0,0), \quad \mathbf{r}_y = \mathbf{r}_y(x,0,0), \quad \mathbf{r}_z = \mathbf{r}_z(x,0,0) \tag{5.4}$$

where $\mathbf{r}_x = \dfrac{\partial \mathbf{r}}{\partial x}, \mathbf{r}_y = \dfrac{\partial \mathbf{r}}{\partial y}$, and $\mathbf{r}_z = \dfrac{\partial \mathbf{r}}{\partial z}$. In the shear deformable ANCF element, the displacement

field is assumed to be cubic in x and linear in y and z. Hence, the subscript "0" is only used

with $\mathbf{r}_x$. The Green-Lagrange strains and curvatures components along the beam centerline can

be defined as (Schwab and Meijaard, 2010)

$$\left.\begin{aligned}
\varepsilon_{011} &= \frac{1}{2}(\mathbf{r}_{0x}^T \mathbf{r}_{0x} - 1), \quad \varepsilon_{22} = \frac{1}{2}(\mathbf{r}_y^T \mathbf{r}_y - 1), \quad \varepsilon_{33} = \frac{1}{2}(\mathbf{r}_z^T \mathbf{r}_z - 1), \\
\gamma_{012} &= \mathbf{r}_{0x}^T \mathbf{r}_y, \qquad \gamma_{013} = \mathbf{r}_{0x}^T \mathbf{r}_z, \qquad \gamma_{23} = \mathbf{r}_y^T \mathbf{r}_z, \\
\theta &= \frac{1}{2}(\mathbf{r}_{yx}^T \mathbf{r}_z - \mathbf{r}_y^T \mathbf{r}_{zx}), \quad \bar{\kappa}_{0y} = -\mathbf{r}_z^T \mathbf{r}_{0xx}, \quad \bar{\kappa}_{0z} = \mathbf{r}_y^T \mathbf{r}_{0xx}
\end{aligned}\right\} \tag{5.5}$$

In Eq. 5.5, ε_{011}, ε_{22}, and ε_{33} are the normal strains, γ_{012}, γ_{013}, and γ_{23} are the shear

strains, θ is the twist, and $\bar{\kappa}_{0y}$, and $\bar{\kappa}_{0z}$ are the expressions of the bending curvature. The total

strain energy of three-dimensional beam can be written as the summation of extension, shear,

bending and torsion energies as

$$U = U_l + U_s + U_b + U_t \tag{5.6}$$

The strain energy U_l due to the extension can be written as a function of the normal strain

$\boldsymbol{\varepsilon}_l = [\varepsilon_{0xx} \quad \varepsilon_y \quad \varepsilon_z]$ and the stress vector $\boldsymbol{\sigma}_l$ as

$$U_l = \frac{1}{2} A \int_0^l \boldsymbol{\sigma}_l{}^\mathrm{T} \boldsymbol{\varepsilon}_l \, dx \tag{5.7}$$

where, A is the cross section area. Assuming homogeneous isotropic linear elastic material, the normal stress vector can be written as

$$\boldsymbol{\sigma}_l = \mathbf{E} \boldsymbol{\varepsilon}_l \tag{5.8}$$

where $\mathbf{E}$ is the elastic coefficients matrix that can be written as function of the shear modulus G and Poisson ratio v as

$$\mathbf{E} = \frac{2G}{(1-2v)} \begin{bmatrix} 1-v & v & v \\ v & 1-v & v \\ v & v & 1-v \end{bmatrix} \tag{5.9}$$

The second part of the strain energy is the transverse shear strain energy. This can be written in terms of the shear strains as

$$U_s = \frac{1}{2} \int_0^l GA(\gamma_{012}^2 + \gamma_{013}^2 + \gamma_{23}^2) \, dx \tag{5.10}$$

The third part of the strain energy is the bending strain energy. The bending strain energy can be defined as function of the curvature as

$$U_b = \frac{1}{2} \int_0^l [EI_y (\bar{\kappa}_{0y})^2 + EI_z (\bar{\kappa}_{0z})^2] \, dx \tag{5.11}$$

Finally, the last part of the strain energy is the torsion energy which can be defined as function of the twist angle θ as

$$U_t = \frac{1}{2}\int_0^l GI_p \theta^2 \mathrm{d}x \tag{5.12}$$

5.3. <u>Comparison of the Different Approaches</u>

In order to compare between the strain components obtained using the general Continuum Mechanics approach and the other approaches, the global position vector can be rewritten as (Sugiyama et al, 2006)

$$\mathbf{r} = \mathbf{r}_0 + y\mathbf{r}_y + z\mathbf{r}_z \tag{5.13}$$

where $\mathbf{r}_0$ is the position vector of an arbitrary point on the beam centerline. The tangent to the center line $\mathbf{r}_x$ can be rewritten as follows

$$\mathbf{r}_x = \mathbf{r}_{0x} + y\mathbf{r}_{yx} + z\mathbf{r}_{zx} \tag{5.14}$$

Assuming an initially straight beam and using the preceding displacement field and the Green-Lagrange strain definition, the strain components are obtained as

$$\left.\begin{aligned}
\varepsilon_{11} &= \frac{1}{2}(\mathbf{r}_x^T\mathbf{r}_x - 1) = \frac{1}{2}(\mathbf{r}_{0x}^T\mathbf{r}_{0x} - 1) + y\mathbf{r}_{0x}^T\mathbf{r}_{yx} + z\mathbf{r}_{0x}^T\mathbf{r}_{zx} + \frac{1}{2}(y\mathbf{r}_{yx} + z\mathbf{r}_{zx})^T(y\mathbf{r}_{yx} + z\mathbf{r}_{zx}), \\
\varepsilon_{22} &= \frac{1}{2}(\mathbf{r}_y^T\mathbf{r}_y - 1), \quad \varepsilon_{33} = \frac{1}{2}(\mathbf{r}_z^T\mathbf{r}_z - 1), \qquad \gamma_{12} = \mathbf{r}_x^T\mathbf{r}_y = \mathbf{r}_{0x}^T\mathbf{r}_y + y\mathbf{r}_{yx}^T\mathbf{r}_y + z\mathbf{r}_{zx}^T\mathbf{r}_y, \\
\gamma_{13} &= \mathbf{r}_x^T\mathbf{r}_z = \mathbf{r}_{0x}^T\mathbf{r}_z + y\mathbf{r}_{yx}^T\mathbf{r}_z + z\mathbf{r}_{zx}^T\mathbf{r}_z, \qquad \gamma_{23} = \mathbf{r}_y^T\mathbf{r}_z
\end{aligned}\right\} \tag{5.15}$$

Comparing Eqs. 4.8, 5.5 and 5.15, the following differences in deformation modes obtained using the Simplified Euler Bernoulli, elastic line and continuum mechanics approaches are observed:

1. The simplified Euler-Bernoulli elastic force model can work only for small deformation problems. The shear and cross section deformations are neglected.

2. In the continuum mechanics approach, the bending strain is defined by the term $y\mathbf{r}_{0x}^T\mathbf{r}_{yx} + z\mathbf{r}_{0x}^T\mathbf{r}_{zx}$. On the other hand, in the elastic line approach, the bending strain is defined using the curvature expression $\bar{\kappa}_{0y} = -\mathbf{r}_z^T\mathbf{r}_{0xx}$ and $\bar{\kappa}_{0z} = \mathbf{r}_y^T\mathbf{r}_{0xx}$. Finally, in the simplified Euler-Bernoulli beam approach, the bending strain is defined using different curvature definition $\kappa = \mathbf{r}_{xx}$. These three definitions for the bending strain are not the same and can lead to different stiffness characteristics that determine the accuracy and robustness of the solution.

3. In the elastic line approach, the higher order strain component $\frac{1}{2}(y\mathbf{r}_{yx} + z\mathbf{r}_{zx})^T(y\mathbf{r}_{yx} + z\mathbf{r}_{zx})$ is neglected. This higher order term has insignificant contribution to the bending strain in small deformation cases.

4. In the continuum mechanics approach, the torsion strain is defined by the term $y\mathbf{r}_{yx}^T\mathbf{r}_y + z\mathbf{r}_{zx}^T\mathbf{r}_y$ and $y\mathbf{r}_{yx}^T\mathbf{r}_z + z\mathbf{r}_{zx}^T\mathbf{r}_z$, while in the elastic line approach the torsion strain is defined using the curvature expression θ. These different definitions for the twist strain may also lead to different results.

5.4. <u>Numerical Results</u>

The flexible-link chain three-dimensional tracked vehicle introduced in the last chapter is used to verify the proposed Euler-Bernoulli beam force model discussed earlier. As mentioned in the previous chapter, this example represents a complex system with large number of bodies connected by large number of revolute (pin) joints. Furthermore, the mathematical models of

116

such vehicles represent a stiff numerical integration problem due to the high frequencies of the contact forces. Hence, one must carefully select the elastic force model that suits the type of analysis performed. Choosing a general force model that takes into consideration all the deformation modes will result in a very slow simulation. Three different elastic force models are used to define the elastic forces associated with the flexible links. The first model uses an Euler-Bernoulli beam element and the elastic forces are calculated based on the simplified Euler-Bernoulli force model presented earlier in section 4.6. The second and third models employ the three-dimensional shear deformable beam element. The second tracked vehicle model elastic forces are calculated based on an elastic line approach. Finally, the last model of the tracked vehicle elastic forces is defined using the general continuum mechanics approach. In order to improve the computational efficiency of the continuum mechanics approach, a reduced integration scheme was used in the numerical integration of the elastic forces. A comparison will be made between the results of the full and reduced integration schemes. The three tracked vehicle chain models are developed using ANCF closed loop chains and the system differential and algebraic equations are solved simultaneously. An implicit HHT (Hilber et al, 1977) method was used for the numerical solution of the system differential equations.

5.4.1 <u>Rigid Body Motion</u>

The angular velocities of the two sprockets of all the three tracked vehicle models were specified to follow the pattern shown in Fig. 53.
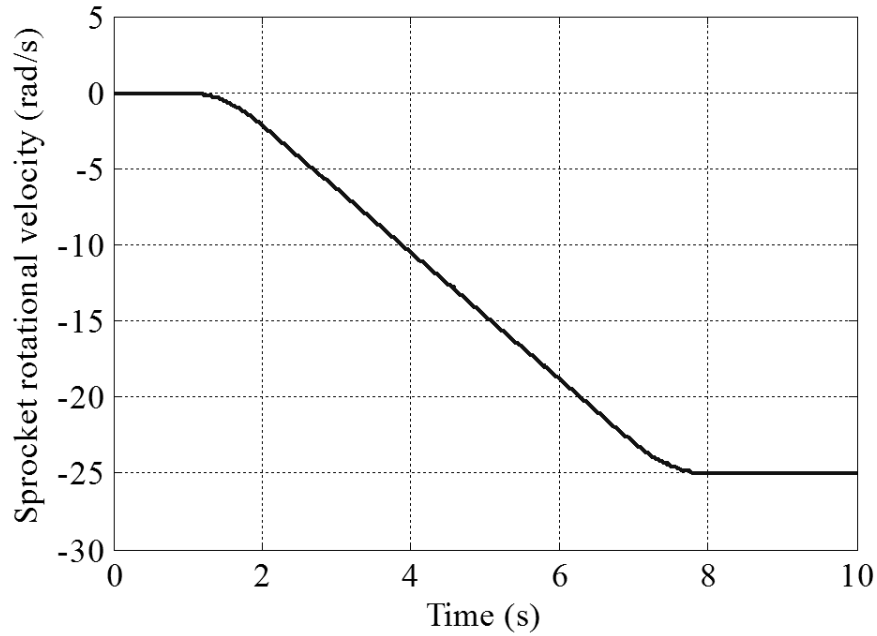
Figure 53 Sprocket rotational velocity

The response of the chassis to this input sprocket velocity is shown in Figs. 54-56. Figure 54 shows the forward velocity of the chassis. As expected, the velocity of the chassis follows the same pattern as the sprocket velocity. The results of Figs. 55 and 56 show the forward and vertical positions of the chassis center of mass. From the results presented in these figures, it is clear that the rigid body motion results of all the flexible chains models are in good agreement. This demonstrates that the new simplified Euler-Bernoulli elastic force model describes the rigid body motion correctly.

Figure 54 Chassis forward velocity
(⊙⋯⊙⋯⊙ Euler-Bernoulli, ⬥·⬥·⬥ Elastic line, ★★★ Continuum mechanics)
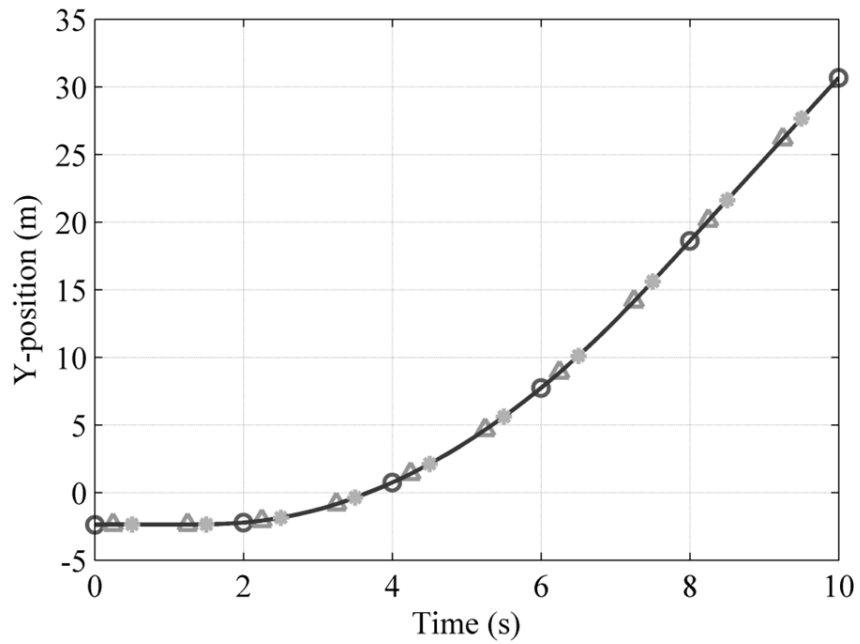
Figure 55 Forward displacement of the chassis
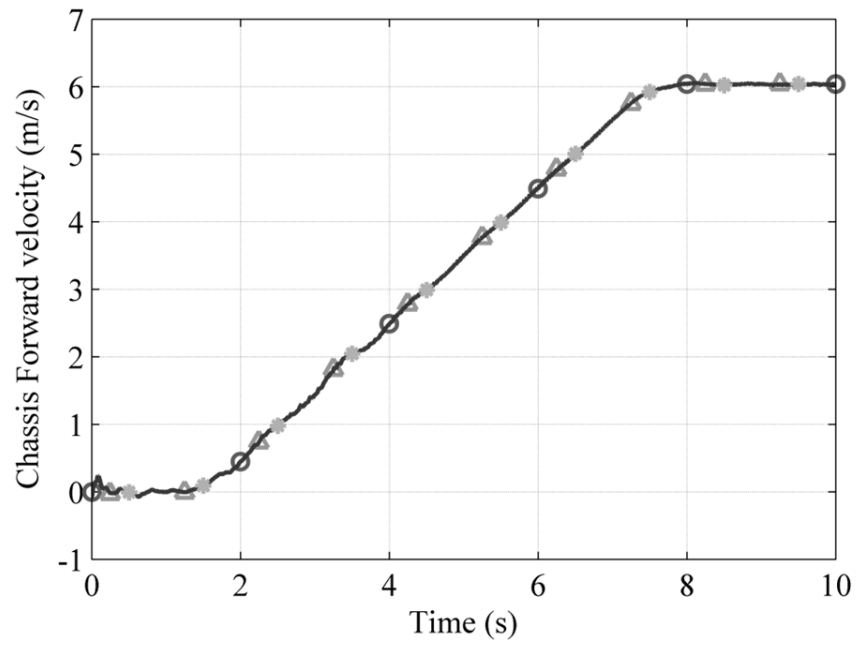(⊙⋯⊙⋯⊙ Euler-Bernoulli, ⬥·⬥·⬥ Elastic line, ★★★ Continuum mechanics)
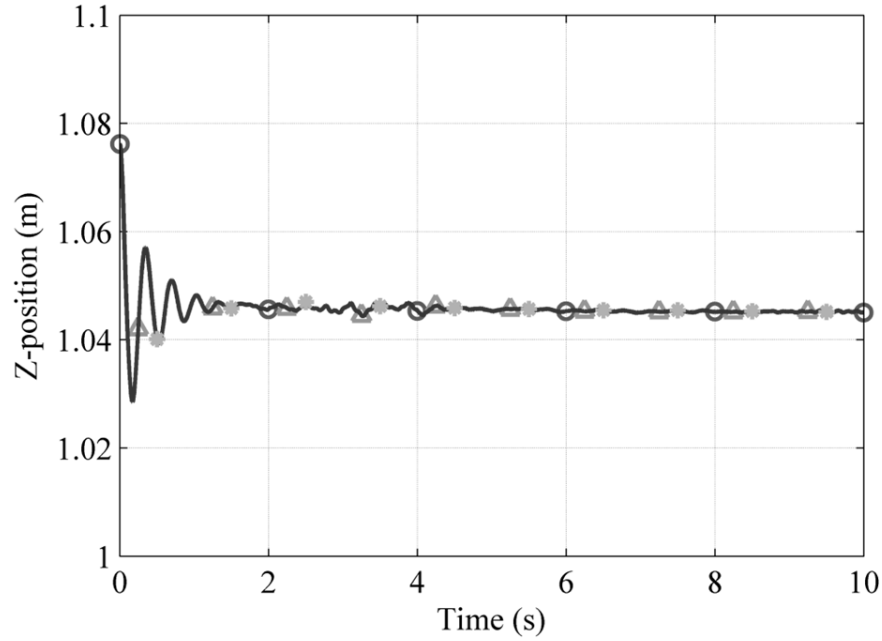
Figure 56 Vertical displacement of the chassis
(·o·o··o· Euler-Bernoulli, ⠔·⠔··⠔·Elastic line, ★★★ Continuum mechanics)

5.4.2 **Deformation Analysis**

As mentioned earlier, an advantage of including the flexibility of the track links is to be able to calculate the strains and stresses online. The online computation of the track link deformation leads to a more realistic prediction of the system dynamics, this is due to the nature of the coupling between different displacement modes and simulation parameters. This subsection introduces a comparison between the different elastic force model strains. Figure 57 shows the axial strain of the right track chain at $t=5$s. The results presented in this figure show good agreement between the three different force models. This agreement demonstrates that the approximation made in the Euler Bernoulli elastic force calculation are acceptable in the case of small deformation.

120
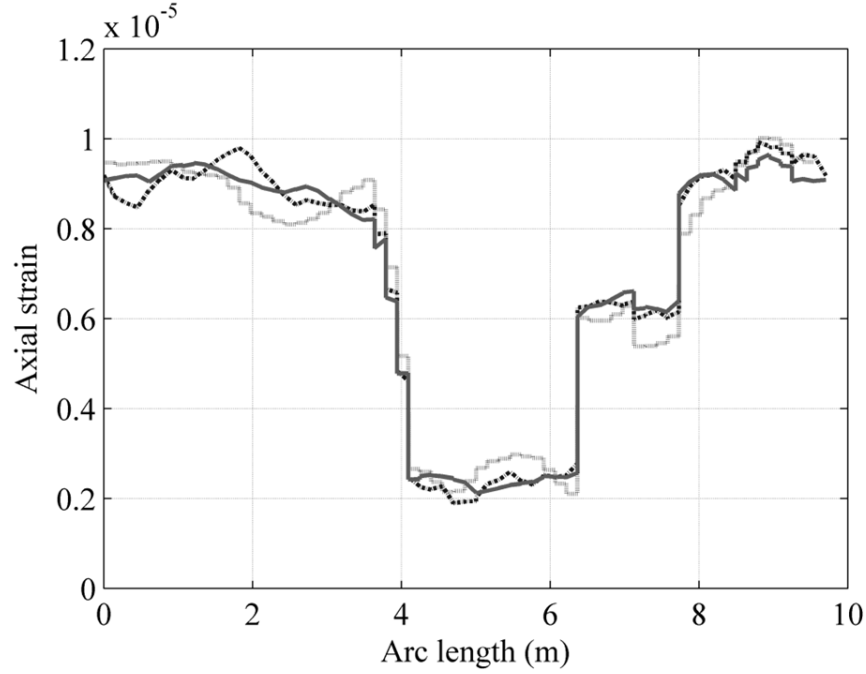
Figure 57 Right chain axial strain at $t = 5$s
($\cdots\cdots\cdots$ Euler-Bernoulli, ------ Elastic line, ———— Continuum mechanics)

As mentioned earlier, the proposed simplified Euler-Bernoulli beam elastic force model does not consider any of the cross section deformation; these deformation modes are function of the cross section gradients that are not considered in the ANCF Euler-Bernoulli beam element. If these modes are of importance, one can use an ANCF fully parameterized spatial beam element instead. Figures 58 and 59 show a comparison between normal strains in y and z directions. These two figures also show good agreement between the elastic line and continuum mechanics approaches. Figure 60 shows a comparison between the shear strain in the x-y plane. This figure shows that the shear strain is very small in both cases and can be neglected.
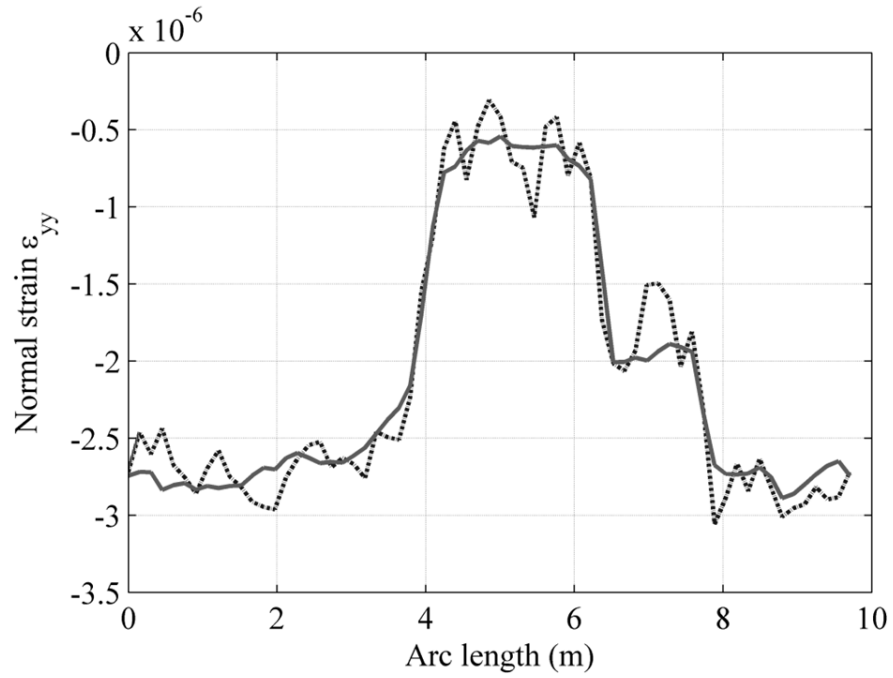
Figure 58 Right chain normal strain ε_{yy} at $t = 5$s
(------ Elastic line, —— Continuum mechanics)
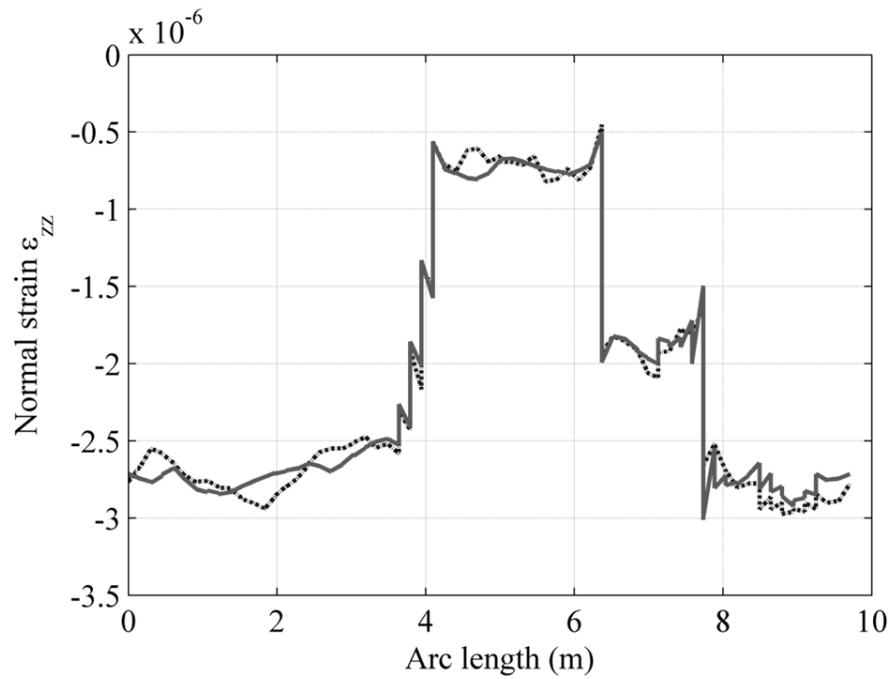
Figure 59 Right chain normal strain ε_{zz} at $t = 5$s
(------ Elastic line, —— Continuum mechanics)
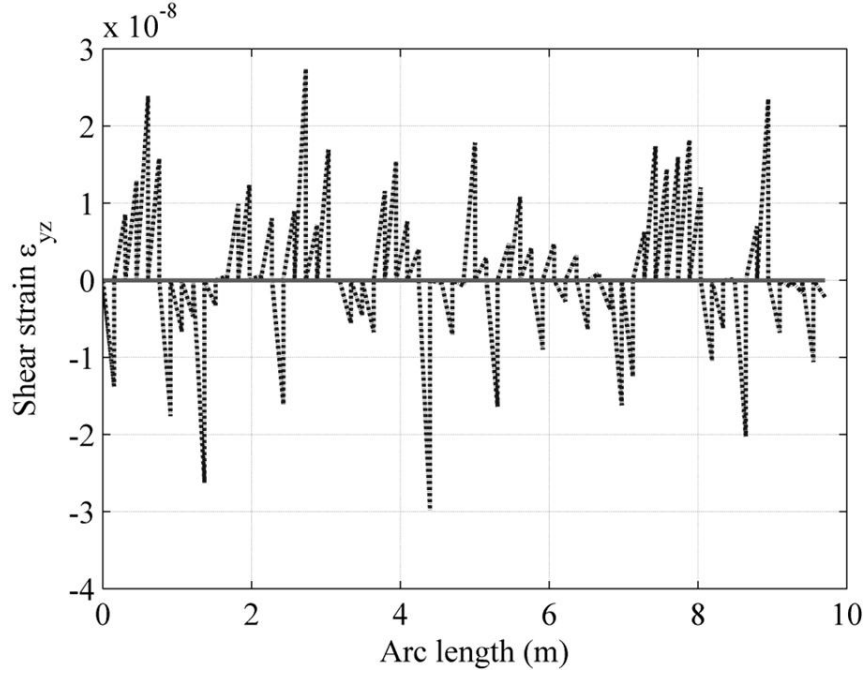
Figure 60 Right chain shear strain ε_{yz} at $t = 5$s

(------ Elastic line, ——— Continuum mechanics)

As previously mentioned, reduced integration was used in an attempt to improve the computational efficiency of the continuum mechanics approach. A comparison between the full and reduced integration is shown in Figs 61-63. These three figures show the normal strains in the x, y, and z directions. It is clear from the results presented in these figures that the solutions obtained using the two schemes are almost identical.
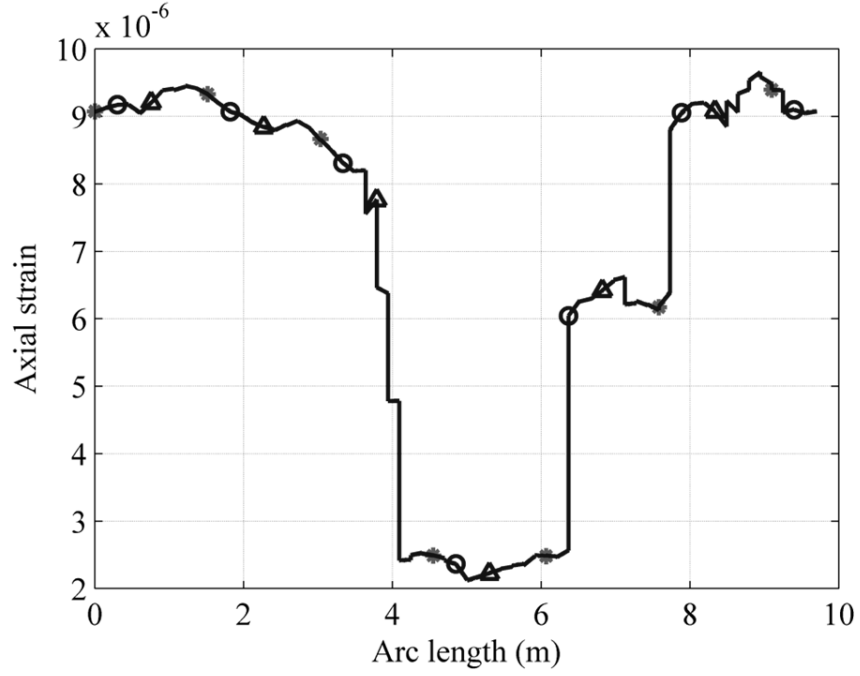
Figure 61 Right chain axial strain ε_{xx} at $t = 5$s

(★★★ Full integration, ⊙⊙⊙ Reduced integration (522), ▵▵▵ Reduced integration (422))
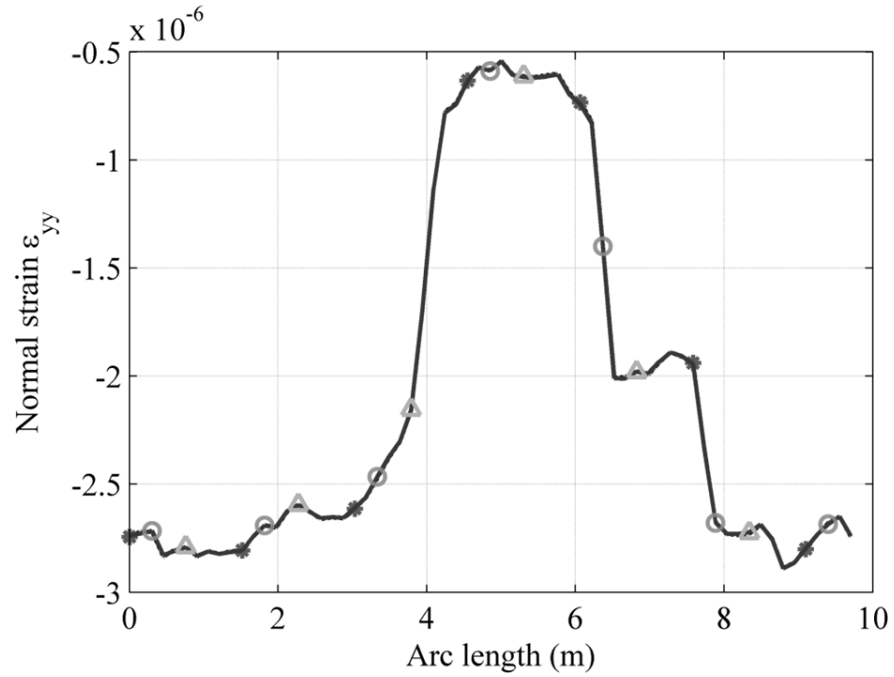
Figure 62 Right chain normal strain ε_{yy} at $t = 5$s

(★★★ Full integration, ⊙⊙⊙ Reduced integration (522), ▵▵▵ Reduced integration (422))

124
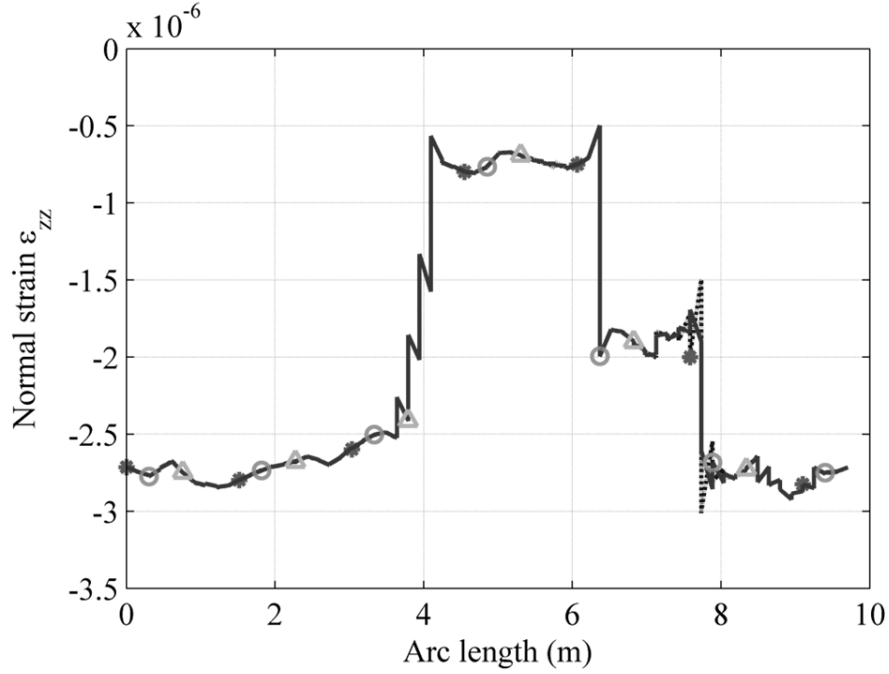
Figure 63 Right chain normal strain ε_{zz} at $t = 5\text{s}$
(★★★ Full integration, ⊙⊙⊙ Reduced integration (522), ▵▵▵ Reduced integration (422))

While all the results of the different models show good agreement, the computational time of the Euler-Bernoulli elastic force model is very small compared to the other two models. Table III shows the computational times of the three force models using the Euler-Bernoulli computational time as the reference.

Table III. Simulation times of the elastic force models

Force model	Number of integration points			Simulation time
	x	y	z	
Euler-Bernoulli	-	-	-	1
Elastic Line	7	-	-	37
Continuum Mechanics	5	3	3	128
Continuum Mechanics (522)	5	2	2	57
Continuum Mechanics (422)	4	2	2	47

The times given in Table III show that the proposed Euler-Bernoulli elastic force model is very efficient compared to the elastic line and continuum mechanics approaches. However, it is important to point out that the simplified Euler-Bernoulli elastic force model considers only the axial and bending deformations, and assumes small longitudinal deformation. If any of the other deformation modes are of interest, or the model under study experiences large deformation, one should use a force model that does not employ such assumptions.

5.5. <u>Concluding Remarks</u>

The proposed simplified Euler-Bernoulli beam force model introduced in the previous chapter is verified by comparing its results with the results obtained using the general continuum mechanics and the elastic line force models. A brief discussion of the main differences between the force models is presented. The proposed force model can be applied only in the case of small deformation and does not take into consideration any of the shear or cross section deformations. A flexible tracked vehicle model is used to verify the new force model. The results show good agreement between the rigid body motion and the axial strain predicted by all force models. The new force model is shown to be very efficient compared to the other force models.

CHAPTER 6

CONCLUSIONS

Existing MBS algorithms and computer programs do not allow structural finite elements (beams, plates, and shells) of a mesh to have arbitrarily large relative rigid body displacements that can introduce non-structural geometric discontinuities. Most algorithms and computer codes define structural FE meshes in which the elements are rigidly connected. In MBS algorithms, components which are not rigidly connected are treated as separate bodies, and nonlinear algebraic equations are used to define the joints that connect these bodies. Furthermore, the mesh inertia matrix becomes highly nonlinear in the case of rigid body rotations. Similarly, relative rigid body rotations lead to highly nonlinear kinematic constraint equations and inertia forces in the case of rigid body dynamics, as demonstrated in chapter 2 using a simple example. FE algorithms, on the other hand, employ co-rotational formulations that lead to highly nonlinear inertia matrix in the case of rigid body motion. For the most part, FE computer programs employ an incremental solution procedure that is not designed for solving MBS differential/algebraic equations. This thesis proposes the development of new FE meshes that can be effectively used in MBS dynamic analysis. The proposed ANCF procedure can be effectively used for modeling non-structural geometric discontinuities by allowing the structural finite elements of a mesh to have arbitrarily large relative rigid body displacements. Connectivity conditions between the finite elements are defined using linear algebraic constraint equations which can be introduced at a preprocessing stage before the dynamic analysis in order to eliminate redundant coordinates; thereby significantly reducing the number of algebraic equations and the associated Lagrange multipliers. Using ANCF finite elements, that correctly describe rigid body displacements and do not require the use of the co-rotational formulation, one obtains a FE mesh that has rigid body

degrees of freedom and at the same time has a constant mass matrix. The relationship between these ANCF continuity conditions and the concept of knot multiplicity used in computational geometry methods such as B-splines and NURBS is discussed and demonstrated using several examples. The examples presented in chapter 2 show that ANCF finite elements can be used to systematically model non-structural discontinuities as well as structural discontinuities including T- and V-junctions.

Chapter 3 addresses the important issue of using computational geometry methods such as B-spline and NURBS as analysis tools. B-spline and NURBS employ recurrence formulas that allow changing the degree of continuity at a breakpoint by adjusting the knot multiplicity at this point. As demonstrated, the recurrence formula has several drawbacks when B-spline representation is used as an analysis tool. Because the recurrence formula does not provide flexibility for choosing the basis functions, B-spline representation can lead to significantly larger number of coordinates and a higher dimensional model. This fact was used to demonstrate the generality of the ANCF geometry. While B-spline geometry can always be converted to ANCF geometry, the converse is not true. It is also shown that the B-spline recurrence formula cannot be used to model structural discontinuity in a straight forward manner. While structural discontinuities are of the C^0 type, they cannot be captured in the B-spline representation by reducing the knot multiplicity by one. This reduction of the knot multiplicity is equivalent to elimination of the relative translation only; and such a reduction in the knot multiplicity leads to a rigid body mode that defines the conditions of a pin joint. In the case of structural discontinuities, on the other hand, the C^0 B-spline representation does not eliminate the rigid body mode since additional algebraic constraint equations are required in order to eliminate the relative rotations between two segments. This chapter also presents a new three-dimensional pin

joint model that leads to linear connectivity conditions and constant mass matrix when used with ANCF finite elements. The implementation of this new model is demonstrated using a flexible-link chain example. The limitations identified in this chapter when B-spline geometry is used as analysis tool suggest the use of the I-CAD-A approach in which a constant transformation can be developed to convert CAD geometry to FE mesh. It should be also clear that NURBS geometry has the same limitations as B-spline representation when used as an analysis tool.

In Chapter 4, Discussion of the new class of ideal compliant joints that account for the distributed inertia and elasticity is continued and used to discuss fundamental issues related to the integration of computer aided design and analysis (I-CAD-A). The ideal compliant joints developed, while more general and capture more modes of displacements, can be, for the most part, formulated using linear algebraic equations. These linear connectivity conditions allow for the elimination of the dependent variables at a preprocessing stage, thereby significantly reducing the problem dimension and array storage needed. Consequently, the constraint equations are automatically satisfied at the position, velocity, and acceleration levels. Therefore, when using the proposed approach to model large scale chain systems, differences in computational efficiency between the augmented formulation and the recursive methods are eliminated, and the CPU times resulting from the use of the two formulations become similar regardless of the complexity of the system. Furthermore, the elimination of the joint constraint equations and the associated dependent variables contribute to the solution of a fundamental *singularity problem* encountered in the analysis of closed loop chains and mechanisms, and there is no need to repeatedly change the chain or mechanism independent coordinates.

Using the concept of the ideal compliant joints, the fundamental problems that can be encountered when using computational geometry methods, can be explained. The concept of the

129

knot multiplicity used in computational geometry methods is not suited for the formulation of ideal compliant joints that may require different degrees of continuity for different variables or elements of the gradient vector or require imposing constraints on the gradient vectors along directions that differ from the B-spline and NURBS coordinate lines. As explained, this issue is closely related to the inability of B-spline and NURBS to model *structural discontinuities*.

This chapter also demonstrates that large deformation ANCF finite elements can be effective in solving small deformation problems. The necessity of using the new concepts developed in modeling complex systems is demonstrated using a heavily constrained tracked vehicle with flexible link chains. Without using the proposed approach modeling, such a complex system with flexible links can be a challenging task. The analysis presented in this chapter also demonstrates that adding significant model details does not necessarily imply increasing the complexity of the MBS algorithm. In fact, including significant details such as body flexibility and joint deformations can be accomplished using MBS algorithms that are much simpler than the algorithms currently used for rigid body system analysis.

It was observed that the flexible tracked vehicle under study experiences small deformation. This motivated employing an elastic force model that makes use of the small deformation assumption in an attempt to improve the computational efficiency of the vehicle. A simplified spatial elastic Euler-Bernoulli beam force model was developed. This force model accounts for the coupling between bending and axial deformations. The model employs constant stiffness matrices that can be calculated at a preprocessing stage. This helps in reducing the computational effort needed to evaluate the elastic forces.

In Chapter 5, the proposed simplified Euler-Bernoulli beam force model introduced in chapter 4 is verified by comparing its results to the general Continuum Mechanics and the Elastic

Line force models. A brief discussion of the main differences of the force models is presented. A flexible tracked vehicle model is used to verify the new force model. The results show good agreement between the rigid body motion and the axial strain detected by all the force models. The new force model is shown to be very efficient compared to the other force models.

APPENDIX A
SPRINGER COPYRIGHTS TRANSFER

Copyright Transfer Statement

The copyright to this article is transferred to Springer (respective to owner if other than Springer and for U.S. government employees: to the extent transferable) effective if and when the article is accepted for publication. The author warrants that his/her contribution is original and that he/she has full power to make this grant. The author signs for and accepts responsibility for releasing this material on behalf of any and all co-authors. The copyright transfer covers the exclusive right and license to reproduce, publish, distribute and archive the article in all forms and media of expression now known or developed in the future, including reprints, translations, photographic reproductions, microform, electronic form (offline, online) or any other reproductions of similar nature.

An author may self-archive an author-created version of his/her article on his/her own website and or in his/her institutional repository. He/ she may also deposit this version on his/her funder's or funder's designated repository at the funder's request or as a result of a legal obligation, provided it is not made publicly available until 12 months after official publication. He/ she may not use the publisher's PDF version, which is posted on www.springerlink.com, for the purpose of self archiving or deposit. Furthermore, the author may only post his/her version provided acknowledgement is given to the original source of publication and a link is inserted to the published article on Springer's website. The link must be accompanied by the following text: "The final publication is available at www.springerlink.com".

Prior versions of the article published on non-commercial pre-print servers like arXiv.org can remain on these servers and/or can be updated with the author's accepted version. The final published version (in pdf or html/xml format) cannot be used for this purpose. Acknowledgement needs to be given to the final publication and a link should be inserted to the published article on Springer's website, accompanied by the text "The final publication is available at springerlink.com".

The author retains the right to use his/her article for his/her further scientific career by including the final published journal article in other publications such as dissertations and postdoctoral qualifications provided acknowledgement is given to the original source of publication.

The author is requested to use the appropriate DOI for the article.

Articles disseminated via www.springerlink.com are indexed, abstracted and referenced by many abstracting and information services, bibliographic networks, subscription agencies, library networks, and consortia.

After submission of the agreement signed by the corresponding author, changes of authorship or in the order of the authors listed will not be accepted by Springer.

ASME COPYRIGHTS TRANSFER

ASME Journals Digital Submission Tool
Guidelines and Information
Copyright Transfer
Rev. 08/2012

ASME requests that authors/copyright owners assign copyright to ASME in order for a journal paper to be published by ASME. Authors exempt from this request are direct employees of the U.S. Government, whereby papers are not subject to copyright protection in the U.S., or non-U.S. government employees, whose governments hold the copyright to the paper.

The copyright transfer agreement has been incorporated into the ASME Journal Tool to collect digital signatures from each author.

Upon submission of a paper, an email will be sent to each author for electronic signature.

If an author is not authorized to sign the form (e.g., employer owns copyright) the email needs to be forwarded to the individual authorized to sign on the author's behalf. The digital copyright form contains options for the following:

(1) Papers Owned by One Author or Joint Authors

(2) Designated Authors

If an author is going to have a co-author act as a Designated Author, they need to forward the email with the electronic signature request to the Designated Author and provide the Designated Author with written authorization to sign on their behalf.

A Designated Author may sign the digital document on behalf of the other authors ONLY IF the designated author has secured written authorization from the other author. The Designated Author MUST be able to produce such written authorization if requested.

(3) Papers Created by Authors of U.S. Federal Government Contractor, National Lab, etc.

(4) U.S. Government Employees and non-U.S. Government Employees.

WHO SHOULD SIGN

Only the copyright owner(s) of the Paper, or an authorized representative, can sign the copyright form. If one of the following applies, you may not own the copyright to the paper, or you may not be authorized to sign the agreement, and you may need to have the appropriate copyright owner(s) or organization representative sign the Agreement:

(1) You created the Paper within the scope of your employment, and your employer is the copyright owner.

(2) You created the Paper under an independent contractor agreement.

Note to U.S. Government Contractors: If you created the Paper under contract with the U.S. Government, e.g., U.S. Government labs, the paper may be subject to copyright, and you or your employer may own the copyright. Please review your company/institutional policies and your contractor agreement. Your Paper may also require a footer acknowledging contract information and also the following statement:

"The United States Government retains, and by accepting the article for publication, the publisher acknowledges that the United States Government retains, a non-exclusive, paid-up, irrevocable, worldwide license to publish or reproduce the published form of this work, or allow others to do so, for United States Government purposes."

It is your responsibility to ensure that the final PDF version of the Paper you submit includes all necessary footers and statements required under your contract.

(3) You received a grant that funded your Paper.

Please review your company policies regarding copyright, and if you are not authorized to sign this agreement, please forward to the appropriate organization representative. Please review applicable company, institutional, and grant policies and your employment/independent contractor agreement to determine who holds the rights to your Paper.

RETAINED RIGHTS OF AUTHORS

Authors retain all proprietary rights in any idea, process, procedure, or articles of manufacture described in the Paper, including the right to seek patent protection for them. Authors may perform, lecture, teach, conduct related research, display all or part of the Paper, and create derivative works in print or electronic format. Authors may reproduce and distribute the Paper for non-commercial purposes only. Non-commercial applies only to the sale of the paper per se. For all copies of the Paper made by Authors, Authors must acknowledge ASME as original publisher and include the names of all author(s), the publication title, and an appropriate copyright notice that identifies ASME as the copyright holder.

COPYRIGHT ASSIGNMENT: TERMS

The terms of copyright assignment refer to content that is subject to copyright.

REPRESENTATIONS, OBLIGATIONS, ACKNOWLEDGEMENTS, AND INDEMNIFICATION

The signee assigns irrevocably to ASME all worldwide rights under copyright in the Paper and represents and acknowledges that:

(A) This Paper represents: either the first publication of material or the first publication of an original compilation of information from a number of sources as specifically noted by footnotes and/or bibliography.

(B) You have the right to enter into this Copyright Form and to make the assignment of rights to ASME. If the Paper contains excerpts from other copyrighted material (including without limitation any diagrams, photographs, figures or text), you have acquired in writing all necessary rights from third parties to include those materials in the Paper, and have provided appropriate credit for that third-party material in footnotes or in a bibliography.

(C) If you are signing this Form on behalf of any co-authors or other copyright holders, you have obtained express authorizations from all those authors and/or copyright holders to make this assignment of rights to ASME.

(D) To the best of the author's knowledge, all statements contained in the Paper purporting to be facts are true or supported by reasonable scientific research, the Paper does not contain any defamatory or libelous material and does not infringe any third party's copyright, patent, trade secret, or other proprietary rights and does not violate the right of privacy or publicity of any third party or otherwise violate any other applicable law; furthermore that to the best of your ability, you are responsible for ensuring the accuracy of your research and the Paper's content.

(E) If the Paper was produced in the course of an author's employment by, or contractual relationship with, the U.S. Federal or State Government and/or contains classified material, it has been appropriately cleared for public release and such is indicated in the paper.

(F) The Paper is not subject to any prior claim, encumbrance or form and is not under consideration for publication elsewhere.

(G) You have appropriately cited and acknowledged all third parties who have contributed significantly in the Paper's technical aspects.

(H) ASME is not responsible for any misrepresentation, errors or omissions by those signing this copyright form.

(I) All print and electronic copies of the Paper submitted to ASME become ASME's physical property regardless of whether or not ASME publishes the Paper, and that ASME is not obligated to publish your paper (see the Termination Section below if your paper is not published).

(J) ASME is not responsible for any of your expenses incurred in connection with preparing the Paper or attending meetings to present it, nor will ASME pay you any financial compensation if it publishes your Paper.

(K) Subject to and to the maximum extent permitted by law, you agree to indemnify and hold harmless ASME from any damage or expense related to a breach of any of the representations and warranties above.

TERMINATION

If ASME decides not to publish your Paper, this Form, including all of ASME's rights in your Paper, terminates and you are thereafter free to offer the Paper for publication elsewhere.

GENERAL PROVISIONS

This Copyright Form, the Terms & Conditions, and ASME Copyright Guidelines, constitutes the entire agreement between you and ASME, and supersedes all prior or current negotiations, understandings and representations, whether oral or written, between you and ASME concerning the Paper.

This Agreement is governed by, and should be construed in accordance with, the laws of the State of New York, United States of America, applicable to agreements made and performed there, except to the extent that your institution is prohibited by law from entering contracts governed by New York law, in which limited case this Agreement is governed by, and should be construed in accordance with, the laws of the jurisdiction in which your institution is located.

Any claim, dispute, action or proceeding relating to this Agreement may be brought only in the applicable state and federal courts in the State and County of New York, and you expressly consent to personal jurisdiction and venue in any of those courts.

CITED REFERENCES

Abbas, L.K., Rui, X., and Hammoudi, Z.S.: Plate/Shell Element of Variable Thickness Based on the Absolute Nodal Coordinate Formulation. <u>IMechE Journal of Multibody Dynamics</u> 224: 127-141, 2010.

Bando, K., Yoshida, K. and Hori, K.: The Development of the Rubber Track for Small Size Bulldozers. <u>International Off-Highway & Powerplants Congress & Exposition, Milwaukee, WI</u>, 1991.

Berzeri, M., Campanelli, M. and Shabana, A.A.: Definition of the Elastic Forces in the Finite-Element Absolute Nodal Coordinate Formulation and the Floating Frame of Reference Formulation. <u>Multibody System Dynamics</u> 5: 21-54, 2001.

Choi, J.H., Lee, H.C. and Shabana, A.A.: Spatial Dynamics of Multibody Tracked vehicles, Part I: Contact Forces and Simulation Results. <u>Vehicle System Dynamics</u> 29: 27–49, 1998.

Choi, J.H., Lee, H.C. and Shabana, A.A.: Spatial Dynamics of Multibody Tracked vehicles, Part II: Contact Forces and Simulation Results. <u>Vehicle System Dynamics</u> 29: 113-137, 1998.

Dmitrochenko, O. N. and Pogorelov, D. Y.: Generalization of Plate Finite Elements for Absolute Nodal Coordinate Formulation. <u>Multibody System Dynamics</u> 10: 17-43, 2003.

Dmitrochenko, O.N, Hussein, B.A, and Shabana, A.A: Coupled Deformation Modes in the Large Deformation Finite Element Analysis: Generalization. <u>Journal of Computational and nonlinear dynamics</u> 4: 021002-2, 2009.

Dufva, K.E., Sopanen, J.T., and Mikkola, A.M.: A Two-Dimensional Shear Deformable Beam Element Based on the Absolute Nodal Coordinate Formulation. <u>Sound and Vibration</u> 280: 719-738, 2005.

Dufva, K., Kerkkänen, K. Maqueda, L.G., and Shabana, A.A.: Nonlinear Dynamics of Three-Dimensional Belt Drives Using the Finite-Element Method. <u>Nonlinear Dynamics</u> 48: 449-466, 2007.

Galaitsis, A.G.: A Model for Predicting Dynamic Track Loads in Military Vehicles. <u>Journal of Vibration, Acoustics, Stress, and Reliability in Design</u> 106: 286-291, 1984.

Garcia-Vallejo, D., Escalona, J.L., Mayo, J., and Dominguez, J.: Describing Rigid-Flexible Multibody Systems Using Absolute Coordinates. <u>Nonlinear Dynamics</u> 34: 75-94, 2003.

Garcia-Vallejo, D., Mayo, J., and Escalona, J. L.: Three-Dimensional Formulation of Rigid-Flexible Multibody Systems with Flexible Beam Elements. <u>Multibody System Dynamics</u> 20: 1-28, 2008.

Gerstmayr, J., and Matikainen, M. K.: Analysis of Stress and Strain in the Absolute Nodal Coordinate Formulation. <u>Mechanics Based Design of structure and Machines.</u> 34(4): 409–430, 2006.

Gerstmayr, J. and Irschik, H.: On the Correct Representation of Bending and Axial Deformation in the Absolute Nodal Coordinate Formulation with an Elastic Line Approach. <u>Journal of sound and vibration</u> 318: 461-487, 2008.

Gerstmayr, J., Matikainen, M. K., and Mikkola, A. M.: A Geometrically Exact Beam Element Based on the Absolute Nodal Coordinate Formulation. <u>Multibody System Dynamics</u> 20(4): 359–384, 2008.

Gerstmayr, J. and Shabana, A.A.: Analysis of Thin Beams and Cables Using the Absolute Nodal Co-ordinate Formulation. <u>Nonlinear Dynamics</u> 45: 109-30, 2006.

Hamed, A.M., Shabana, A.A., Jayakumar, P., and Letherwood, M.D.: Non-Structural Geometric Discontinuities in Finite Element/Multibody System Analysis. <u>Nonlinear Dynamics</u> 66: 809-824, 2011.

Hamed, A.M., Jayakumar, P., Letherwood, D.M., Gorsich, D.J. Recuero, A.M., Shabana, A.A.: Ideal Compliant Joints and Integration of Computer Aided Design and Analysis. <u>Journal of Computational and Nonlinear Dynamics</u>, under review, 2014.

Hilber, H.M., Hughes, T.J.R., and Taylor, R.L: Improved Numerical Dissipation for Time Integration Algorithms in Structural Dynamics. <u>Earthquake Engineering & Structural Dynamics</u> 5: 283-292, 1977.

Hughes, T.J.R., Cottrell, J.A. and Bazilevs, Y.: Isogeometric Analysis: CAD, Finite Elements, NURBS, Exact Geometry and Mesh Refinement. <u>Computer Methods in Applied Mechanics and Engineering</u> 194: 4135–4195, 2005.

Hussein, B.A., Sugiyama, H., and Shabana, A.A: Coupled Deformation Modes in the Large Deformation Finite-Element Analysis: Problem Definition. <u>Journal of Computational and nonlinear dynamics</u> 2: 146-154, 2007.

Hussein, B., Negrut, D., and Shabana, A.A.: Implicit and Explicit Integration in the Solution of the Absolute Nodal Coordinate Differential/Algebraic equations. <u>Nonlinear Dynamics</u> 54: 283-296, 2008.

Hussein, B.A., Weed, D., and Shabana, A.A.: Clamped End Conditions and Cross Section Deformation in the Finite Element Absolute Nodal Coordinate Formulation. <u>Multibody System Dynamics</u> 21: 375-393, 2009.

Kerkkänen, K.S., García-Vallejo, D., and Mikkola, A.M.: Modeling of Belt-Drives using a Large Deformation Finite Element Formulation. <u>Nonlinear Dynamics</u> 43: 239-256, 2006.

Korkealaakso, P., Mikkola, A., Rantalainen, T. and Rouvinen, A.: Description of Joint Constraints in the Floating Frame of Reference Formulation. <u>Proceedings of the Institution of Mechanical Engineers, Part K: Journal of Multi-body Dynamics</u> 223: 133-144, 2009.

Lan, P., and Shabana, A.A.: Integration of B-spline Geometry and ANCF Finite Element Analysis. <u>Nonlinear Dynamics</u> 61: 193-206, 2010.

Leamy, M.J., and Wasfy, T.M.: Analysis of belt-drive mechanics using a creep-rate-dependent friction law. <u>ASME Journal of Applied Mechanics</u> 69: 763-771, 2002.

Maqueda, L.G., Mohamed, A.A. and Shabana, A.A.: Use of General Nonlinear Material Models in Beam Problems: Application to Belts and Rubber Chains. <u>ASME Journal of Computational and Nonlinear Dynamics</u> 5: 849-859, 2010.

Mikkola, A.M., and Matikainen, M.K.: Development of Elastic Forces for a Large Deformation Plate Element Based on the Absolute Nodal Coordinate Formulation. <u>Journal of Computational and nonlinear dynamics</u> 1: 103-108, 2006.

Mikkola, A., Shabana, A.A., Rebollo, C.S., and Octavio, J.R.J.: Comparison Between ANCF and B-spline Surfaces. <u>Multibody System Dynamics</u> 30: 119-138, 2013.

Mohamed, A.A.: Visco-Elastic Nonlinear Constitutive Model for the Large Displacement Analysis of Multibody Systems. <u>Thesis dissertation, University of Illinois at Chicago</u> 2011.

Mohamed, A.A. and Shabana, A.A.: Nonlinear Visco-Elastic Constitutive Model for Large Rotation Finite Element Formulation. <u>Multibody System Dynamics</u> 26: 57-79, 2011.

Nachbagauer, K., Gruber, P., and Gerstmayr, J.: Structural and Continuum Mechanics Approaches for a 3D Shear Deformable ANCF Beam Finite Element: Application to Static and Linearized Dynamic Examples. <u>Journal of Computational and nonlinear dynamics.</u> 8(2): 021004, 2013.

Nakanishi, T. and Shabana, A.A.: On the Numerical Solution of Tracked Vehicle Dynamic Equations. <u>Nonlinear Dynamics</u> 6: 391-417, 1994.

Ogden, R.W.: <u>Non-Linear Elastic Deformations</u> Dover, New York, 1984.

Omar, M.A. and Shabana, A.A.: A Two-Dimensional Shear Deformation Beam for Large Rotation and Deformation. <u>Journal of Sound and Vibration</u> 243: 565-576, 2001.

Piegl, L. and Tiller, W.: <u>The NURBS Book</u> 2nd edn. Springer, New York 1997.

Roberson, R.E., and Schwertassek, R.: <u>Dynamics of Multibody Systems</u> Springer Verlag, Berlin, Germany, 1988.

Sanborn, G.G. and Shabana, A.A.: On The Integration of Computer Aided Design and Analysis Using The Finite Element Absolute Nodal Coordinate Formulation. Multibody System Dynamics 22: 181–197, 2009.

Schiehlen, W.O.: Multibody System Dynamics: Roots and Perspectives. Multibody System Dynamics 1: 149-188, 1997.

Schwab, A. L., and Meijaard, J. P.: Comparison of Three-Dimensional Flexible Beam Elements for Dynamic Analysis: Finite Element Method and Absolute Nodal Coordinate Formulation. Proceedings of the IDETC/CIE 2005, ASME 2005 International Design Engineering Technical Conferences and Computers and Information in Engineering Conference Long Beach, CA, 2005.

Schwab, A. L., and Meijaard, J. P.: Comparison of Three-Dimensional Flexible Beam Elements for Dynamic Analysis: Classical Finite Element Formulation and Absolute Nodal Coordinate Formulation. Journal of Computational and Nonlinear Dynamics 5: 011010-(1-10), 2010.

Shabana, A.A., and Wehage, R.A.: Spatial Transient Analysis of Inertia-Variant Flexible mechanical Systems. ASME Journal of Mechanisms, Transmissions, and Automation in Design 106: 172-178, 1984.

Shabana, A.A.,: An Absolute Nodal Coordinate Formulation for the Large Rotation and Deformation Analysis of Flexible Bodies. Technical Report No. MBS96-1-UIC 1996.

Shabana, A.A.: Computer Implementation of the Absolute Nodal Coordinate Formulation for Flexible Multibody Dynamics. Nonlinear Dynamics 16: 293–306, 1998.

Shabana, A.A., and Mikkola, A.M.: Use of the Finite Element Absolute Nodal Coordinate Formulation in Modeling Slope Discontinuity. ASME Journal for Mechanical Design 125: 342–350, 2003.

Shabana, A. A.: Computational Dynamics Second edition, Wiley, New York, 2010.

Shabana, A.A.: General Method for Modeling Slope Discontinuities and T-Sections using ANCF Gradient Deficient Finite Elements. ASME Journal of Computational and Nonlinear Dynamics 6: 024502-(1-6), 2010.

Shabana, A.A.: Computational Continuum Mechanics Cambridge University Press, Cambridge, 2012.

Shabana, A.A., Hamed, A.M., Mohamed, A.A. , Jayakumar, P, and Letherwood, M.D.: Use of B-spline in the Finite Element Analysis: Comparison with ANCF Geometry: Journal of Computational and Nonlinear Dynamics 7: 81-88, 2012.

Shabana, A.A.: Dynamics of Multibody Systems Fourth Edition, Cambridge University Press, Cambridge, 2014.

Simo, J.C: A Finite Strain Beam Formulation. The Three-Dimensional Dynamic Problem. Part I. Computer Methods in Applied Mechanics and Engineering, 49: 55-70, 1984.

Sopanen, J. T., and Mikkola, A. M: Description of Elastic Forces in Absolute Nodal Coordinate Formulation. Nonlinear Dynamics. 34: 53–74, 2003.

Sugiyama, H., Escalona, J.L. and Shabana, A.A.: Formulation of Three-Dimensional Joint Constraints Using the Absolute Nodal Coordinates. Nonlinear Dynamics 31: 167-195, 2003.

Sugiyama, H., Gerstmayr, J., and Shabana, A.A.: Deformation modes in the finite element absolute nodal coordinate formulation. Journal of Sound and Vibration 298: 1129-1149, 2006.

Tian, Q., Chen, L.P., Zhang, Y.Q., Yang, J.Z.: An Efficient Hybrid Method for Multibody Dynamics Simulation Based on Absolute Nodal Coordinate Formulation. ASME Journal of Computational and Nonlinear Dynamics 4: 021009-(1-14), 2009.

Tian, Q., Zhang, Y., Chen, L., and Yang, J.: Simulation of Planar Flexible Multibody Systems with Clearance and Lubricated Revolute Joints. Nonlinear Dynamics 60: 489-511, 2010.

Vallejo, D.G., Escalona, J.L., Mayo, J., and Dominguez, J.: Describing Rigid-Flexible Multibody Systems Using Absolute Coordinates. Nonlinear Dynamics, 34: 75-94, 2003.

Vallejo, D.G., Escalona, J.L., Mayo, J., and Dominguez, J.: Efficient Evaluation of the Elastic Forces and the Jacobian in the Absolute Nodal Coordinate Formulation. Nonlinear Dynamics, 35: 313-329, 2003.

Vallejo, D.G., Valverde, J. and Domínguez, J.: An Internal Damping Model for the Absolute Nodal Coordinate Formulation. Nonlinear Dynamics, 42: 347–369, 2005.

Yakoub, R.Y., and Shabana, A. A.: Three Dimensional Absolute Nodal Coordinate Formulation for Beam Elements: Implementation and Application. ASME Journal for Mechanical Design 123: 614–621, 2001.

Yoo, W.S., Lee, J.H., Park, S.J., Sohn, J.H., Pogorelov, D., and Dimitrochenko, O.: Large Deflection Analysis of a Thin Plate: Computer Simulation and Experiment. Multibody System Dynamics 11: 185-208, 2004.

<div align="center">**VITA**</div>

Name	Ashraf M Hamed

Education   **University of Illinois at Chicago, Chicago IL**.
Ph.D. / Department of Mechanical & Industrial Engineering (2011-present).
M.Sc. / Department of Mechanical & Industrial Engineering (2010-2011).
Cairo University , Egypt
B.Sc. / Department of Mechanical Engineering (2001-2005).

Teaching   **University of Illinois at Chicago, Chicago IL, USA** (2012)**.**
Experience Teaching assistant for the following courses:
- Mechanisms and Dynamics of Machinery

Cairo University, Egypt, (2006-2009)**.**
Teaching assistant for the following courses:
- Theory of Machines
- Control Theory and Design
- Vibration Analysis
- Robotics
- Machine drawing
- Machine Design

Professional   – Society of Automotive Engineers (SAE)
Membership   – American Society of Mechanical Engineers (ASME)

Reviewing   – ASME IDETC/CIE International Conference on Multibody Systems, Nonlinear Dynamics and Control, 2011-2014.
    – ASME IMECE International Mechanical Engineering Congress & Exposition, 2012.

Publications   **Journal Publications**

- * **Hamed, A.M**., Jayakumar, P., Letherwood, D.M., Gorsich, D.J. Recuero, A.M., Shabana, A.A.: Ideal Compliant Joints and Integration of Computer Aided Design and Analysis. Journal of Computational and Nonlinear Dynamics, under review, 2014.

- Walin, M., Aboubakr, A.K., Jayakumar, P., Letherwood, D.M., **Hamed, A.M.**, Shabana, A.A.: A Comparative Study of Joint Formulations: Application to Multibody System TrackedVehicles. Journal of Nonlinear Dynamics, 5(3):031006-031015, 2013.

- * Shabana, A.A., **Hamed, A.M.**, Mohamed, A. A., Paramsothy Jayakumar, Letherwood, D.M: Use of B-spline in the Finite Element analysis: Comparison with ANCF Geometry. Journal of Computational and Nonlinear Dynamics, 2012.

- *** Hamed, A.M.**, Shabana, A.A, Jayakumar, P., Letherwood, D.M.: Non-structural Geometric Discontinuities in Finite Element/Multi-body System Analysis. Journal of Nonlinear Dynamics, 2011.

  * Used in making the current thesis.

Conference papers

- **Hamed, A.M**., Jayakumar, P., Letherwood, D.M., Gorsich, D.J. Recuero, A.M., Shabana, A.A: Ideal Compliant Joints and Integration of Computer Aided Design and Analysis. Proceedings of the ASME 2014 International Design Engineering Technical Conference, 2014. (Accepted)

- **Hamed, A.M**, Jayakumar, P., Letherwood, D.M., Recuero, A.M, Shabana, A.A.: New Multibody System Simulation Capability for Flexible-Link Chain Tracked Vehicles", Society of Automotive Engineers Commercial Vehicle Engineering Congress Oct 1-3, 2013.

- Walin, M.S, Aboubakr, A.K., Jayakumar, P., Letherwood, D.M., **Hamed, A.M.**, Shabana, A.A: Evaluations of Cmpliant Mechanical Joint Models: A Comparative Study. ECCOMAS Thematic Conference on Multibody Dynamics, July 1-4, 2013.

- Shabana, A.A., **Hamed, A.M.**, Paramsothy Jayakumar, Letherwood, D.M.: Limitations of B-Spline Geometry in the Finite Element/Multibody System Analysis. Proceedings of the ASME 2011 International Design Engineering Technical Conference, August 28-31, 2011.

- Paramsothy Jayakumar, Contreras, U, Letherwood, D.M, **Hamed, A.M.**, Mohamed, A. A., Shabana, A.A.: New Finite Element / Multi-body System Algorithm for Modeling Flexible Tracked Vehicles. 2011 NDIA Ground vehicle Systems Engineering and Technology Symposium Mdeling & Simulation, Testing and Validation (MSTV) Mini-Symposium, Dearborn, Michigan, August 9-11, 2011. (**Best Paper Award**)

- Shabana, A.A., **Hamed, A.M.**, Paramsothy Jayakumar, Letherwood, D.M.: Limitations of B-Spline and NURBS Geometry in Mechanical System Analysis. Multibody Dynamics, ECCOMAS Thematic Conference J.C. Samin, P. Fisette (eds.) Brussels, Belgium, July 4-7, 2011.

- Shabana, A.A., **Hamed, A.M**, Paramsothy Jayakumar, Letherwood, D.M.: Integration of Geometry and Finite Elements in the Analysis of Nonlinear Systems. <u>ECCOMAS Thematic Conference on Computational Methods in Structural Dynamics and Earthquake Engineering M. Papadrakakis, M. Fragiadakis, V. Plevris (eds.)</u> Corfu, Greece, May 26–28, 2011.